DISSERTATION

RNA REPLICATION BY POLIOVIRUS RNA-DEPENDENT RNA POLYMERASE: EFFECTS OF RESIDUE 5 ON ELONGATION COMPLEX STABILITY AND PROCESSIVITY

Submitted by

Sarah E. Hobdey

Department of Biochemistry and Molecular Biology

In partial fulfillment of the requirements

for the Degree of Doctor of Philosophy

Colorado State University

Fort Collins, Colorado

Spring 2011

Doctoral Committee:

Advisor: Olve Peersen

Laurie Stargell
Chaoping Chen
Carol Wilusz

ABSTRACT

RNA REPLICATION BY POLIOVIRUS RNA-DEPENDENT RNA POLYMERASE: EFFECTS OF RESIDUE 5 ON ELONGATION COMPLEX STABILITY AND PROCESSIVITY

The poliovirus (PV) RNA-dependent RNA polymerase (RdRP) is a small, single-subunit, enzyme that is responsible for the replication of the viral genome. PV genome replication is much more involved than just repetitively incorporating a single nucleotide into an oligonucleotide primer. The polymerase must first go through multiple steps of initiation before processive replication can happen. During primer-dependent initiation, the polymerase must bind the primer/template RNA substrate and undergo a conformational change to form a stable RNA-polymerase complex. After the stable RNA-polymerase complex is formed the polymerase undergoes a second conformational change associated with the addition of the first nucleotide to the primer. It is only after these few steps of initiation that the polymerase can begin processive elongation. The work presented in this dissertation addresses a structure-function relationship related to initiation and processivity of the PV RdRP. Specifically, my work shows that the PV RdRP residue 5 is involved in forming and maintaining the stable, elongation-competent complex. Also, the complex stability can be modulated by downstream RNA interactions or by the number of nucleotides that are incorporated to form the stable complex. Lastly, my data demonstrate evidence of an RNA rearrangement during elongation complex

formation and show that the maintenance of a stable elongation complex is required for processive RNA replication, which is required for virus replication. To end, these data elucidate a more complete understanding of the structure-function relationships of the viral RNA polymerase and could eventually facilitate in the design of specific polymerase inhibitors.

ACKNOWLEDGMENTS

I would like to acknowledge my advisor Olve Peersen for all of his support throughout my time as a graduate student. Olve has given me a great deal of guidance in many areas of my research, those that have led to publications and those that have not, for both, I am grateful. I would also like to thank the members of my lab for all their advice and assistance. I am grateful to my thesis committee for offering their time and scientific insight. Thank you to my friends for keeping me sane throughout this process. Finally, I am grateful to my family for their support and encouragement.

TABLE OF CONTENTS

Abstract of Dissertation ii
Acknowledgements iv
Table of Contents v
List of Figures ix
Chapter 1. Introduction **1**
1.1 Poliovirus History: Discovery, Disease and Taxonomy 1
1.1.1 Discovery 1
1.1.2 Disease 2
1.1.3 Taxonomy 5
1.2 Poliovirus Eradication Efforts and Debate 5
1.3 Poliovirus "Life-Cycle" 6
1.3.1 Replication in the human 7
1.3.2 Replication in the cell 8
1.3.3 Replication in the cell-free HeLa extract system 17
1.3.4 Replication in classical biochemical systems 18
1.4 Poliovirus RNA Replication 19
1.4.1 Negative-strand RNA synthesis 20
1.4.2 Positive-strand RNA synthesis 22
1.4.3 PV polymerase fidelity 22
1.5 Mechanisms of RNA Replication by $3D^{pol}$ 23
1.5.1 Kinetic mechanism of initiation 24
1.5.2 Kinetic mechanism of elongation 24
1.5.3 Mechanism of termination 26
1.6 Poliovirus $3D^{pol}$ Structure 26
1.7 Structure-Function Relationships of PV $3D^{pol}$ 31

1.7.1 Replication fidelity 32
1.8 Scope of this Dissertation 32
Chapter 2. Materials and Methods **34**
2.1 Plasmids and Viral cDNA 34
2.1.1 pET26UbDH 34
2.1.2 pRNA2 34
2.1.3 pGRNA2-polio 35
2.2 Protein Expression and Purification 35
2.3 RNA Oligonucleotides 37
2.3.1 IRdye labeled RNA 37
2.3.2 Fluorescein labeled RNA 37
2.3.3 2-aminopurine labeled RNA 37
2.4 RNA Binding Assay 40
2.5 Elongation Complex Formation 40
2.5.1 EC formation on IRdye labeled single stranded RNA templates 40
2.5.2 EC formation on IRdye labeled downstream duplex RNA 42
2.5.3 EC formation on 2-aminopurine RNA templates 43
2.6 RNA Elongation 44
2.6.1 Fluorescein labeled RNA elongation 44
2.6.2 2-aminopurine elongation 46
2.7 Elongation Complex Stability 46
2.8 $3D^{pol}$ Solubility 48
2.9 Elongation Processivity 48
2.9.1 Primer extension 48
2.9.2 Self-priming RNA 51
2.10 Cell-free Replication 52
2.11 Transfection of HeLa Cells and Virus Quantification 53
2.12 Sequence of $3D^{pol}$ cDNA from Virion RNA 53
Chapter 3. Poliovirus Polymerase Residue 5 Plays a Critical Role in Elongation Complex Stability **55**
3.1 Introduction 55

3.2 Results 59
3.2.1 Residue 5 mutations were made PV $3D^{pol}$ 59
3.2.2 Residue 5 mutations have no effect on RNA binding and little effect on elongation complex formation 60
3.2.3 Residue 5 mutants have no effect on elongation rate 63
3.2.4 Residue 5 mutations have significant effects on elongation complex stability 68
3.3 Discussion 73
Chapter 4. Impact of Elongation Complex (In)Stability on Genome Replication 78
4.1 Introduction 78
4.2 Results 80
4.2.1 PV $3D^{pol}$ Residue 5 mutants affect replication processivity 80
4.2.2 Processivity effects caused by residue 5 mutations result in decreased RNA synthesis in a cell-free replication system 90
4.2.3 A processive polymerase is required for viral propagation 93
4.3 Discussion 96
Chapter 5. Poliovirus $3D^{pol}$ Downstream RNA Interactions and Elongation Complex Lock Length 104
5.1 Introduction 104
5.2 Results 107
5.2.1 Downstream duplex has no effect on elongation complex formation and replication 107
5.2.2 Downstream duplex has stabilizing effects on the elongation complex 112
5.2.3 Nucleotide lock length on elongation complex stability +4>+1>+7 112
5.2.4 There is a detectable 2-aminopurine florescence change associated with elongation complex formation 116
5.2.5 There is a detectable fluorescence change associated with 2-aminopurine treading through the active site of $3D^{pol}$ 125
5.3 Discussion 132
Chapter 6. Discussion and Future Directions 141
6.1 Introduction 141
6.2 The PV Elongation Complex Stability and Processivity 142
6.3 Future Directions 146

6.3.1 Effects of Zn^{++} on EC stability 146
6.3.2 Abortive elongation “hot-spots” 147
6.3.3 Fidelity of residue 5 mutants 149
6.4 Conclusion 151
References **152**

List of Figures

Chapter 1

1.1 Postulated model of PV pathogenesis....3

1.2 Postulated model of post-polio syndrome....4

1.3 Poliovirus “life-cycle” overview....9

1.4 Poliovirus positive-strand RNA genome....10

1.5 Poliovirus host cell entry....12

1.6 Model of the poliovirus replication complex....14

1.7 Asymmetrical RNA replication....15

1.8 PV genome circularization, negative-strand synthesis....21

1.9 Kinetic mechanisms for RNA replication by $3D^{pol}$....25

1.10 Crystal structure of the complete PV $3D^{pol}$....28

1.11 Crystal structure of the PV $3D^{pol}$ – RNA elongation complex....30

Chapter 2

2.1 IRdye label and thymidine modification....38

2.2 Fluorophores used in elongation, binding and EC formation assays....39

2.3 RNA polymerase elongation template elements (PETE)....41

2.4 RNA elongation using 5’ fluorescently labeled PETE....45

2.5 2-aminopurine PETE RNA elongation fluorescence....47

2.6 Poliovirus RNA genome used for processivity experiments....50

Chapter 3

3.1 Crystal structure showing residue 5 and RNA used for elongation complex experiments....58

3.2 Elongation complex formation 61

3.3 $3D^{pol}$ elongation rates 64

3.4 $3D^{pol}$ elongation stability 67

3.5 Elongation complex stability 69

3.6 Salt effects on elongation complex stability 71

3.7 Solubility of $3D^{pol}$ during stability assays 72

Chapter 4

4.1 Poliovirus RNA genome used for processivity experiments 81

4.2 DNA primer extension assay 84

4.3 Discovery of RNA self-priming 85

4.4 Elongation processivity of self-primed poliovirus RNA 87

4.5 Comparison of processivity for residue 5 mutants 88

4.6 Elongation processivity minus 5' NTR 91

4.7 Negative-strand RNA synthesis in a cell-free translation-replication system 92

4.8 Viability of poliovirus engineered to express residue 5 mutations 95

4.9 One-step growth curve of wild-type and Trp5Phe poliovirus 97

Chapter 5

5.1 Possible PV RNA interactions 106

5.2 Elongation complex formation kinetics 109

5.3 Elongation of through duplex RNA 111

5.4 EC_{+4} stability 113

5.5 EC_{+4} stability kinetics 114

5.6 Cartoon models of expected $EC_{+1,+4}$ and $_{+7}$ formations 117

5.7 Kinetics of $EC_{+1,+4}$ and $_{+7}$ stability 118

5.8 UNAfold predicted RNA secondary structures of 2AP templates before EC formation....120

5.9 Model of EC formation on 2AP templates....122

5.10 2AP fluorescence during wild-type EC_{+4} formation....123

5.11 2AP fluorescence during W5L EC_{+4} formation....126

5.12 2AP fluorescence associated with $3D^{pol}$ elongation....128

5.13 Comparison of normalized 2AP signals during elongation....130

5.14 NTP series on ap9 template by wild-type and residue 5 mutants....131

5.15 Final model of EC formation with data adaptions....137

Chapter 6

6.1 Analysis of primer extension by wild-type PV $3D^{pol}$....143

6.2 Snap-back/self-primed RNA template elongation....145

6.3 $3D^{pol}$ crystal structure showing potential Zn^{++} binding site....148

Chapter 1

Introduction

1.1 Poliovirus History: Discovery, Disease and Taxonomy

1.1.1 Discovery

Poliovirus (PV) was first recorded as an infectious virus in 1908 by Landsteiner and Popper after the epidemic emergence of poliomyelitis, a human central nervous system disease that leads to paralysis (50, 86). Landsteiner and Popper demonstrated bacterially sterile transmission of the disease from human to rhesus monkeys by injection of spinal fluid from a symptomatic child into the peritoneum of the monkey. Although, this was the first scientific evidence of poliovirus as an infectious virus, the first record of poliomyelitis has been dated back as far as 1500-1333 B.C. to the early Egyptians (50).

Detailed studies of PV began around the early 1950s when Enders, Weller and Robbins first cultivated the virus in human tissue (51, 158). This work, along with the ongoing PV epidemic, pushed the scientific community to begin intensive research of the PV that eventually led to the development of two vaccines, the inactivated virus vaccine developed by Jonas Salk and the attenuated virus oral vaccine by Albert Sabin (50, 138). Since the development of the vaccine, PV research has led to many firsts in the field of virology, including the first infectious clone of an animal virus RNA genome (130) and the first high resolution three-dimensional image of a human virus (72); also, of particular importance to the research in this dissertation, studies by Baltimore *et. al.* provided the

first direct evidence of RNA replication in a human by the PV RNA-dependent RNA polymerase (RdRP) (18).

1.1.2 Disease

Polioviruses are enteroviruses, generally meaning viruses that infect or can be found in the intestines and are spread in a fecal-oral transmission cycle. The poliovirus receptor, PVR or CD155, is only expressed in human cells and thus PV has no other vectors of transmission (98, 129). Since PV is spread through fecal-oral transmission, the virus initially infects and replicates in the gut of the host, which commonly leads to the virus entering the bloodstream. PV may invade the central nervous system where it can destroy motor neurons, causing muscular paralysis known as poliomyelitis (Fig. 1.1). The incubation period for poliomyelitis is about 10 days and occurs in 1 out of 150 PV infections (106, 107). In about 10% of PV infected individuals, a secondary illness occurs called abortive poliomyelitis. Abortive poliomyelitis can cause multiple non-specific infections such as upper respiratory tract infection, gastrointestinal illness, and influenza like infections (65, 83). In 25-50% of cases, abortive poliomyelitis leads to what is now known as post-polio syndrome or PPS (40). PPS is caused by residual effects of poliovirus infection and causes axonal sprout degeneration but the actual cause of degeneration is unknown (Fig. 1.2) (85). Symptoms include muscle weakness, pain and fatigue and usually occur 15-30 years after acute infection (34). As the PV infected individuals age, PPS is becoming more of a medical concern and is currently an area of significant research.

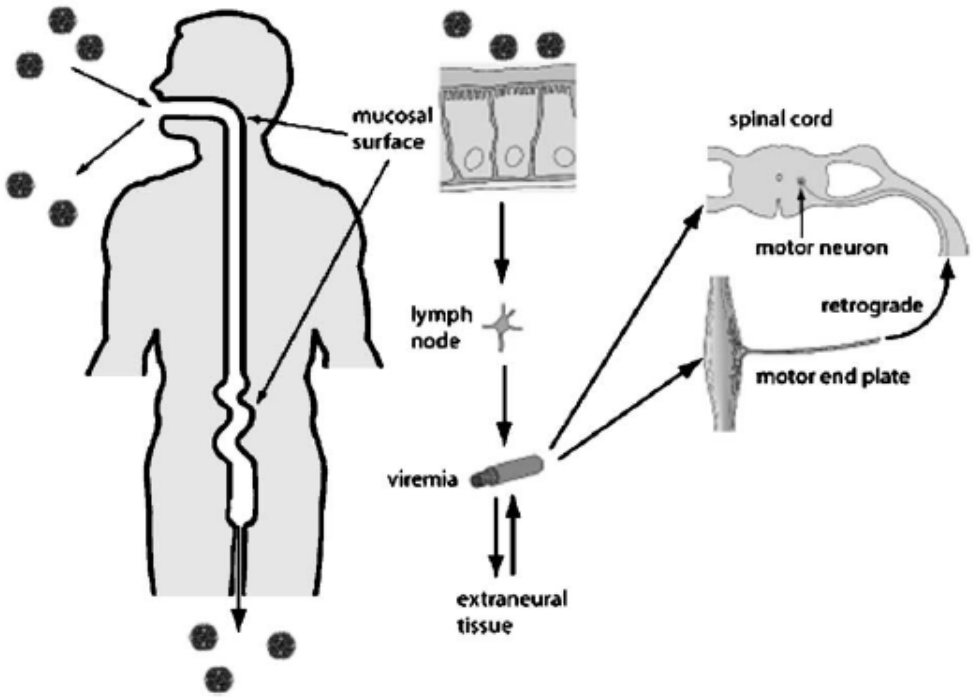

FIG 1.1. Postulated model of PV pathogenesis. PV enters the human host through fecal-oral transmission. Upon infection the virus replicates in the mucosal cells of the gastrointestinal tract where it commonly drains into the lymph nodes to reach the blood stream.. In a few cases the virus in the blood stream is spread to extraneural tissues (fat and muscle cells) where more replication occurs, resulting in sustained vireama, ultimately increasing the chances of virus invasion of the spinal cord where the virus causes axonal degeneration causing paralytic poliomyelitis. *Racaniello 2006 Virology.* (129)

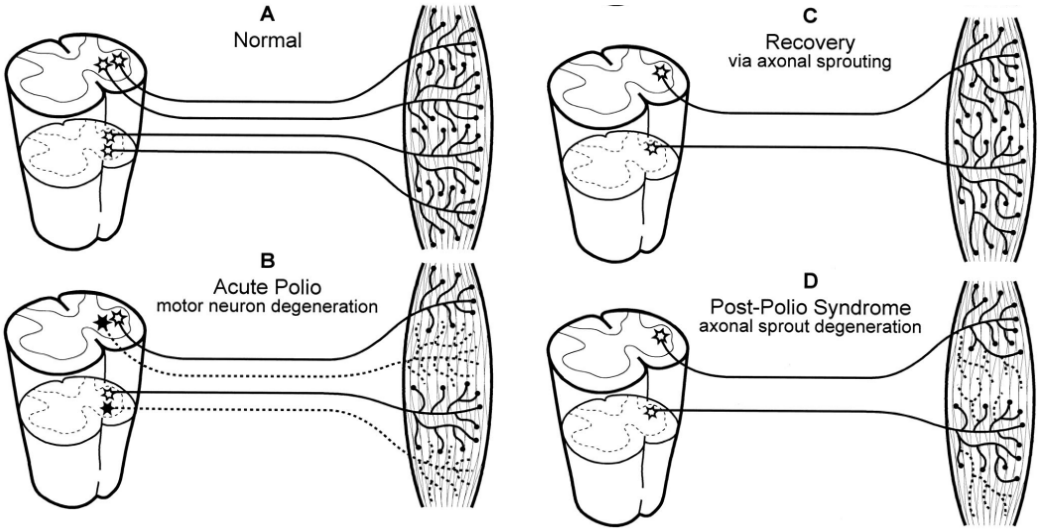

FIG 1.2. Postulated model of post-polio syndrome. (A) Healthy muscular motor neuron . The cell body is located in the spinal cord *(left)* and muscle fibers *(right)* are penetrated by the axon and axonal sprouts. (B) Infection of motor cells by PV causes neuron degeneration. (C) Axonal sprouting to make up for neurons lost by PV infection. (D) Hypothesized axonal sprout degeneration induce by post-polio syndrome. *Lambert et al. 2005 Anesthesiology.* (85)

1.1.3 Taxonomy

Poliovirus is a member of the *Picornaviridae* family of small (*Pico*-) non-enveloped, icosahedral viruses that have a single-stranded positive-sense RNA genomes (142). The *Picornaviridae* includes several closely related and medically important viruses such as poliovirus, rhinovirus, hepatitis A virus, coxsackievirus and echovirus. These viruses cause a wide range of acute diseases in humans, including poliomyelitis, the common cold, liver disease, heart disease, and aseptic meningitis. Poliovirus is the best known and most studied member of the *Picornaviridae* family and is generally considered the prototypical picornavirus.

Recently the International Committee in Taxonomy of Viruses (ICTV) has developed a new system of virus classification where viruses are grouped by order, family, genus and species. The PV now belongs to the new *Picornavirales* order that includes plant and animal viruses from five families including *Picornaviridae* family, genus *Enterovirus*, species human enterovirus C (155). This virus classification system is an ongoing effort in which thousands of viruses still remain unclassified while new viruses are added each year. For example the Picornaviridae family included eight genera in 2008 and 12 genera in 2009, which is the most recent report to date.

1.2 Poliovirus Eradication Efforts and Debate

In 1988 the World Health Organization (WHO) launched the first campaign for the eradication of poliovirus. Since that time the world has seen a 99% decrease in polio cases. However, there are a few areas of the world where PV remains endemic in the human population, including northern India, Nigeria and the border between Afghanistan and Pakistan (1). Poliovirus eradication seemed likely when first proposed as a vaccine

had been developed, we had diagnostic techniques that were able to detect PV, and the virus was maintained completely in a human host, where spread would be relatively easy to control. The oral poliovirus vaccinations (OPV), designed by Albert Sabin in 1941, contain three attenuated strains of poliovirus that induce strong immunity against infection (50, 138). The human immune response is generally able to recognize and destroy the attenuated virus before it causes significant disease. However, in the short time that the virus is replicating (~2 weeks) in the vaccinated host, some of the attenuated vaccine strains have been observed to revert back to wild-type poliovirus and are shed as virulent virus (49). If a percentage of the population is not immunized, the newly shed virulent virus may cause an outbreak of poliomyelitis among non-immune individuals, thus remaining a significant threat in some areas of the world. The inactivated virus vaccine (IPV) used in the developed world circumvents this problem, but it is too expensive for the global eradication campaign (105). Thus, there is a strong argument for the development of antivirals or better vaccines.

1.3 Poliovirus "Life-Cycle"

The PV "life-cycle" has been studied extensively since its discovery in the early 1900s. However, it wasn't until the development of cell biology techniques that molecular details of viral replication could be better illuminated. The term "life-cycle" is commonly used among virologists to explain virus replication and propagation but is not necessarily scientifically correct, since a living organism is defined by the capacity for metabolism, growth, reproduction and reaction to stimuli. Most viruses fulfill all of these requirements except for the ability metabolize, and no viruses have this capability.

Regardless, here PV replication and propagation will be referred to as the virus "life-cycle" to be in agreement with the literature.

1.3.1 Replication in the human

Oral ingestion is the most common mechanism of PV infection (Fig. 1.1). The ingested virus replicates in the oropharyngeal and intestinal mucosa of the human host (137). After multiplication in the mucosa, the virus drains into the lymph nodes and eventually into the bloodstream, causing mild infection symptoms such as headache and fever; in 99% of PV infected individuals this is the extent of the disease (107). However, in 1% of infected individuals viral replication begins to occur at non-neural tissues such as adipose and muscle cells in the body, increasing viremia and resulting in viral entry into the central nervous system. In these cases the virus replicates in and destroys motor neurons within the spinal cord, brain stem and motor cortex, leading to muscular paralysis (129).

As previously mentioned, humans are the only known natural hosts of poliovirus, being the only animal expressing the poliovirus receptor, CD155. It has been shown that some monkeys can be experimentally infected and cultured mouse cells are permissive, meaning the cells will generate infectious virus upon transfection, but infection cannot be spread (80). To show that mice were not susceptible PV infection due to the fact that they did not have the CD155 receptor, transgenic mice were generated expressing the human cellular receptor CD155 and these mice became permissive to infection through injection, but were still not susceptible through oral transmission (80). The biological function of CD155 (commonly referred to in the literature as the poliovirus receptor,

PVR) was unknown from its discovery in 1989 until 2003 when CD155 was finally established as a cell-cell adhesion molecule (101).

It was originally hypothesized that tissue tropism of the PV was localized to specific cells and tissues determined by expression of CD155 (137); interestingly this is not the case, rather tissue tropism is dependent upon cellular differences in cap-independent translation of the PV RNA genome, mediated by an internal ribosome entry site (IRES) (63, 93). For example, it has been shown that poly(A) and poly(C) binding protein (PABP and PCBP2) variants have the ability to bind the PV genome to mediate translation (68).

1.3.2 Replication in the cell

There are five required events associated with PV infection of the host cell: entry, viral genome translation, viral genome replication, virion assembly, and virus exit (Fig 1.3) (44), and the loss of any one of these steps would be detrimental to viral propagation. The PV virion is a small, non-enveloped, icosahedral protein coat containing 60 copies of each viral protein (VP), VP1, VP2, VP3 and VP4 (72). The virion contains a single strand of positive-sense RNA, shown in Fig. 1.4, that is covalently linked to viral protein VPg on its 5' end (55, 111, 161). Upon infection, VPg is cleaved from the RNA and the positive-sense genomic RNA is translated by host translation machinery to produce a ~250 kD viral polyprotein (5). Translation of viral RNA is initiated by a cap-independent mechanism involving a segment of RNA located in the 5' non-translated region including the IRES. The viral polyprotein is processed co- and post-translationally by virally encoded proteases to form multiple mature viral proteins required for replication of the RNA genome and synthesis of virions (2).

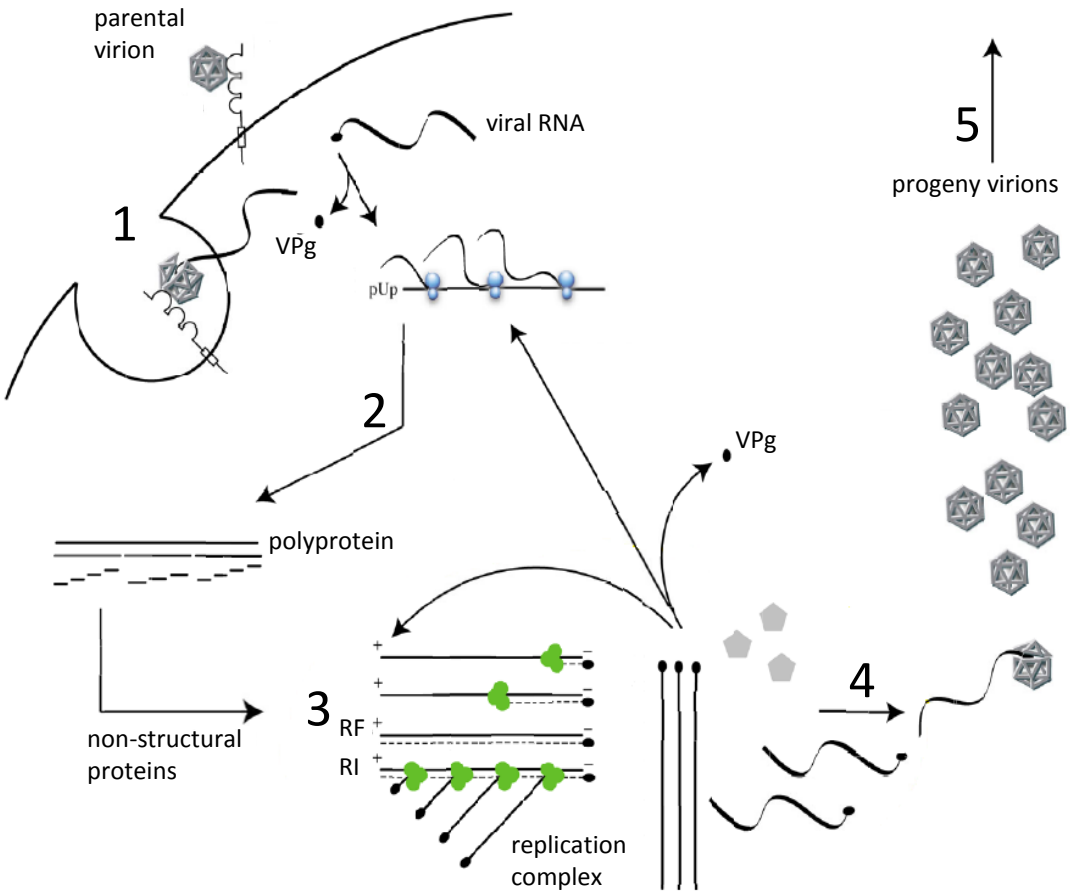

FIG 1.3. Poliovirus "life-cycle" overview. The PV "life-cycle" can be broken down into five main steps. 1, viral entry, including receptor binding, endocytosis and RNA release. 2, cap-independent translation of the viral genome. 3, formation of viral replication complexes for RNA replication by $3D^{pol}$. 4, virion assembly and genome encapsidation and 5, viral exit via cell lysis. Adapted from *De Jesus. Virol J. 2007.* (44)

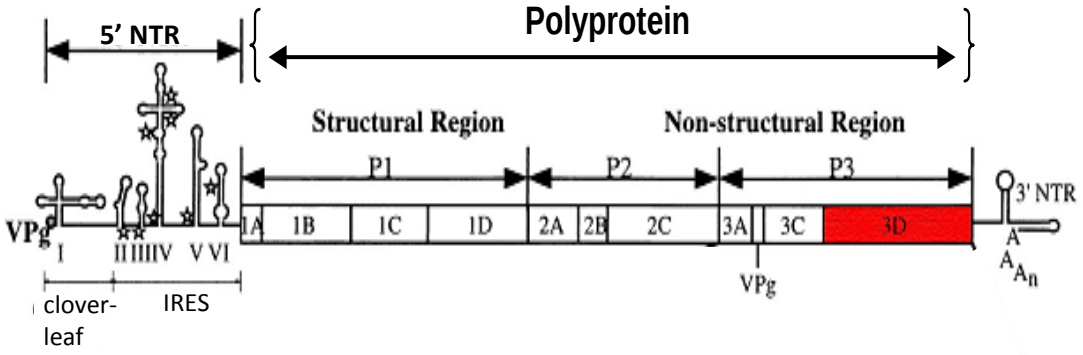

FIG 1.4 Poliovirus positive-strand RNA genome.. The 5'end is VPg linked. The 5' NTP includes the cloverleaf and IRES (internal ribosome entry site). The polyprotein open reading frame consists of viral proteins P1, P2, and P3. P1 proteins make up the structural capsid proteins. The P2 and P3 proteins include all non-structural proteins involved in formation of replication complexes and RNA replication. In red is the RNA-dependent RNA polymerase $3D^{pol}$. After the polyprotein is the 3' NTR followed by a poly(A) tail. Adapted from *Xiang et al. 1998. J. Virol.* (161).

Entry: Like all viruses, the PV is inert outside of the host cell, having no metabolic processes allowing for multiplication; therefore, it is essential for the virus to enter its host to maintain its existence. Inside the host, the PV commandeers host cell machinery required for its replication thus the virus will evolve and multiply, an essential part of virus "life cycle". As previously mentioned, for PV to enter a host cell that cell must be expressing the CD155 receptor. Once the PV – CD155 complex is formed it undergoes endocytosis by the host (Fig. 1.5) (29). After endocytosis there is a conformational change in the capsid structure that results in release of the viral RNA into the host cell cytoplasm (88). The 5' VPg (a protein required for priming RNA replication) is then cleaved from the viral RNA genome by an unknown host cell enzyme and the genome is ready for translation (5, 111).

Translation: PV translation occurs in a cap independent manner facilitated by the presence of an internal ribosome entry site (IRES) (120, 121). The IRES is a highly structured RNA element that can be bound by host translational machinery to initiate translation of the PV genome. The PV genome is translated from a single open reading frame resulting in a large polyprotein. This polyprotein is cleaved co- and post-translationally in *cis* and in *trans* by viral proteases $2A^{pro}$ and $3CD^{pro}$. The large polyprotein is divided into three main groups; P1, P2, and P3. The P1 proteins (VP1, VP2, VP3 and VP4) are structural proteins involved in forming the virus particle (77), the P2 proteins (2A, 2B and 2C) are involved in membrane rearrangement and the processing of other proteins both viral and host, and the P3 viral proteins (3A, 3B [VPg], 3C and 3D) are involved in viral RNA replication. Polyprotein processing also results in intermediate products (2BC, 3AB, and 3CD) that serve functional purposes in viral reproduction (77)

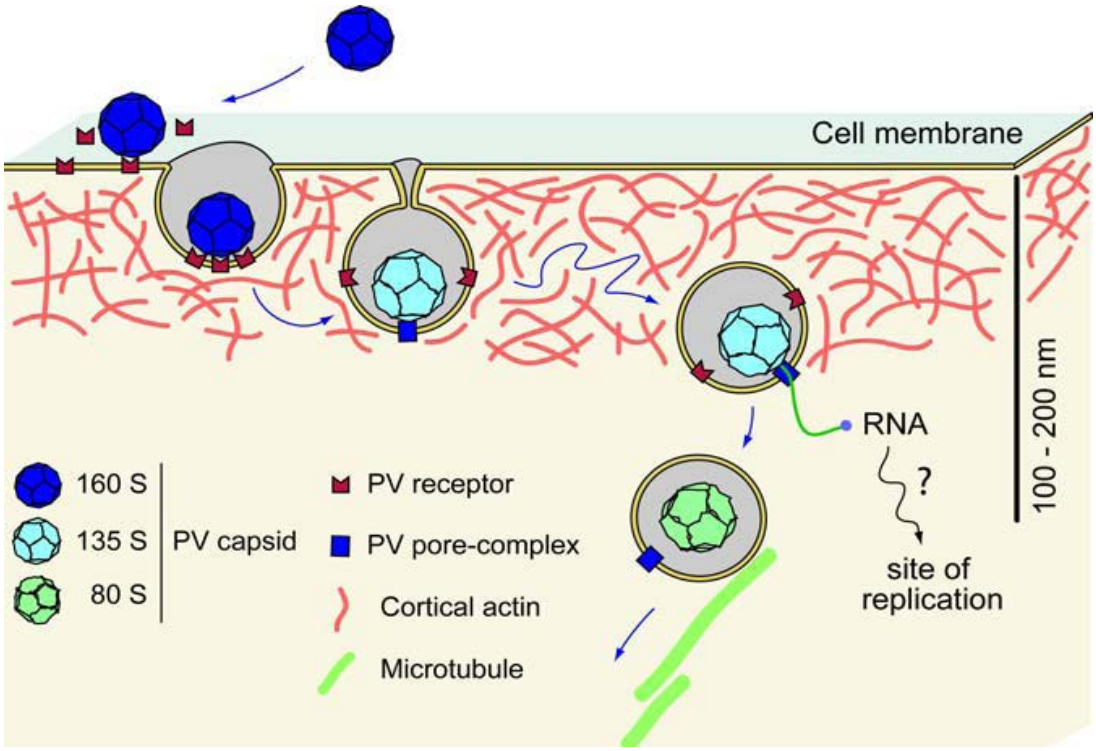

FIG 1.5 Poliovirus host cell entry. The 160S virus particle (dark blue) binds PV receptor, CD155, and undergoes a conformational change to form the 135S particle, which is internalized by an actin and tyrosine kinase-dependent mechanism. Viral RNA is released from the 135S particle 100-200 nm into the host cell and the empty capsid is transported further into the cell via microtubules. *Brandenburg et al. 2007. PLoS biology*. (29)

(also reviewed in (160)). After translation of the first few viral $2A^{pro}$ molecules, the virus is able to take over most of the host translation machinery by cleaving eIF4G host translation protein in such a way that the translation machinery is still functional for virus translation but insufficient for host mRNA translation (52, 139); thus, rendering the host incapable of synthesizing cellular proteins and allowing viral protein production to increase significantly.

RNA Replication: RNA replication occurs in large membrane-bound replication complexes, illustrated in Figure 1.6, that contain P2 and P3 viral proteins and host proteins such as poly(A) and poly(C) binding proteins (70, 103). Within poliovirus replication complexes, positive-sense RNA is circularized through a protein-protein bridge (70). In these replication complexes asymmetrical genome replication takes place by the virally encoded RNA-dependent RNA polymerase, $3D^{pol}$, by first making a negative-strand copy of the genomic RNA, which in turn serves as a template for the generation of multiple copies of nascent positive-strands (Fig. 1.7) (21). New positive strand RNAs are either translated to make additional protein for virion production, replicated to increase the amount of negative strand RNAs, or packaged into virion and released from the cell. When the genomic RNA is isolated from replication complex the negative-strand that is complementary to the positive-strand remains in a duplex, known as replicative form (RF) (17, 21). Upon initiation of positive strand RNA synthesis, the duplex RNA is melted and from this point forward the negative strand RNA exists as a replicative intermediate (RI) where multiple positive strands of RNA are being synthesized from a single template. Unlike negative strand synthesis, the positive strands

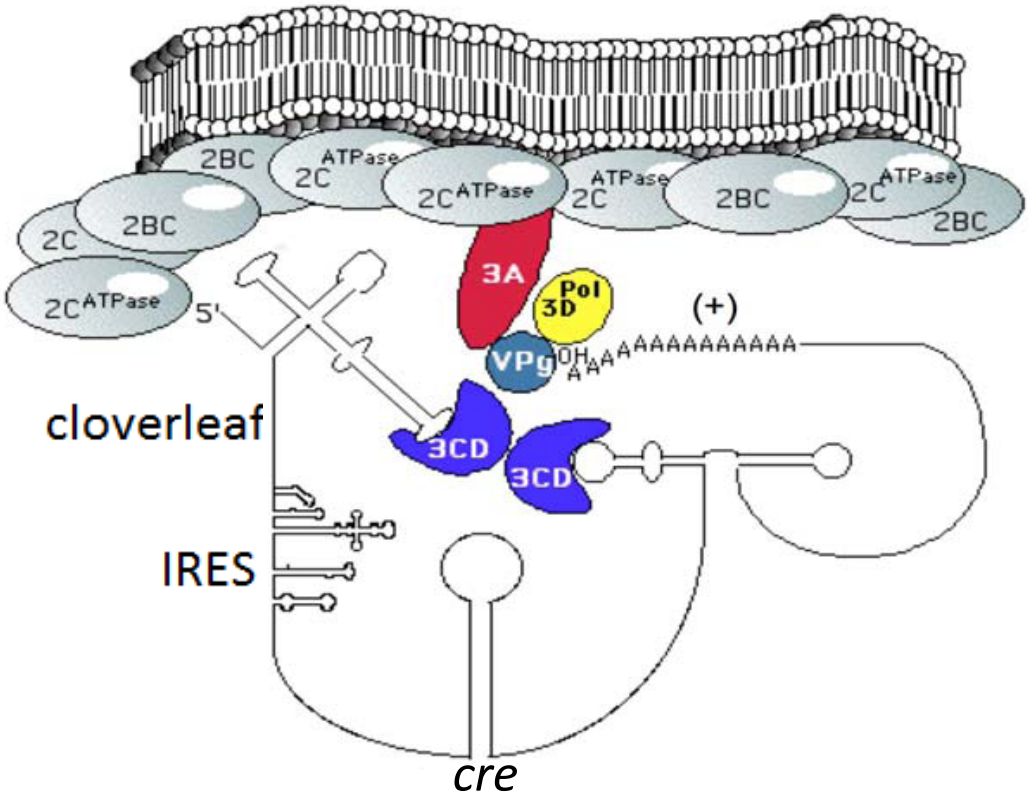

FIG 1.6 Model of the poliovirus replication complex. Cartoon representation of negative-strand synthesis by $3D^{pol}$. PV RNA replication occurs in large ER membrane associated complexes. Viral P2 proteins, $2C^{ATPase}$ and 2BC, sequester host cell membrane and P3 proteins (3A, 3B [VPg], 3CD and $3D^{pol}$) are responsible for RNA replication. The *cre* (*cis*-acting replication element) is required for VPg, primer, uridylylation and RNA replication. Host proteins are not shown. Adapted from *Murray and Barton,.2003. J. Virol.* (103)

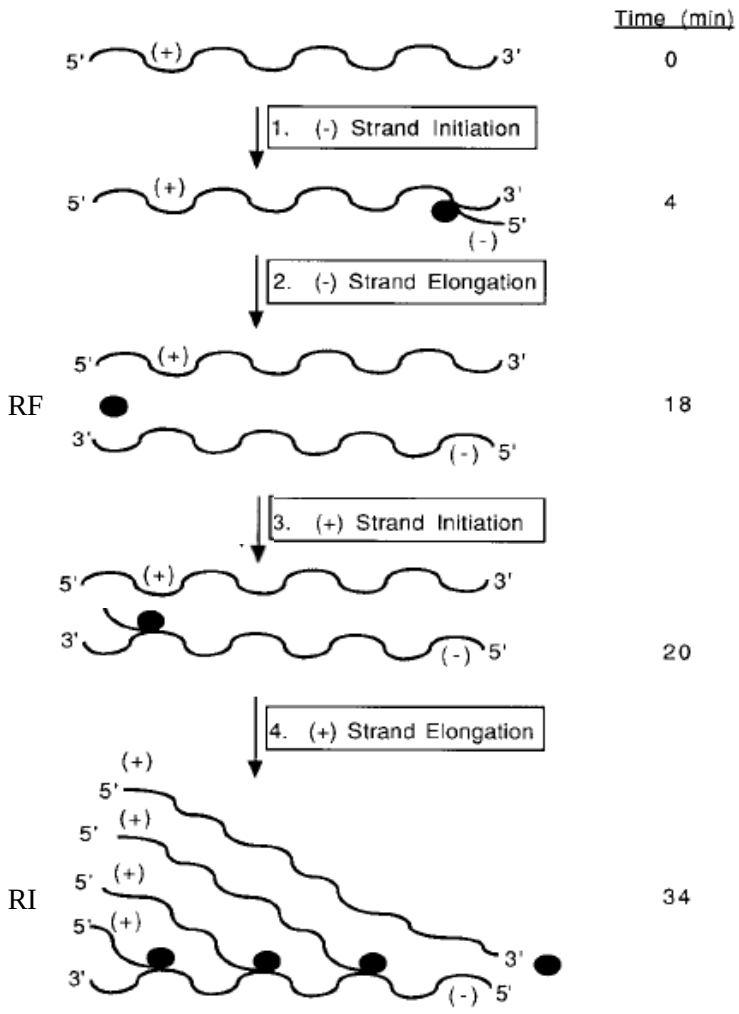

FIG 1.7 Asymmetrical RNA replication. (1) Initiation of negative-strand RNA synthesis from the positive-strand genome. (2) Formation of replicative form (RF) dsRNA. (3) Positive-strand initiation from the negative-strand RNA template. (4) Replicative form (RI) RNA, initiation of multiple positive-strands from a single negative-strand RNA. Time represents RNA replication in HeLa cytoplasmic extracts. Black circle represents RdRP, $3D^{pol}$. Adapted from *Barton and Flanegan. 1997. J. Virol.*(21).

of RNA do not remain in duplex with their template, but rather are believed to be melted by the next replicating polymerase (Fig 1.7, RI) (28).

RNA replication is initiated by a di-uridylylation of viral protein, 3B (VPg). VPg di-uridylylation is templated by a stem-loop RNA structure located at nucleotides 4444-4504 of the PV genome called the *cis*-acting replication element (*cre*) (117). The loop of the *cre* provides a template adenosine (A_5) base for uridylylation of the Tyr 3 hydroxyl ($VPgpUpU_{OH}$) by $3D^{pol}$. The process of uridylylation requires VPg binding to $3D^{pol}$ followed by the binding of this $3D^{pol}$-VPg complex to the RNA *cre* (133). In the current model, VPg is first uridylylated by ester bond formation between α-phosphate of a UTP and the Tyr3 OH, this reaction is catalyzed by the $3D^{pol}$ with the *cre* A_5 as the template. A singly uridylylated VPg ($VPgpU_{OH}$) then slides back to base pair with A_6 of the *cre* loop so that A_5 is used once again as the template for incorporation of the second uridine (119). Interestingly, since *cre* is essential for initiation of replication, they ensure that replication complexes are composed of viral RNA and not host mRNA (116).

Encapsidation: After multiple rounds of RNA replication, positive-strand genomic RNA is packaged into virus particles. Very little is understood about the encapsidation process, however, it is known to be closely coupled to RNA replication so that only RNA genomes that are being replicated are packaged (113). Some early work showed evidence of VPg acting as a packaging signal (111) but new evidence suggests that there may be more than just a single protein responsible for the coordination of RNA replication and packaging. One recent study suggests viral protein 3AB or 3CD permits transit of RNA from replication complexes to virus capsid particles (114). Another

recent study suggests that viral protein $2C^{ATPase}$ is responsible for specificity of viral RNA encapsidation as it threads the viral RNA into the mature virus capsid particle (90).

1.3.3 Replication in the cell-free HeLa extract system

The cell-free system uses HeLa cell cytoplasmic extracts to reconstitute authentic viral replication, a technique that has been used to study poliovirus replication successfully for many years (20, 48, 100). The cell-free coupled translation-replication system allows formation of pre-initiation RNA replication complexes (PIRCs) where synchronous RNA replication occurs. These complexes have been shown to be nearly identical to replication complexes in the host cell and therefore are considered authentic replication complexes (23). Addition of viral RNA to cellular extracts initiates the translation of RNA by host translation proteins. Like *in vivo* viral RNA replication, RNA replication in the cell-free system is synthesized asymmetrically when infected with the positive strand genome (23, 103). Adding 2 mM guanidine HCl cell-free replication prevents viral RNA replication while the RNA is translated; this permits the formation of membrane associated replication complexes. At low concentrations, guanidine HCl restricts the ATPase function of viral protein 2C which inhibits initiation of negative strand synthesis while having no effects on other viral or host proteins (21). Using this system, viral protein synthesis and RNA replication can be measured by pulse-labeling with ^{35}S-Met and ^{32}P-NTP incorporation, respectively. Upon removal of guanidine HCl, negative strand RNA replication is synchronously initiated. These replication reactions can then be quenched at various time points, making it possible to visualize initiation, elongation and termination of RNA on an agarose gel (21). Such aspects have proven extremely beneficial for RNA replication rate studies and examining various aspects of

positive and negative strand synthesis (21, 25). Conveniently, using this system, viral or host proteins can be added in *trans* and drugs that inhibit translation or replication can be added and then can be removed by centrifuging replication complexes and aspiration of the supernatant. Another advantage to using the cell-free system is that many studies can be completed without generating fully infectious virus by deletion of the P1 proteins from the genome, as capsid proteins are not required for the replication of the genome.

While this *in vitro* system recapitulates the steps required for PV replication, it may omit certain aspects of virus-host interactions. For example, cellular responses to viral infections that may affect viral replication, such as cell signaling and apoptosis (3), would remain undetected or deficient in this system. Also, PV replication occurs on virally sequestered ER membranes in the cell (27), certainly ER membranes constitute some of the membrane population in the cell-free system but the ER is not intact and it is likely that replication complexes are generated on any available membrane. Despite these potential pitfalls, the cell-free replication system offers an excellent system to gather insights to PV replication that are unattainable in the cell.

1.3.4 Replication in classical biochemical systems

As well as the cell-free replication system, classical biochemical systems are also used as an *in vitro* system for studying PV replication. This system requires the minimal amount of materials needed for RNA replication. For PV replication the components include RNA-dependent RNA polymerase, $3D^{pol}$, RNA template, primer (can be RNA/DNA oligomer or VPg), NTPs and Mg^{++} (118). Replication rates and efficiency depend greatly on reaction conditions such as pH, temperature and salt concentration (59, 71). Using such systems, detailed kinetic mechanisms and structural insights into RNA

replication by $3D^{pol}$ have been determined (9, 13, 152). The ability to have stringent control of the system can be advantageous over other systems like the cell-free system where various undetected interactions can be occurring with host proteins, making the system unfit for such kinetic details. That being said, replication in these reconstituted systems do not represent authentic replication complexes and lessons gleaned from these assays often require recapitulation in in cell-free and/or cellular assays (71, 81).

1.4 Poliovirus RNA Replication

In the early 1960s David Baltimore and colleagues discovered the enzyme responsible for the replication of the PV genome was an RNA-dependent RNA polymerase (RdRP) contained within the "D" protein from the P3 region of the polyprotein, commonly called $3D^{pol}$ (16, 18). The discovery that the PV polymerase was an RdRP came on the coattails of the discovery of the first RdRP in Mengovirus (131). In that study, the investigators showed that RNA could be synthesized in the presence of actinomycin D, a DNA-dependent RNA polymerase inhibitor (131). Soon after this discovery similar experiments were done for the PV to show that the PV also employed an RdRP for replication of the genome (18).

$3D^{pol}$ synthesizes both positive- and negative-strand RNAs, which can be found in three different conformations: single-stranded positive-sense RNA, double-stranded RNA where positive- and negative- strands are base paired called replicative form (RF) , and replicative intermediate (RI) where multiple positive-strands are being synthesized from a single negative-strand template (17, 19, 41).

1.4.1 Negative-strand RNA synthesis

Negative-strand synthesis differs from positive-strand synthesis mainly in initiation. Negative-strand initiation requires that translation of the viral RNA be shut off to avoid ribosome, 5'→3', polymerase, 3'→5', collisions. Translation is shut-off by 3CD binding to the 5' cloverleaf RNA structure, blocking binding of host translational machinery, specifically eIF4G (56). Translation shut-off is not a problem for synthesis of positive-strand RNA because the negative-strand template is not translated. After translation shut-off, negative-strand synthesis is initiated by circularization of the PV genome through a RNA- protein-protein-RNA bridge that brings the 5' and 3' ends of the genome together (70). In this model host Poly r(A) Binding Protein (PABP) is bound to the 3'poly(A) of the viral RNA and Poly r(C) Binding Protein (PCBP2) is bound to the 5' cloverleaf, along with viral protein 3CD (Fig.1.8) (156). The PABP-PCBP interaction is thought to bring 3CD in proximity to the 3' end of the genome so that when 3CD is proteolytically processed $3D^{pol}$ can bind VPg or $VPgpUpU_{OH}$ and negative-strand synthesis can occur (61, 70).

Along with translation shut off and genome circularization, negative-strand synthesis also requires the ATPase activity of viral protein $2C^{ATPase}$ for initiation but not for subsequent replication (21, 95). This was discovered by GuHCl inhibition studies, where low mM concentrations of GuHCl were shown to inhibit negative-strand RNA initiation and upon removal of GuHCl negative-strand synthesis begins synchronously (21). Sequence analysis of GuHCl resistant virus populations indicated a N179G mutation in the predicted ATPase domain of 2C (15, 125). Later it was shown that these

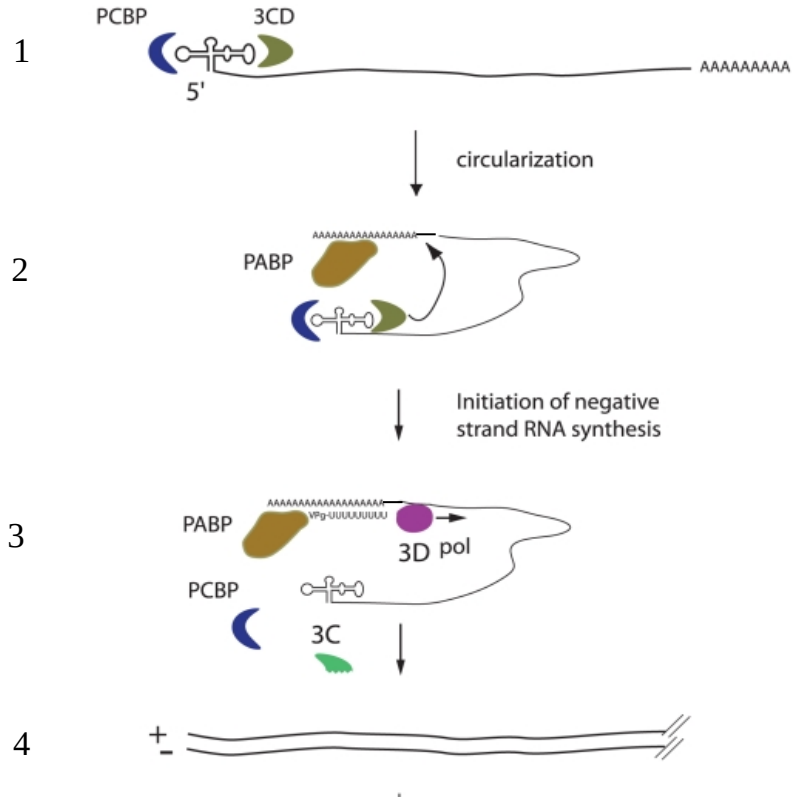

FIG 1.8. PV genome circularization, negative-strand synthesis. (1) Binding of positive-strand RNA 5' cloverleaf by host protein PCBP and viral protein 3CD. (2) Circularization of the RNA through PABP and PCBP protein interactions. (3) Cleavage of 3CD to 3C and $3D^{pol}$ for initiation of negative-strand RNA synthesis. (4) Formation of replicative form (RF) dsRNA. *Vogt and Andino. 2010. PLoS Pathog.* (156).

mutations did inhibit ATPase activity of 2C (124), however, the role of $2C^{ATPase}$ in negative-strand initiation is still unknown.

1.4.2 Positive-strand RNA synthesis

Unlike negative-strand synthesis, positive-stand synthesis absolutely requires priming from a uridylylated VPg (103). As discussed previously, VPg uridylylation occurs by $3D^{pol}$ transferase activity, templated by the RNA *cis*-acting replication element (*cre*). Significantly less is known about the molecular details of positive strand replication than negative-strand replication. For example, it is not well understood how $VPgpUpU_{OH}$ anneals to the 3' end of the negative strand genome (143), nor is it known how the asymmetry of positive: negative-strand replication is regulated (112).

1.4.3 PV polymerase fidelity

An interesting characteristic of many viral RdRPs is that they generally have relatively low fidelity, meaning that they have a greater frequency of misincorporated nucleotides compared to DNA polymerases. Low fidelity has largely been attributed to the fact that RdRPs do not have 3'-exonucleolytic activity, which provides proofreading capabilities in DNA polymerases. Otherwise the core polymerase fidelity is quite comparable (12, 157). The poliovirus $3D^{pol}$ mutation rate (~10^{-4} misincorporations per nucleotide copied) is a very high mutation rate when compared to a DNA-dependent polymerase with exonuclease activity (10^{-9} misincorporations per nucleotide copied) (47). This low fidelity enables the virus to rapidly form subpopulations, or quasispecies, that differ from the parental virus by one or more nucleotides. The generation of quasispecies is thought to be a mechanism by which RNA viruses can evade selective environmental pressures, such as antiviral drugs and host immune response, and facilitate the spread of

the virus from one tissue type to another (46). However, there is a limit to how much the viral genome can vary before propagation is affected. If the virus goes past this limit the population will no longer be able to propagate, an event referred to as "error catastrophe" (38). For example, poliovirus polymerase inserts about one wrong base for every 3800 bases replicated about two misincorporations per genome (153, 154). If this frequency increases to three misincorporations per 3500 bases replicated, the virus may no longer be able to propagate (47). Current antiviral efforts have focused largely on bringing about modifications to the polymerase fidelity that either decrease polymerase fidelity to push the virus towards error catastrophe or increasing polymerase fidelity to reduce viral adaptability (154).

1.5 Mechanisms of RNA Replication by $3D^{pol}$

Although viral replication *in vivo* occurs in large replication complexes, primer dependent polymerization of RNA by purified poliovirus polymerase ($3D^{pol}$) can occur in solution in the absence of all other viral proteins. Most mechanistic details concerning poliovirus RNA replication have been determined in this manner, using purified polymerase and a symmetrical primer/template substrate (sym/sub) RNA complex (10, 12, 30). More recently, the Peersen laboratory has employed a self-priming hairpin RNA, called Primer Elongation Template Element or PETE, to determine kinetic details of PV $3D^{pol}$ function (59, 71, 99). The advantage of using PETE is that the primer and template are a single molecule that can prime from only a single site, as opposed to the self-annealing sym/sub complex where there are two 3'OH that can serve as a primer. Also, the PETE RNA molecules are easily modified for fluorescent detection, convenient for high throughput and kinetic assays (59, 99).

1.5.1 Kinetic mechanism of initiation

In order to determine kinetic details of nucleotide incorporation, it was first necessary to be able to assemble a stable, active, elongation complex (EC). The EC is composed of $3D^{pol}$, RNA substrate and the first NTP. The assembly of the stable EC, or initiation, is a two-step process that is separate from elongation (Fig. 1.9). In the first step $3D^{pol}$ binds the RNA primer/template substrate, this has a slow rate of 0.1 μM^{-1} s^{-1} in no monovalent salt and 5 mM $MgCl_2$ and 60 µM $ZnCl_2$ and a dissociation rate of 0.1 s^{-1}, determined using kinetic simulations (9). The dissociation constant of the polymerase-RNA complex is dependent upon experimental conditions and the structure of the RNA substrate, but is generally reported to be in the low µM range (9, 99). The addition of the first nucleotide in initiation is ~2-3 orders of magnitude slower than the addition of sequential nucleotides in elongation (0.0001 s^{-1} vs. 0.06 s^{-1}), but increases the EC stability ~4 fold (7, 9, 71). This suggests that there is a conformational change in the polymerase involved with the formation of the EC, but such a change remains to be seen, even after the crystal structure of the PV $3D^{pol}$ EC was solved (60).

1.5.2 Kinetic mechanism of elongation

Using the sym/sub assay, the complete kinetic mechanism for single nucleotide incorporation by $3D^{pol}$ has been determined (11, 13). The incorporation of a single nucleotide is a complex process involving multiple functions of a single polymerase. Kinetic studies of all known classes of polymerase indicate that they share a five step mechanism for the addition of a single nucleotide: 1) nucleotide triphosphate binding, 2) a conformational change, 3) phosphodiester bond formation, 4) a second conformational change and 5) pyrophosphate release (Fig. 1.9). Two steps in the mechanisms are

initiation

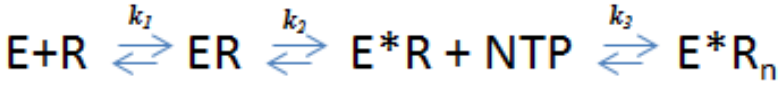

elongation

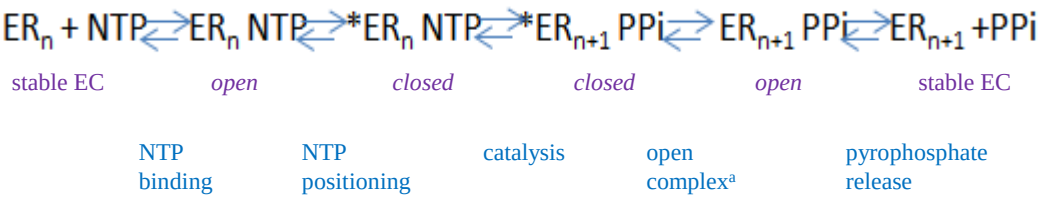

FIG 1.9. Kinetic mechanisms for RNA replication by 3D^{pol}. The kinetic mechanism for initiation (*top*) is a three step mechanism. After enzyme (E) and RNA (R) binding (k_1) an E conformational change takes place (k_2) followed by the slow incorporation of the first NTP to form a very stable elongation –competent complex. The kinetic mechanism for elongation (*bottom*) occurs after initiation, and is a five step mechanism, each step is represented by blue arrows and the functions are described below in also in blue. The polymerase states are described in purple

[a] indicates possible step for RNA translocation or where an extra step may be required for translocation.

* indicates the conformational change associated with active site closure

believed to be rate limiting, assuming there are sufficient quantities of nucleotides available: the first conformational change (step 2) and phosphodiester bond formation (step 3). It has been shown that small alterations in the first conformational change required for phosphodiester bond formation could significantly affect the ability of the polymerase to determine correct base pairing, which would have a large effect on fidelity (14). Fidelity of incorporation is largely based on the ability of the polymerase to determine whether the bound nucleotide is correctly paired to its complementary nucleotide on the template strand prior to catalysis (steps 2 and 3). If an NTP does not correctly pair with its complementary base, it is released from the polymerase active site before phosphodiester bond formation.

1.5.3 Mechanism of termination

To date, there is no known mechanism of elongation termination other than the $3D^{pol}$ falling of the 5' end of the template or spontaneous dissociation during elongation. However, *in vivo* $3D^{pol}$ is able to generate abortive products suggesting that there may be some mechanism for termination. It has been found that the bacteriophage φ6 RdRP has terminal nucleotidyltransferase activity that aids in RNA replication termination (127). Such transferase activity has also been discovered in the PV $3D^{pol}$ but has not been directly linked to RNA replication termination (108).

1.6 Poliovirus $3D^{pol}$ Structure

The first RdRP crystal structure, published in 1997, was of the PV $3D^{pol}$ (67). This structure was important to the field because it showed that RdRPs had the same overall right-hand conformation as other DNA-dependent DNA and RNA polymerases (DdDP and DdRP) (79, 140) . However, this structure was incomplete due to the entire

"fingers" domain being disordered (residues: 1-12, 38-66, 98-181 and 270-290); therefore, many structural details of this domain remained elusive. The disordered regions of the polymerase were likely due to the crystal packing conformation resulting from the oligomerization of the polymerase on two interfaces, I and II (67). Interface I has a head-to-tail orientation where the thumb domain of one polymerase interacts with palm domain of another. Via this head-to-tail orientation it is possible that long fibers of polymerase could form. Before the crystallization of PV $3D^{pol}$ there were reports of the polymerase acting as an oligomer, as polymerization was found to be concentration dependent and displayed cooperative binding to RNA; also, chemical cross-linking after initiation indicated a direct protein-protein interaction that was pH dependent (115). Later it was shown by electron microscopy that mutations in residues of Interface I disrupted polymerase oligomerization (94). Interface II is between the thumb domain of one polymerase and the N-terminus of the next and suggested that two polymerase molecules interacted in *trans* to form the active polymerase. However, since this report there has been no data supporting the interaction of Interface II (152).

In 2004 the crystal structure of the complete Mahoney type 1 PV polymerase was determined by Thompson and Peersen (Fig. 1.10) (152). By interruption of Interface I, via L446D/R455D mutation in the thumb domain, the polymerase was stable in a different crystal packing conformation where all residues had good density. The overall structure of poliovirus $3D^{pol}$ is similar to other viral RdRPs and conforms to the canonical right hand analogy where the active site palm domain is enclosed by the fingers and thumb domains. The fingers domain can be broken down into four separate amino acid stretches referred to as the index (residues 1-69), middle (residues 269-285), ring

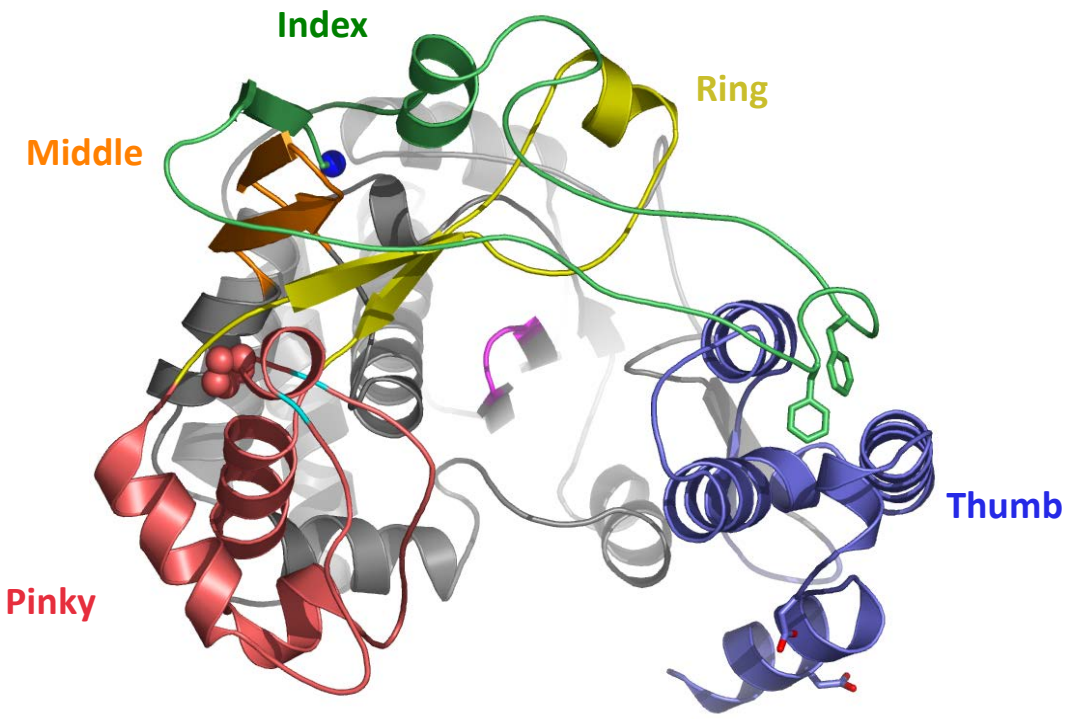

FIG 1.10. Crystal structure of the complete PV 3D^{pol}. Top view of "right hand". Palm domain in grey, magenta loop indicates the catalytic site. Thumb domain in blue. Fingers domain in green, orange, yellow and pink represent index, middle, ring and pinky fingers respectivly. Blue ball of index finger represents the N-terminus. *Thompson and Peersen. 2004. EMBO.* PDB code 1RA6. (151)

(residues 150-179) and pinky (residues 96-149 and 180-190) fingers. This allowed for clear description of amino acid, RNA and NTP interactions, also these regions are conserved in other picornavirus RdRPs (32). Of functional importance, this structure elucidated the structural basis for N-terminal burial required for polymerase activation (152). As seen with the partial structure, functionally required regions of the polymerase are highly conserved among all the RdRPs in the *Picornaviridae* family. For example, regions involved in NTP binding and catalysis are nearly identical in structure and sequence, suggesting that changes to the structures or sequence of these domains could result in noticeable alterations in polymerase activity.

Recently the crystal structure of the active PV $3D^{pol}$-RNA elongation complex was solved by Gong and Peersen (60). This is the first crystal structure of an active RdRP that has undergone multiple rounds of nucleotide incorporation. The structure has a significant amount of up- and downstream RNA, and shows evidence of active site closure upon NTP binding (Fig. 1.11) (60). This structure was solved by the formation of a very stable EC by the incorporation of four nucleotides on a PETE RNA substrate that has both upstream and downstream duplexes. The overall structure shows that the polymerase forms a clamp, composed of the $3D^{pol}$ pinky and thumb, around the upstream duplex RNA and suggests that dsRNA separation takes place as the template enters the polymerase active site by the index finger (Fig. 1.11). The structure shows that template nucleotides +1, +2 and +3 are single stranded, threading through the active site. The +1 nucleotide is base stacked against the upstream -1 nucleotide and poised for base paring with the incoming nucleotide. The +2 nucleotide is completely un-stacked from +1 and +3 nucleotides by a pocket within the index finger and Pro20, respectively. The +3

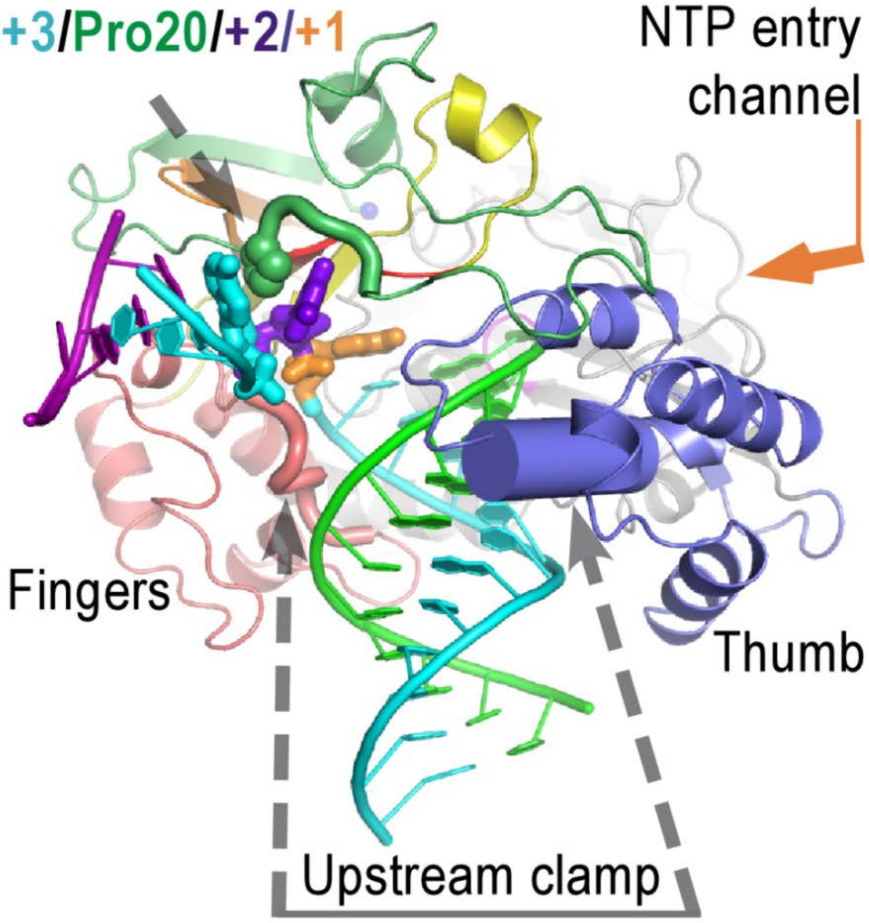

FIG 1.11. Crystal structure of the PV 3D^{pol}-RNA elongation complex. Template RNA strand is in cyan, downstream non-template strand in magenta and upstream non-template is in bright green. Template nucleotides +1, +2 and +3 are colored orange, purple and cyan, respectively. The polymerase palm domain is colored in grey, thumb in blue. The index, middle, ring and pinky fingers are in green, orange, yellow and pink, respectively. *Gong and Peersen .2010. PNAS.* PDB code, 3OL6 (60)

nucleotide is newly separated from its complementary strand by $3D^{pol}$ residues 18 and 19 in the index finger. By the addition of cognate CTP and CTP analogues, a series of structures were produced showing various aspects of the catalytic cycle. Different from other DdDPs and DdRPs, it was found that active site closure in PV $3D^{pol}$ RdRP is generated from movements in the palm domain, rather than the fingers commonly seen with other polymerases. Importantly, this report also suggested that $3D^{pol}$ requires a sixth step in the kinetic mechanism of nucleotid incorporation wherein translocation occurs. Although no structural evidence was seen for translocation, the absence of the translocation associated with any other steps and comparisons with other DNA and RNA polymerase structures, suggests that a conformational change associated with translocation could require a novel sixth step in the kinetic mechanism. In all, the determination of the PV $3D^{pol}$ and EC has been greatly beneficial in understanding the structure function relationships of all RdRPs and to the generation of this dissertation.

1.7 Structure-Function Relationships of PV $3D^{pol}$

The essential role of the RdRP in viral propagation makes it an important enzyme for understanding viral replication. Positive-strand virus RdRPs are highly homologous in structure and unique to viruses and some plants, making them a possible target for small molecule inhibitors. Currently the only antiviral against RNA viruses is a broad-spectrum nucleotide analogue, ribavirin, used to aid in treatment of hepatitis C but is not effective against all RNA viruses like the poliovirus (62). Therefore, there is a significant need for better antiviral therapeutics that more specifically target structural or functional aspects of the RdRPs. Even though the kinetic mechanisms for PV $3D^{pol}$ initiation and elongation

are known (9, 11, 13), and the complete structure and EC have been solved (60, 152), our present understanding of the structure-function relationships is still incomplete.

1.7.1 Replication fidelity

Investigation of antiviral resistance in the poliovirus polymerase revealed a Gly64Ser mutation in $3D^{pol}$ that produced a virus that is resistant to the mutagenic nucleotide analog ribavirin (39). This mutation promoted ribavirin resistance by producing a slower replicating virus with a higher fidelity RdRP (123). It was later found that the slower replication rate of Gly64Ser $3D^{pol}$ could be attributed to a 3-fold decrease in the first conformational change (step 2) of the kinetic mechanism (14). Structural analysis concluded that the Gly64Ser mutation caused an increase in stabilization in the polymerase through hydrogen bonding interactions at the amino terminus that in turn caused a prolonged stabilization in a "fidelity check point" which resulted in increased fidelity (14).

1.8 Scope of this Dissertation

This dissertation uses *in vitro* RNA replication systems, cell-free systems and infectious virus replication to elucidate structure-function relationships in the poliovirus (PV) RNA-dependent RNA polymerase. The first report (Chapter 3) investigates the functional role of residue 5 in RNA binding, elongation complex (EC) formation, elongation rate and EC stability. I initially hypothesized that residue 5 was involved in NTP incorporation but found instead it had a significant effect on EC stability. In Chapter 4, I describe the investigation of the significance of EC stability for viral replication. I showed that the most significant effect can be seen in the processivity of elongation, where less stable ECs result in less processive polymerization. The data suggested

evidence of a downstream RNA interaction, which I further investigated in Chapter 5. In Chapter 5, I show data that support the hypothesis that PV $3D^{pol}$ does interact with single- and double-stranded downstream RNA and that a downstream duplex has significant effects on EC stability. However, it remains unclear as to whether residue 5 is directly involved in RNA interactions. Finally, in Chapter 6 I describe the impact of my investigations and discuss future directions.

Chapter 2

Materials and Methods

2.1 Plasmids and Viral cDNA

2.1.1 pET26UbDH

pET26UbDH was kindly provided by Craig E. Cameron (Penn State University). pET26UbDH contains the open reading frame of the complete poliovirus (PV) $3D^{pol}$ from Mahoney 1 linked to an N-terminal ubiquitin (Ub) (58). A C-terminal GSSS-His_6 tag and a $3D^{pol}$ L446D point mutation, which interrupts the Interface I (67, 152) interaction so that the polymerase can function as a monomer, were added. The ubiquitin is co-translationally cleaved by a ubiquitin-specific carboxyl-terminal protease to generate an authentic $3D^{pol}$ N-terminus with glycine as its first residue (58).

2.1.2 pRNA2

pRNA2 was supplied by David J. Barton (University of Colorado, Aurora). pRNA2 contains sub-genomic wild-type PV cDNA with a deletion of the capsid genes, nucleotides 1175-2956 (36). The 5' end has two non-viral guanosines which are required for *in vitro* T7 RNAP based transcription of the plasmid into viral RNA. T7 transcription of MluI-linearized pRNA2 results in a wild-type PV, positive-strand, replicon. The two non-viral guanosines at the 5’ end of the transcripts allow authentic replication of negative-strand RNA in the cell-free system, but inhibit initiation of subsequent positive-strand synthesis (24).

$3D^{pol}$ mutations were generated using the QuikChange Site-Directed Mutagenesis Kit protocol (Stratagene, Inc.) and verified by sequencing. Plasmids were isolated from *E.coli* and digested with KasI and MluI to produce a minimal fragment containing the desired $3D^{pol}$ mutation and this fragment was sub-cloned into the full-length pRNA2 vector that has not undergone PCR to decrease the chance of introducing additional point mutations.

2.1.3 pGRNA2-polio

pGRNA2-polio was generated from pGEM-polio provide by the Kirkegaard Lab. pGEM-polio contains the full PV open reading frame to generate fully infectious virus (45). The 5' end contains two non-viral guanosines, required for *in vitro* transcription via T7 RNAP. The two non-viral guanosines are maintained after T7 transcription resulting in a quasi-infectious virus after transfection. However, after only a few replications of the genome the non-viral guanosines are lost and viral replication occurs as normal (69).

pGRNA2-polio and $3D^{pol}$ mutations were sub-cloned from pRNA2 plasmid digested with KasI or BglII and MluI. The pGRNA2 plasmid has a longer poly$(A)_{80}$ (80 adenosine) tail than the original pGEM-polio. Mutant plasmids are named pG for pGEM, 3D to indicated mutated protein followed by residue, position, and mutation, e.g. pG3DW5F.

2.2 Protein Expression and Purification

pET26bUbDH containing PV $3D^{pol}$, was transformed into *E. coli* BL21 (PCG1) cells for expression. By this method, $3D^{pol}$ is initially translated as an ubiquitin fusion protein that is then cleaved *in vivo* by co-expressed ubiquitin-specific carboxyl terminal protease Ubp1, resulting in full-length polymerase with the native N-terminal glycine

residue (58). Cells were grown overnight at room temperature in NZCYM medium with 25 µg/ml kanamycin, 20 µg/ml chloramphenicol, and 0.4% (w/v) D-glucose to reach an OD_{600} of ≈1.0 and 5 ml of the overnight culture was then used to inoculate 1 liter of NZCYM medium with 25 µg/ml kanamycin. The cells were grown at 37 °C to an OD_{600} of 0.6-0.8, cooled to room temperature, IPTG was added to a final concentration of 0.5 mM, and the cells were grown for an additional 12-18 hours. The resulting cell pellet was resuspended in a lysis buffer of 50 mM Tris, pH 8.0, 300 mM NaCl, 20% (v/v) glycerol, and 0.02% (w/v) NaN_3 and lysed at 18000 psi in a model M-110L microfluidizer (Microfluidics, Newton, MA). The lysate was centrifuged for 40 minutes at 17,000 rpm in a Sorvall SS-34 rotor and the supernatant was loaded onto a nickel charged Chelating Sepharose Fast-Flow column (GE Healthcare), followed by step elution with 350 mM imidazole in 50 mM Tris, pH 8.0, 300 mM NaCl, 20% (v/v) glycerol, and 0.02% (w/v) NaN_3. Fractions containing the polymerase were pooled and diluted to reduce the NaCl concentration to ≈0.11 M prior to loading onto a HiTrap Q HP column (GE Healthcare) and eluting with a linear gradient to 1 M NaCl in 25 mM Tris, pH 8.5, 20% (v/v) glycerol, 0.02% (w/v) NaN_3. The pooled fractions were concentrated to ≈0.8 ml and run over a Superdex 200 gel filtration column (GE Healthcare) equilibrated in 200 mM NaCl, 20% (v/v) glycerol, 5 mM Tris, pH 7.5, 0.02% (w/v) NaN_3. Pooled fractions were supplemented with 5 mM TCEP, concentrated to ≈400 µM, flash frozen with liquid nitrogen, and stored at -80 °C in 5-10 µl aliquots. Protein concentrations were determined based on absorbance at 280 nm and extinction coefficients were calculated based on the amino acid sequence using the ExPASy Proteomics Server (http://www.expasy.ch/tools/protparam.html).

2.3 RNA Oligonucleotides

2.3.1 IRdye labeled RNA

RNA oligonucleotides were synthesized by Integrated DNA Technologies (www.idtdna.com) with an amino modifier deoxythymidine residue at the variable N position of the GNRA-type RNA tetraloop (i.e. GTAA) (Fig. 2.1). The oligonucleotides were labeled at this site with IRdye 800RS NHS ester (LI-COR Biosciences) in a buffer containing 200 mM Na_2CO_3/$NaHCO_3$, pH 9.5, and 12.5 mM EDTA, ethanol precipitated, resuspended in TE buffer, and any remaining unreacted label was removed via Biospin P6 columns (Bio-Rad). Labeling efficiency was determined by the relative absorbance of the final material at 260 nm and 767 nm. The intramolecular hairpin structure that serves as a $3D^{pol}$ primer-template was formed by heating the RNA to 95°C for 3 minutes in 50 mM NaCl, 5 mM $MgCl_2$, 10 mM Tris, pH 8.0, followed by snap cooling on ice, which favors the intermolecular hairpin rather than the formation of oligomeric dimers.

2.3.2 Fluorescein labeled RNA

5’ fluorescein labeled RNA oligonucleotides were synthesized by Integrated DNA Technologies (www.idtdna.com) (Fig. 2.2A). The RNA was resuspended in TE buffer (1 mM EDTA, 10 mM Tris, pH 8.0) then heated to 95^{o}C for 3 minutes and snap cooled on ice to fold the elongation competent PETE (Polymerase Template Elongation Element) RNA.

2.3.3 2-aminopurine labeled RNA

RNA templates containing the 2-aminopurine nucleotide analogue were synthesized by Dharmacon RNAi Technologies (Thermo Scientific, www.dharmacon.com) (Fig. 2.2B). The intramolecular hairpin structure was formed by

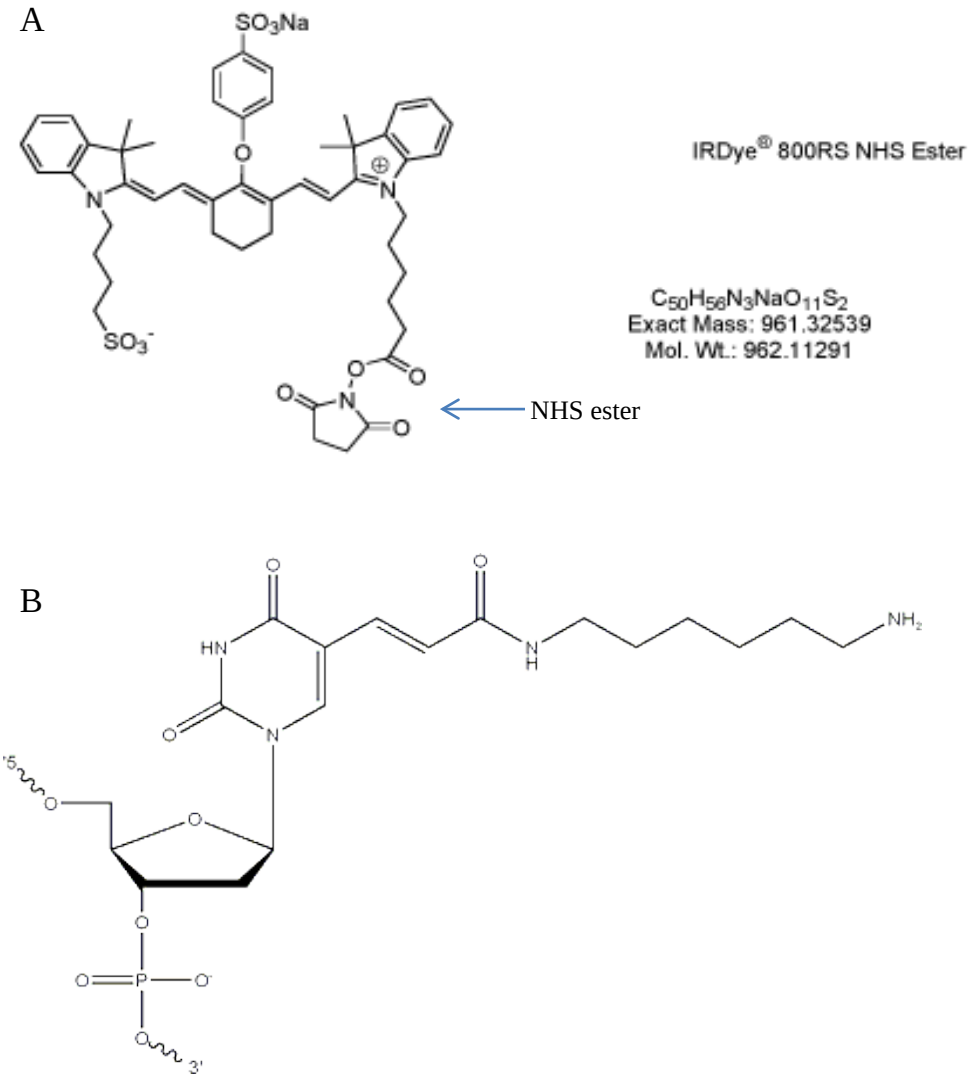

FIG 2.1. IRdye label and thymidine modification. (A) IRdye 800RS labeled used in labeling modified thymidine. Image from LI-COR website www.licor.com. (B) C6 dT amino modified base in GTAA tetraloop to attach LI-COR IRdye for RNA detection. Image from IDT website, www.idtdna.com. IRdye NHS group attaches to amine of modified base.

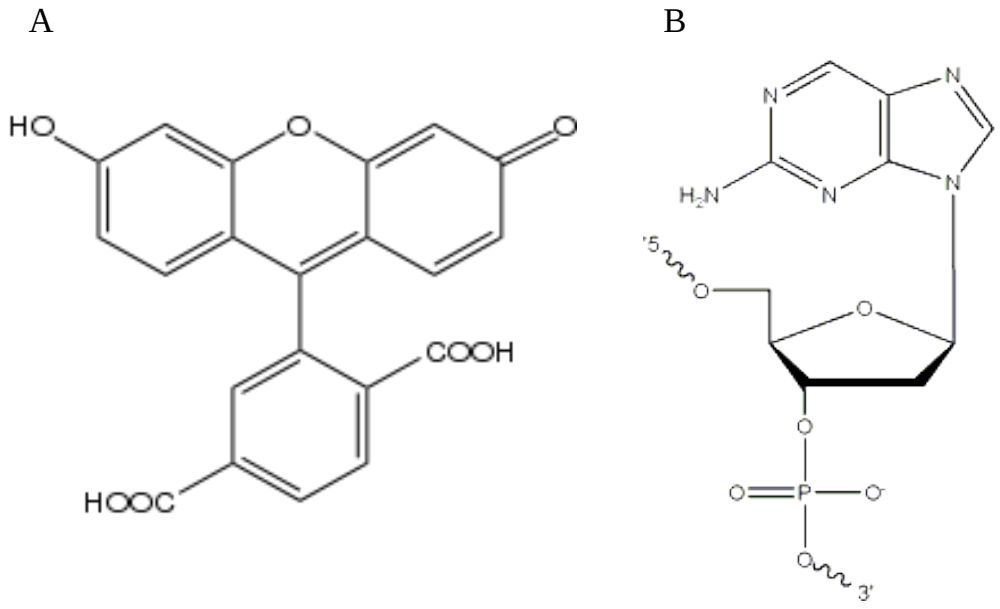

FIG 2.2. Fluorophores used in elongation, binding and EC formation assays. (A) Fluorescein used to label 5' end of 10_26 and 8_6 PETE RNAs in elongation and RNA binding assays (B) 2-aminopurine adenine base analogue used as fluorescent reporter in 2-aminopurine elongation and complex formation assays.

heating the RNA to 95°C for 3 minutes in 50 mM NaCl, 5 mM $MgCl_2$, 10 mM Tris, pH 8.0, followed by snap cooling on ice.

2.4 RNA Binding Assay

RNA binding reactions were performed as previously described using 10 nM 8-6 PETE RNA which has a 8 bp hairpin stem with a 6 nt template in 75 mM NaCl, 50 mM HEPES, pH 6.5, 1.5 mM $MgCl_2$, 0.1% NP40, 4 mM DTT (Fig. 2.3) (99). Fluorescence polarization data were collected in a Perkin-Elmer Victor V multimode microplate reader using black 384-well polystyrene plates. RNA dissociation constants were determined by curve fitting the data to a single-site binding isotherm with a Hill coefficient to account for the apparent cooperativity of the polarization data using Kaleidagraph (Synergy Software).

2.5 Elongation Complex Formation

2.5.1 EC formation on IRdye labeled single stranded RNA templates

Elongation complex formation assays were performed using two different RNA molecules in the same reaction to allow us to determine the formation rates of the +1 and +2 complexes simultaneously. PETE RNA molecules used in these experiments were 9+2-24 and 10+1-12 (Fig. 2.3A), which are named using a *X*+*Y*-*Z* convention, where *X* is the number of base pairs in the priming stem, *Y* is the number of nucleotides that are incorporated into the RNA to form the "locked" elongation complex, and *Z* is the number of remaining nucleotides in the single stranded template. Both RNAs contain a unique guanosine as the sixth nucleotide from the 5' end, allowing us to pause elongation at this point and avoid any end effects by omitting CTP from the reaction. Elongation complexes were formed by mixing 15 μM $3D^{pol}$, 1 μM each 10+1-12 and 9+2-24 RNA,

FIG 2.3. RNA Polymerase Elongation Template Elements (PETE).
(A) IRdye labeled RNA used for EC formation and stability assays. The nucleotides in grey indicate elongation upon incubation with GTP, ATP and UTP. Asterisk indicates modified base for IRdye label. (B) IRdye labeled RNA used for downstream duplex assays. The nucleotides colored blue indicate elongation upon incubation with GTP, ATP and CTP. (C) RNA templates containing 2-aminopurine (2AP) nucleotide analogue for downstream interaction assays. (2AP) is represented in green. In all RNA templates the nucleotides incorporated during elongation complex formation are colored red.

and 40 μM each ATP and GTP in a reaction buffer of 75 mM NaCl, 50 mM HEPES, pH 6.5, 1.5 mM $MgCl_2$, and 5 mM TCEP. Elongation complex reactions were quenched at the indicated times by addition of an equal volume of quench buffer consisting of 20 mM EDTA, 50 mM HEPES, pH 6.5, 75 mM NaCl. Identical reactions also containing 40 μM UTP were carried out to follow the direct formation of longer +7 or +20 products that stop six nucleotides from the end of the template. Reaction products were separated on 15% polyacrylamide, 7M urea gels that were imaged using a LI-COR Odyssey Infrared Imager 9120 and quantified using the manufacturer's Odyssey software. Data from PAGE was plotted as percentage of total RNA that elongated at each time point and fitted to a single exponential curve, $A*(1-\exp^{-t/\tau})+C$, where τ is the time constant for complex formation.

2.5.2 EC formation IRdye labeled downstream duplex RNA

Elongation complex formation assays were performed as described above on RNA containing downstream duplex. PETE RNA molecules used in these experiments were dblPETE 8+4_0+9, dblPETE 8+4_3+8 and PETE 8+4_3_3 (Fig. 2.3B). These RNA templates are named by an *X+Y_A+B*, or *X+Y_Z_Z* for the control, convention where *X* is the number of nucleotides in the 3' hairpin, *Y* is the number of nucleotides incorporated during complex formation, *A* is the number of single stranded nucleotides at the 5' end, *B* is the number of base pairs in the downstream hairpin. The "dblPETE" or double PETE designates RNA templates that have downstream duplex and PETE 8+4_3_3 served as a control having the same overall sequence with no downstream duplex. Elongation complexes were formed by mixing 15 μM $3D^{pol}$, 1 μM each RNA, and 40 μM each ATP and GTP in a reaction buffer of 75 mM NaCl, 50 mM HEPES, pH 6.5, 1.5 mM $MgCl_2$,

and 5 mM TCEP. Elongation complex reactions were quenched at the indicated times by addition of an equal volume of quench buffer consisting of 20 mM EDTA, 50 mM HEPES, pH 6.5, 75 mM NaCl. Reaction products were separated on 15% polyacrylamide, 7M urea gels that were imaged using a LI-COR Odyssey Infrared Imager 9120 and quantified using the manufacturer's Odyssey software. Data from PAGE was plotted as percentage of total RNA that elongated at each time point and fitted to a single exponential curve, $A*(1-\exp^{-t/t})+C$, where τ is the time constant for complex formation.

2.5.3 EC formation on 2-aminopurine RNA templates

Elongation complex formation of 2-aminopurine containing RNA was performed in an Applied Photophysics SX-20 stopped-flow instrument where equal volumes of $3D^{pol}$-RNA complex were mixed with or without ATP and GTP. 45 µM $3D^{pol}$ and 2.5 µM 9+4apN_13 RNA were added in a reaction buffer of 75 mM NaCl, 50 mM HEPES, pH 6.5, 1.5 mM $MgCl_2$, and 5 mM TCEP. Reactions were incubated on ice for 20 minutes followed by a 22^{o}C incubation for 10 minutes. The RNA templates were named in an *X+YapN_Z* format where *X* is the number of base pairs in the priming stem, *Y* is the number of nucleotides that are incorporated into the RNA to form the locked elongation complex, *Z* is the number of remaining nucleotides in the single stranded template and *apN* indicates the position of the 2-aminopurine after the locked complex formation (Fig. 2.3C). The stopped-flow instrument was set for excitation at 315 nm and emission detection using a 370-nm high pass filter. Reactions were loaded into reaction syringe and equal volume of RNA-protein complex and 80 µM ATP and GTP were mixed, for a 2 fold dilution and total fluorescence was monitored for evaluation.

2.6 RNA Elongation

2.6.1 Fluorescein labeled RNA elongation

Elongation rates were measured at 22.5 °C in an Applied Photophysics SX-20 stopped-flow instrument where equal volumes of pre-formed $3D^{pol}$-RNA elongation complex with 10-26 PETE RNA (Fig. 2.4A) and NTP solutions were mixed to initiate the reaction (59). Fluorescence excitation was at 492 nm from a monochromator source with bandwidth set to 9.3 nm and emission from fluorescein was detected using 515 nm high pass filters. Total fluorescent (TF) and fluorescence anisotropy (FA) signals (Fig. 2.4B) were calculated from the parallel and perpendicular polarization signals after background and G-factor correction, as per standard fluorescence methods (84). Stable +1 elongation complexes were assembled prior to the elongation reaction using a 30-minute incubation with 15 μM polymerase, 1 μM RNA and 20 μM ATP and then diluted 10-fold in reaction buffer and stored on ice until being loaded into the stopped flow instrument. Once loaded, the samples were allowed to temperature equilibrate for at least five minutes prior to data collection. The final solution measured in the stopped flow experiment after rapid mixing contains 50 nM RNA, 750 nM polymerase and 5–120 μM each NTP in reaction buffer. Elongation rates in nucleotides per second were calculated from the length of the lag phase observed at of each NTP concentration and plotted against substrate concentration to determine V_{max} and apparent K_m values (59).

A

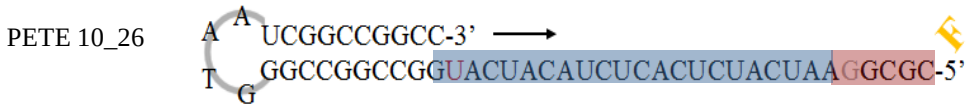

B

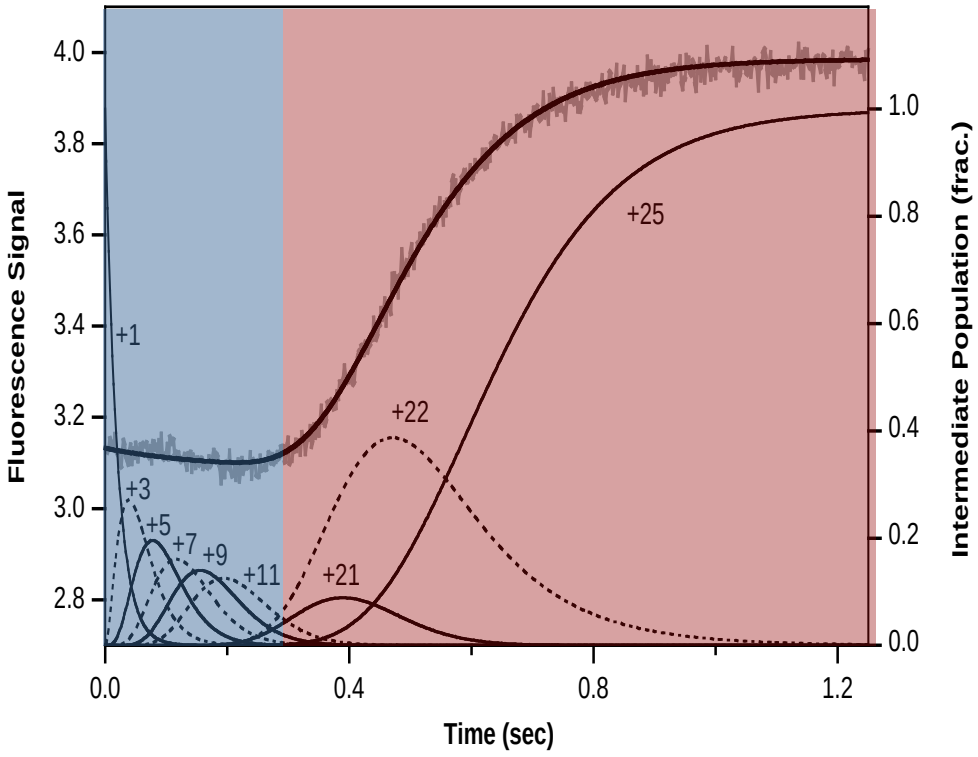

FIG 2.4. RNA elongation using 5’ fluorescently labeled PETE. (A) Cartoon representation of 5’ fluorescein labeled PETE RNA. The red nucleotide represents elongation complex formation. (B) Raw data showing the fluorescence signal change during elongation of PETE 10_26 RNA obtained in a stopped-flow, *y*-axis. y2-axis indicates the intermediate population characterizes as PETE 10_26 is elongated. Adapted from Gong *et al*. 2009. (59)

2.6.2 2-aminopurine elongation

Elongation of RNA templates containing 2-aminopurine were measured by an Applied Photophysics SX-20 stopped-flow instrument where equal volumes of pre-formed $3D^{pol}$-RNA elongation complex with 9+4ap*N*_13 (Fig. 2.5A) and NTP solutions were mixed to initiate the reaction. Elongation complexes were pre-formed prior to injection by the incubation on 15 µM $3D^{pol}$, 5 µM RNA and 40 µM each ATP and GTP in 75 mM NaCl, 1.5 mM $MgCl_2$, 4 mM TCEP and 50 mM HEPES pH 6.5. The complexes were incubated on ice for 20 minutes and then at 22^{o}C for 10 minutes. The reactions were loaded into the injection port for data collection. Fluorescence excitation was at 315 nm and emission was detected with 370 nm high pass filter. TF data was acquired after background auto correction (Fig. 2.5B).

2.7 Elongation Complex Stability

Elongation complexes were formed as described above in section 2.4.1 for the 9+2_24 RNA template and section 2.4.2 for 8+4_0+9, 8+4_3+8 and 8+4_3_3 RNA (Fig. 2.3). RiboLock RNase Inhibitor (Fermentas) was added to 3 units/µl with a room temperature incubation period of 5-15 minutes, depending on complex formation rates from Tables 3.1 and 5.1. Reactions were then diluted up to 10-fold in reaction buffer consisting of 50 mM HEPES, pH 6.5, 5 mM TCEP, 1.5 mM $MgCl_2$ and either 75 mM or 325 mM NaCl (300 mM NaCl final concentration) to limit polymerase-RNA rebinding and reinitiation. For the 9+2_24 template, dilutions were also carried out in 75 mM NaCl with 100 ng/µl heparin to prevent RNA rebinding, and an equivalent concentration of the 10+1-12 RNA was added to the reaction immediately after the dilution step to serve as a degradation and reinitiation control. At indicated time points, small aliquots of the

A

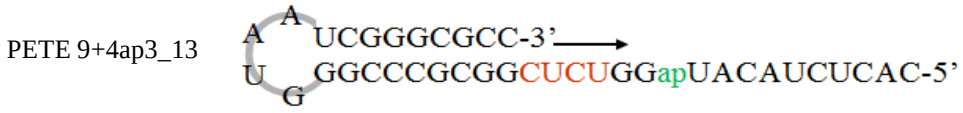

B

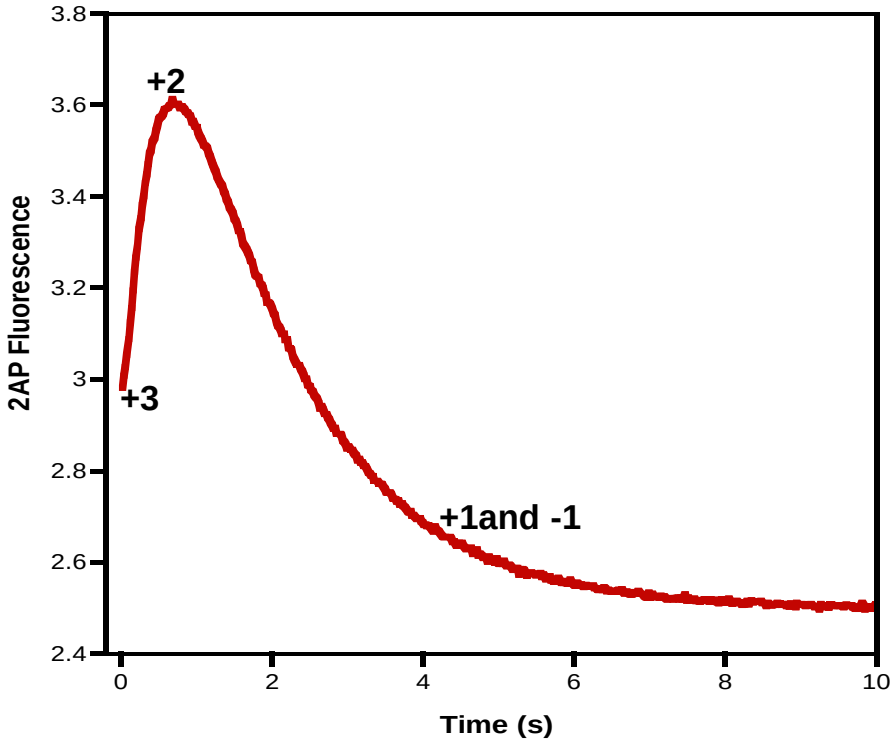

FIG 2.5. 2-aminopurine PETE RNA elongation fluorescence. (A) Cartoon of RNA used for elongation, experiment shown in panel B. (B) Fluorescence signal collected in stopped flow instrument using 370 high pass filter. Data is from 5 µM pre-locked PETE 9+4ap3_13 elongation by 15 µM wild-type $3D^{pol}$ upon addition of 5 µM NTPs. Labels +3, +2 and +1 to -1 indicate fluorescence of 2AP when at positions +3, +2 and +1 to -1 relative to the polymerase active site.

reaction were chased to longer full-length products, unless specified otherwise, by the addition of an equal volume of 40 μM UTP solution, resulting in 20 μM final concentrations of GTP, UTP and ATP; elongation to product was allowed to proceed for 3 or 5 minutes. For 9+4_24, CTP was omitted from the chase step to stop the reaction six nucleotides from the end of the template strand and avoid potential end effects. Reaction products were analyzed by denaturing PAGE and the fraction of active elongation complexes was determined by dividing the amount of elongated RNA by the sum of the fully elongated and non-elongated RNA. Data analysis by exponential curve fitting was performed using Kaleidagraph (Synergy Software).

2.8 $3D^{pol}$ Solubility

Elongation complexes were assembled as described above in 75 and 300 mM NaCl without heparin, diluted 10-fold and incubated at either room temperature or 37 °C, and at various time points (0-180 minutes) after the 10-fold dilution samples were taken and centrifuged at 17,000 x g for 10 minutes at 4^{o}C. The supernatant was removed and soluble protein was analyzed by SDS-PAGE stained with Coomassie Brilliant Blue.

2.9 Elongation Processivity

2.9.1 Primer extension

DNA primers SpeI-2201 (5'- $_{2073}$ ACTCTATGTAATTGGTGATGCCTTGTTCC ATGG$_{2040}$-3') and AvrII-5424 (5'-$_{4521}$TCTTTAGTCCATTATTGATTCATGAA$_{5394}$-3') were designed to anneal to the 3' end of a T7 transcribed PV sub-genomic replicon after linearization with SpeI at nucleotide 2201 and AvrII at nucleotide 5242 at a position in the RNA template with extensive base repeats ($GAGA_n$) so that the elongation complex could be formed and stalled. DNA primers were ordered from Integrated DNA

Technologies (www.idtdna.com) with a 5' LI-COR label. RNA template strands were T7 transcribed from pRNA2 plasmid linearized by SpeI, or AvrII to generate 2201 and 5424 nucleotide RNA products, respectively (Fig. 2.6 B). DNA primers were annealed to the RNA template by mixing 0.5 µM RNA template with 0.5 µM DNA primer in 16 mM NaCl, 1.6 $MgCl_2$ 1.6 mM TRIS pH 7.5 and 2% v/v RiboLock RNase inhibitor (Fermentas) (159). Annealing reactions were then heated to 90^{o}C and step cooled to 30^{o}C in 0.33 degree per minute increments. Annealing efficiency was determined by native 0.7% agarose gel electrophoresis. Primer extensions followed by agarose gel electrophoresis were performed by incubation 0.4 µM primer/template substrate, 10 µM $3D^{pol}$ and 40 µM each ATP, UTP, GTP and CTP formation buffer (75 mM NaCl, 4 mM TCEP, 4 mM $MgCl_2$ and 50 mM HEPES pH 6.5) on ice for 20 minutes followed by a room temperature incubation at 30-35 minutes. Reactions were quenched by the addition of an equal volume of high salt buffer (600 mM NaCl, 20 mM EDTA, and 50 mM HEPES, final). 50% of the reaction volume was loaded on to a native 0.7% agarose gel and separated by electrophoresis. Gels were imaged using a LI-COR Odyssey Infrared Imager 9120 and quantified using the manufacturer's Odyssey software then EtBr stained and imaged again using UVP Bioimaging System and LightLabs software. Primer extensions analyzed by PAGE were performed by pre-incubation of 0.25 µM primer/template substrate, 20 µM $3D^{pol}$ and 500 µM each of CTP and UTP in formation buffer to make the stalled elongation complex. Reactions were then incubated on ice for 20 minutes then moved to room temperature and incubated for 40 minutes. Reactions were then diluted 5-fold into high salt buffer (300 mM NaCl final) containing 125 µM of ATP and GTP for a final NTP concentration of 100 µM.

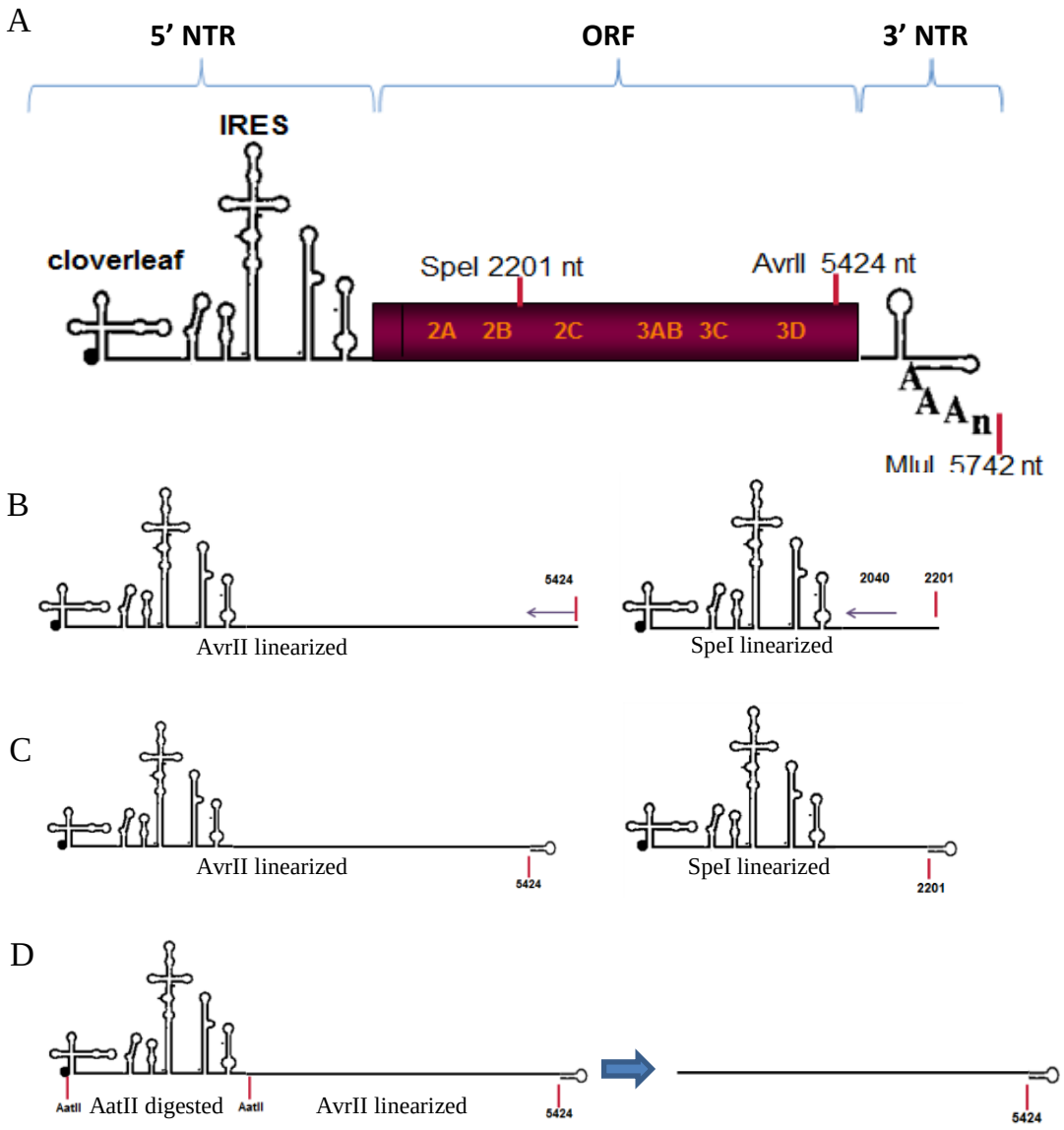

FIG. 2.6. Poliovirus RNA genome used for processivity experiments.
(A) Genomic RNA 5' NTR (non-translated region) with cloverleaf and IRES (internal ribosome entry site) RNA secondary structures. Followed by the ORF, missing the capsid domain, and 3' NTR. Red bars indicated restriction enzyme cut sites : SpeI, 2201 nt; AvrII, 5424 nt; MluI, 5742 nt. (B) RNA template used in primer extension assays. DNA primers are represented by purple arrows. Number represents the nucleotide cut site and 5' position of DNA primer. (C) Self-priming RNA. Hairpin forms at the 3' end. Numbers represent cut site. (D) Removal of 5'UTR via AatII restriction enzyme cut sites.

2.9.2 Self-priming RNA

RNA transcripts were T7 transcribed from pRNA2 plasmid linearized by SpeI, AvrII, or MluI to generate 2201, 5424, or 5742 nucleotide RNA products, respectively (Fig. 2.6A and C). For experiments the required deletion of the 5' NTR, quick-change PCR amplification was performed inserting an AatII restriction enzyme cut site 15 nucleotides into the cDNA on the pRNA2 plasmid (qc-aatII ins pRNA2). The pRNA2 plasmid was digested with the AatII restriction enzyme to remove nucleotides 15-1123 of the PV genome, this fragment was separated by gel purification and the large fragment containing the remainder of the RNA genome was purified and circularized using T4 ligase and reaction buffer from New England Biolabs (Fig. 2.6D). For transcription, the plasmid now called pRNA2-I (for pRNA2 minus IRES) was linearized by the AvrII restriction enzyme, as described above. These RNA transcripts initiate elongation complex formation via snap-back priming from the 3' end of the transcripts. Elongation reactions were initiated by incubating 20 µM protein, 0.4 µM RNA and 500 mM each NTP at room temperature for 7-15 minutes in buffer containing 50mM NaCl, 1.5 mM $MgCl_2$, 4 mM TCEP, 50 mM HEPES pH 6.5, and 1 units/µl RiboLock RNase inhibitor (Fermentas). The resulting elongation complexes were then diluted five fold into a high salt buffer (356 mM NaCl [300 mM final], 200 mM NTPs, 1.5 mM $MgCl_2$, 4 mM TCEP, 50 mM HEPES pH 6.5) to allow elongation to the end of the template without further initiation. Reaction samples were quenched with 16 mM ETDA after various times, phenol:chloroform:isoamyl alcohol extracted, precipitated and relative product RNA lengths were analyzed by native gel electrophoresis in an ethidium bromide stained, 0.7% agarose gel.

2.10 Cell-Free Replication

These experiments were performed by me under the mentorship of Ben Steil in the Barton lab at the University of Colorado Health Sciences Center, in Aurora, CO.

pRNA2, referred to as wild-type, encodes a poliovirus RNA replicon from which the P1 capsid genes have been deleted (nucleotides 1175 to 2956) (36). The T7 transcription of MluI-linearized pRNA2 cDNA yields positive-sense replicon RNA, which was used to program HeLa cytoplasmic extracts.

Cytoplasmic extracts and translation initiation factors were prepared from HeLa cells as previously described (23). Reactions contained 50% cytoplasmic extract, 20% initiation factors, 1x nucleotide reaction mix (10mM ATP, 2.5 mM GTP, and 2.5 mM CTP; 600 mM KCH_3CO_2; 300 mM creatine phosphate; 4 mg/ml creatine kinase; and 155 mM HEPES-KOH, pH 7.4), and T7 transcripts of poliovirus replicon RNA at 45 µg/ml. Pre-initiation RNA replication complexes were formed in the presence of 2 mM guanidine HCl as previously described (21).

Viral protein synthesis from poliovirus replicon mRNA was monitored by incorporation of [^{35}S] methionine (1.2 mCi/ml), which was quantified by acid-precipitation followed by scintillation counting. Pre-initiation replication complexes were isolated from HeLa S10 reactions mixtures and resuspended in [α-^{32}P] NTP-labeling reaction mix (27 mM HEPES-KOH, pH7.4; 60 mM KCH_3CO_2; 2.3 $Mg(CH_3CO_2)_2$, 2.6 mM dithiothreitol, 2.3 mM KCl; 50 µg/ml puromycin; 1 µCi/µl [α-^{32}P] UTP (10 µM labeled UTP), 1 mM ATP, 250 µM GTP and CTP; with or without 2mM guanidine HCl), and incubated at 37^{o}C for indicated time periods. Replication complexes were isolated by centrifugation at 17,000 x g for 15 min at 4^{o}C, resuspended in 0.5% SDS buffer (0.5%

SDS, 1 mM EDTA, 100 mM NaCl, 10 mM Tris, pH7.5,), phenol-chloroform extracted, ethanol precipitated, and the resulting product RNA was analyzed by nondenaturing 1% agarose 1x Tris-borate-EDTA (TBE) gel electrophoresis. The agarose gel was dried and radiolabeled product RNA was detected by phosphorimaging.

2.11 Transfection of HeLa Cells and Virus Quantification

With the exception of cDNA plasmid mutagenesis, these experiments were performed by Dr. Brian Kempf in the Barton lab at the University of Colorado Health Sciences Center, Aurora, CO.

Residue 5 mutations were introduced into poliovirus cDNA by subcloning from pRNA2 via the KasI and MluI restriction sites. Poliovirus RNA encoding wild-type, Trp5Phe, or Trp5Leu $3D^{pol}$ were derived by T7 transcription of MluI linearized cDNAs (Type 1 Mahoney). HeLa cells (~10^6 cells per 35mm well) were transfected with 2 µg of poliovirus RNAs using Transmessenger transfection reagent (Qiagen) according to manufacturer's instructions. Transfected HeLa cells were grown in 2 ml of cell culture media (DMEM containing 10% fetal bovine serum, 100 U/ml penicillin, and 100 µg/ml streptomycin) and incubated at 37^{o}C. Cells were examined for cytopathic effect (CPE) at 24, 48, and 72 hours post-transfection (hpt). At 48 and 72 hpt the cells were subjected to 3 cycles of freeze-thaw. Poliovirus titers at 48 and 72 hpt were determined by plaque assay as previously described (66).

2.12 Sequence of $3D^{pol}$ cDNA from Virion RNA

These experiments were performed by Dr. Brian Kempf in the Barton lab at the University of Colorado Health Sciences Center, Aurora, CO.

Poliovirus RNA was isolated from purified virus particles and converted into cDNA for sequencing. In brief, poliovirus from transfections and infections was purified from cell culture media by layering 8 ml of the virus onto 3 ml 30% (w/v) sucrose in PBS followed by centrifugation at 36,000 rpm for 4 hours at 4^{o}C using a Beckman SW41 rotor. The pelleted virus particles were resuspended in 400 µl 0.5% SDS buffer (0.5% SDS, 10 mM Tris-HCl, pH7.5 100 mM NaCl). PV RNA was isolated by phenol:chloroform:isoamyl alcohol extractions and ethanol precipitation.

Poliovirus RNAs were transcribed into cDNA using Superscript III Reverse Transcriptase (Invitrogen) and a primer complementary to nucleotides 6930 to 6947 of the poliovirus open reading frame (5'-$_{6947}$GGTGGTCTAAATCTATGC$_{6930}$-3'). cDNA corresponding to the 3D^{pol} region of poliovirus RNA was amplified by 35 PCR cycles with high fidelity PHUSION DNA polymerase (New England Biolabs) using a forward primer (5'-$_{5284}$GGCAATGACAATTCTACAAGC$_{5304}$-3') and a reverse primer (5'-$_{6519}$GCTTCAATTAATCTGGATTTC$_{6497}$-3') complementary to the indicated poliovirus RNA sequences. PCR products were sequenced using the forward primer corresponding to poliovirus nucleotides 5816-5838. When mixed populations of virus sequence were detected in the sequence of PCR products (as for Trp5Leu at 48 hpt), PCR products were TOPO-TA cloned (Invitrogen) and the sequences of representative cDNA clones were determined. PCR products and cDNA clones were sequenced in the University of Colorado Cancer Center DNA Sequencing Core Laboratory.

Chapter 3

Poliovirus Polymerase Residue 5 Plays a Critical Role in Elongation Complex Stability

3.1 Introduction

*This chapter has been published as part of Hobdey, S.E., Kempf, B.J., Steil, B.P., Barton, D.J., and Peersen, O.B. (2010) J Virol **84**,8072-8084.*

The work in this chapter was completed by me, Sarah E. Hobdey. Contributions from other authors can be found in Chapter 4 of this dissertation.

Members of the *Picornaviridae* family of small RNA viruses cause a wide range of diseases in humans, including liver disease, heart disease, aseptic meningitis, the common cold, and poliomyelitis. The picornaviruses include the most common human viruses, the rhinoviruses that spread through respiratory pathways and the second most common, enteroviruses that spread by fecal-oral transmission. These viruses have ≈7.5 kB positive-sense genomes containing a single large open reading frame encoding for a ≈250 kDa polyprotein that is cleaved into about a dozen different proteins by viral proteases (77). Their genome lifecycle is completely RNA based, with replication being driven by the viral $3D^{pol}$ protein, an RNA-dependent RNA polymerase (RdRP).

After viral RNA translation and polyprotein processing, $3D^{pol}$ replicates the infecting positive-strand RNA template into a negative-strand intermediate that is subsequently used as a template for positive-strand synthesis. During these processes, $3D^{pol}$ interacts with multiple templates, substrates and other viral proteins; however,

many aspects of these events remain obscure. The crystal structures of several picornavirus $3D^{pol}$ enzymes have been solved and these all conform to the "right hand" analogy commonly used to describe polymerases as having palm, thumb, and fingers domains (32, 54, 64, 92, 110, 152). Based on the recently publish PV $3D^{pol}$ elongation complex structure and homology to other polymerases, the fingers domain interacts with template RNA, the palm domain contains the active site aspartate residues that coordinate the metals needed for catalysis, and the pinky and thumb domains contact the exiting duplex RNA product in a clamp-like structure (60). This is similar to structures of the closely related foot-and-mouth disease and Norwalk viruses solved in complex with nucleic acids (53, 109, 163).

Poliovirus is among the most studied picornaviruses and its polymerase has been thoroughly characterized biochemically (11, 57) and structurally (151, 152). Processive RNA synthesis requires the formation of a stable $3D^{pol}$ elongation complex through a multi-step process involving at least two conformational changes (9, 60). First, following RNA binding there is a slow ($t_{1/2} \approx 12$ sec) conformational change that results in a $3D^{pol}$ RNA complex poised for NTP incorporation. Second, following the addition of the first nucleotide to the primer there is another conformational change to produce a very stable elongation complex with an *in vitro* half-life on the order of several hours. The polymerase begins processive elongation after the formation of this stable elongation complex and each nucleotide addition cycle involves a five step mechanism, of which NTP repositioning and NTP catalysis are rate limiting (11). Similar experiments using the homologous foot-and-mouth disease virus polymerase reveal an analogous set of complexes resulting in an elongation complex with a half-life of 27 hours (6). Although

these viral polymerase complexes have been well-characterized biochemically, there is relatively little known about any structural changes involved in elongation complex formation or the catalytic cycle itself; all the $3D^{pol}$ structures solved thus far show essentially the same conformation with no evidence for significant conformational changes upon RNA or NTP binding.

The activation of several picornavirus polymerases is dependent upon correct cleavage of $3D^{pol}$ from the viral $3CD^{pro}$ precursor protein in order to create a new N-terminus that can be buried in a pocket at the base of the $3D^{pol}$ fingers domain. This buried N-terminus has been observed in polio, coxsackie, rhino, and foot-and-mouth disease virus polymerases (32, 54, 92, 152). In solving the structure of poliovirus polymerase, we observed that burying the N-terminus resulted in a subtle but important conformational change in the active site whereby Asp238 was repositioned to make a key hydrogen bond with the 2' hydroxyl of a bound NTP (152). Addition or deletion of a single residue at the N-terminus abolished enzyme activity, and mutations of Gly1 to alanine resulted in a partially active enzyme with slightly altered positioning of Asp238. Further data from coxsackievirus polymerase showed that the addition of a second N-terminal glycine also inactivated the enzyme, but activity could be restored by also deleting Glu2, indicating that there is a specific length requirement in the N-terminal sequence of the enzyme (32). A prime candidate for involvement in such a length requirement is residue Phe5 of coxsackievirus $3D^{pol}$ that corresponds to Trp5 in poliovirus $3D^{pol}$. In the $3D^{pol}$ structures there is a backbone distortion in the β-strand composed of residues 1-9 that results in this large hydrophobic amino acid being solvent exposed rather than buried into an adjacent hydrophobic pocket (Fig. 3.1A). This

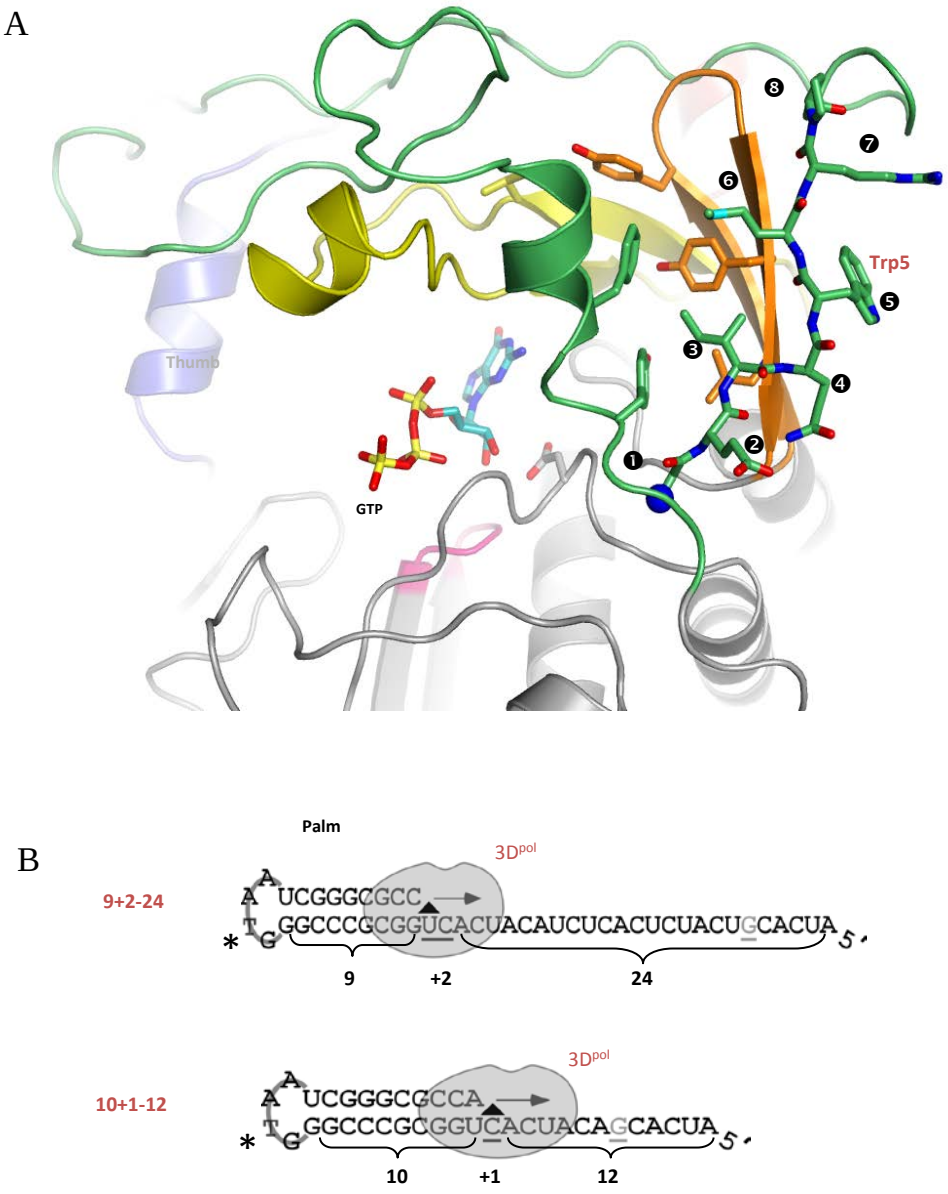

FIG. 3.1. Crystal structure showing residue 5 and RNA used for elongation complex experiments.. (A) Structure of poliovirus polymerase-GTP complex (IRA7) showing the distortion of the β-sheet conformation between residues 3 and 4 that results in Trp5 being solvent exposed adjacent to a large hydrophobic patch composed of residues from the index (green) and middle (orange) fingers. (B) Cartoon of the PETE (*polymerase elongation template element*) RNAs used in complex formation assays. Both RNAs are G-less until the 6th nucleotide from the end, which limits secondary structure and stops elongation before the 5' end to avoid possible end effects. The * indicates the position of the amino-modified deoxythymidine where the IRDye label is covalently attached.

unusual conformation at residue 5 is conserved among picornaviral polymerase structures and substitution mutations at this residue had significant effects on coxsackievirus polymerase activity (32). Large hydrophobic amino acids at residue 5 increased $3D^{pol}$ activity while small amino acids at residue 5 decreased $3D^{pol}$ activity (32). Based on these data we proposed that the $3D^{pol}$ catalytic cycle involves a conformational change wherein residue 5 flips into an adjacent hydrophobic patch on the polymerase to aid in NTP positioning, and such a conformational change would require the N-terminus to be correctly buried to act as a stable pivot for the rotational movement.

In this work we have investigated the role of residue 5 in $3D^{pol}$ in further detail by examining how a series of mutations in poliovirus $3D^{pol}$ affect RNA binding, elongation complex formation, elongation rate, and elongation complex stability. The data show that residue 5 mutations have major effects on the stability of the elongation complex with minor effects on elongation complex formation and no effect on RNA binding affinities and elongation rates.

3.2 Results

3.2.1 Residue 5 mutations were made to PV $3D^{pol}$

Residue 5 point mutations were introduced in the PV $3D^{pol}$ using quick change PCR, as described in Chapter 2 Section 2.1.1. The rationale behind selected PV residue 5 mutations was based on work done in Coxsackievirus; planar hydrophobic residues at position 5 resulted in active polymerase while small hydrophobic residues decreased activity (32). DNA mutations were designed so that the maximum number of nucleotides in the codon sequences were mutated to reduce the chances of reversions when introduced into the full virus (Chapter 4).

3.2.2 Residue 5 mutants have no effect on RNA binding and little effect on elongation complex formation compared to wild-type

The effects of residue 5 mutations on polymerase RNA affinity were determined using a fluorescence polarization based PETE binding assay with residue 5 mutations to a planar aromatic phenylalanine and a smaller non-planar valine residue, described in Chapter 2, Section 2.4. Neither mutation had a significant effect on the affinity for PETE 8-10 RNA (Table 2), indicating that residue 5 does not play a direct role in RNA binding in the absence of nucleotides and elongation. We then examined what effects the mutations have on formation of stable $3D^{pol}$ elongation complexes as measured by the incorporation rate for the initial nucleotides on a self-priming PETE RNA, as described in Chapter 2, Section 2.5.1. Two PETE RNAs were used simultaneously in these experiments: one has a 10 bp hairpin followed by a 13 nt template that allowed the incorporation of only a guanosine when incubated with GTP and ATP, and the other has a 9 bp hairpin with a 26 nt template that allowed the incorporation of both adenosine and guanosine (Fig. 3.1B). This RNA design allowed us to compare the two RNAs in the same reaction to determine if there are differences between +1 and +2 product formation. The final products of the elongation complex formation reaction have identical structures and differ only in the length of their remaining template. Product formation rates were determined by polyacrylamide gel analysis of the quenched samples followed by band quantitation of the IRdye labeled RNAs to determine the relative amounts of starting and elongated material (Fig. 3.2A).

The formation rates for the +1 and +2 products by wild-type $3D^{pol}$ and the various Trp5 mutants are shown in Fig. 3.2B and Table 3.1. All mutants exhibited single

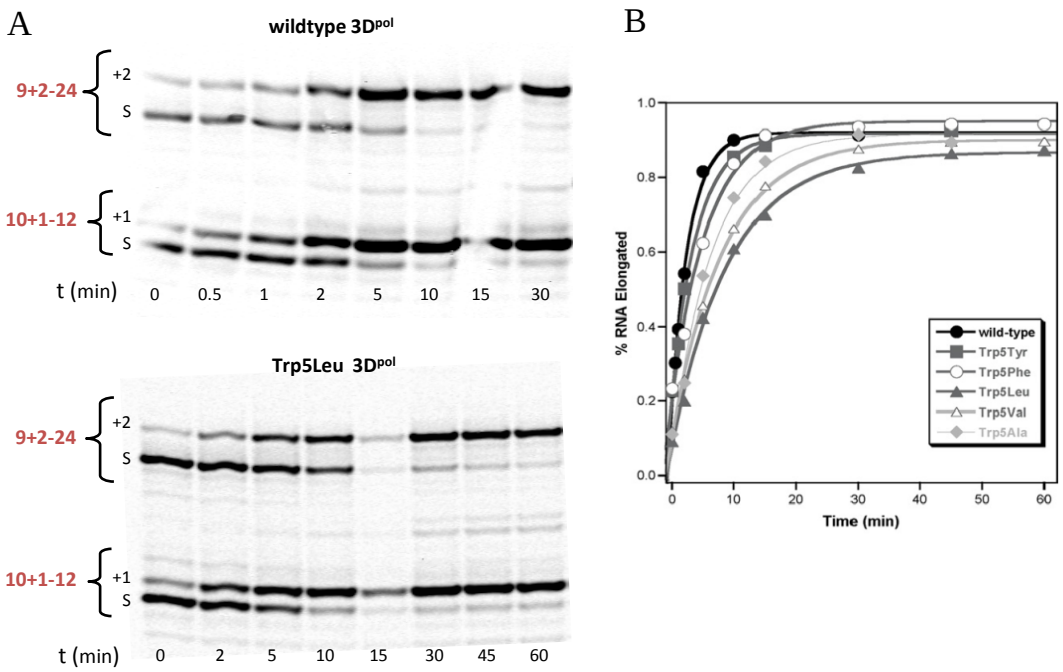

FIG. 3.2. Elongation complex formation. (A) Denaturing PAGE showing the time course for formation of the +1 and +2 products from the two RNAs. Elongation complexes were formed by incubating 1 µM of each PETE RNA, 15 µM 3D^{pol}, and 40 µM of ATP and GTP at 22 °C for various times as indicated. (B) Kinetics of +2 complex formation rates obtained from band intensity data curve fit to a single exponential. The resulting formation time constants are listed in Table 1.

Table 3.1. Initiation product formation rates of Trp5 mutants[c]

Initiation product formation rate (minutes)				
3D^{pol}	**+1 product[a]**	**+7 product[b]**	**+2 product[a]**	**+20 product[b]**
wild-type	2.0 ± 0.1	2.5 ± 0.5	3.0 ± 0.2	3.0 ± 0.5
Trp5Tyr	4.5 ± 0.5	5.5 ± 0.1	4.2 ± 0.3	4.0 ± 0.5
Trp5Phe	4.0 ± 0.1	7.5 ± 0.5	5.9 ± 0.5	9.0 ± 1.5
Trp5Leu	5.5 ± 0.5	4.0 ± 0.5	9.4 ± 0.6	5.0 ± 1.0
Trp5Val	7.0 ± 0.5	5.0 ± 0.5	8.5 ± 0.3	8.0 ± 0.5
Trp5Ala	7.5 ± 0.5	7.5 ± 0.5	6.6 ± 0.7	7.5 ± 0.5

[a] Product formation in the presence of 40 µM each ATP and GTP only.
[b] Product formation in the presence of 40 µM each ATP, GTP and UTP.
[c] Time constants in minutes base on single exponential curve fits of integrated band intensities.

exponential kinetics for +1 and +2 product formation and the rates were determined by numerical curve fitting. The Trp5 mutations reduced both the +1 and +2 complex formation rates when compared to wild-type, but the effects were fairly small with only a ≈3-fold reduction at most (Table 3.1). The rate reduction also correlated with the size of the replacement residue, with tyrosine and phenylalanine having fairly small effects while leucine, valine, and alanine had greater effects. Prior studies of $3D^{pol}$ enzymology have shown that the incorporation of the first nucleotide is the rate-limiting step during initiation that is followed by the fast incorporation of additional nucleotides (13). Consistent with this, the rates for formation of the longer +7 and +20 products in the presence of ATP, GTP, and UTP are comparable to those of the +1 and +2 product formation for each polymerase (Table 3.1).

3.2.3 Residue 5 mutants have no effect on elongation rate

To determine $3D^{pol}$ elongation rates we used the PETE assay in a stopped-flow kinetic format where we detect how long it takes $3D^{pol}$ to reach the end of a 5' fluorescein labeled template RNA, methods described in Chapter 2, Section 2.6.1 (59). The experiments utilized a 10-26 PETE RNA with a 10 bp priming hairpin and a 26 nucleotide G-less template sequence designed to minimize the possibility of secondary structure (Fig. 3.3A). For these experiments, stalled +1 elongation complexes were generated prior to the stopped-flow experiment. The stopped-flow data traces show an initial lag phase that is followed by an increase in anisotropy as the polymerase reaches the end of the template and immobilizes the fluorescein label (Fig. 3.3B). The length of the lag phase is indicative of the time required for the polymerase to elongate through the twenty nucleotide portion of the template, allowing for the calculation of an elongation

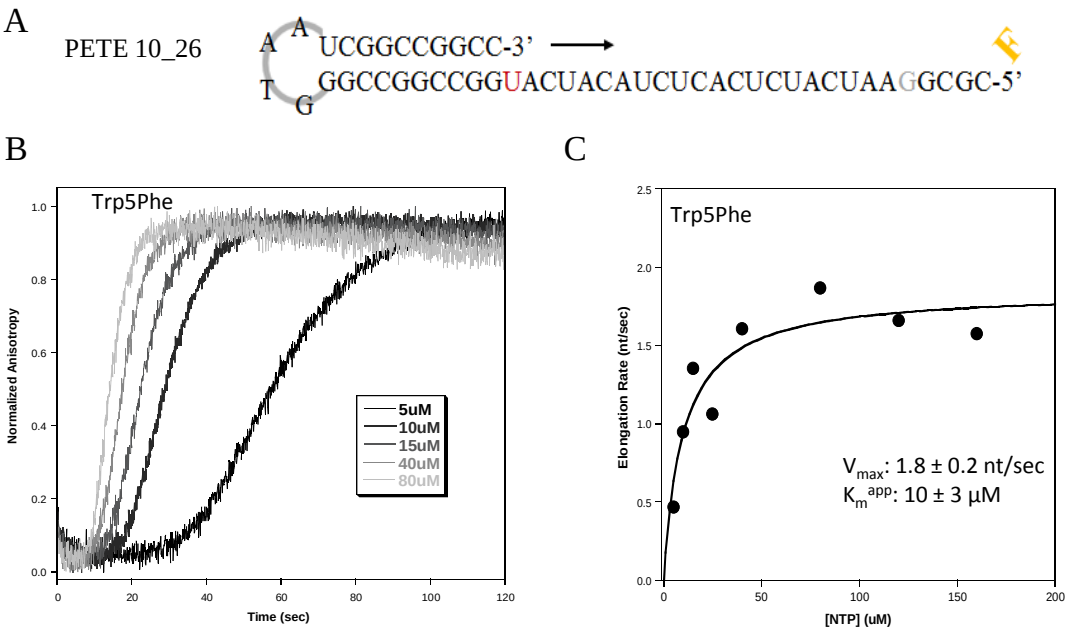

FIG. 3.3. 3D^{pol} elongation rates. (A) Schematic of 5' fluorescein (**F**) end-labeled PETE RNA used to determine elongation rate by stopped-flow fluorescence anisotropy. (B) Normalized anisotropy data showing the signal increase during elongation of 10-26 PETE RNA by Trp5Phe 3D^{pol} at various concentrations of NTPs. The lag phase represents elongation through the 20 nucleotide G-less segment of the template, which shortens with increasing NTP concentration due to faster elongation rates. The increase in anisotropy signal is associated with the addition of the terminal 5 nucleotides as the polymerase contacts the fluorescein at the 5' end of the RNA. (C) Michaelis-Menten plot showing the maximum elongation rate (V_{max}) and apparent K_m for Trp5Phe 3D^{pol}.

rate in nucleotides per second (nt/sec) (59). $3D^{pol}$ elongation rates were measured at a number of NTP concentrations and plotted as a Michaelis-Menten curve from which V_{max} and an apparent K_m values were determined (Fig. 3.3C, Table 3.2). The results indicate that all of the mutants exhibited essentially wild-type maximal elongation rates (V_{max}) and apparent K_m values of ≈2 nt/sec and 20 μM, respectively, indicating that the nature of residue 5 does not significantly affect the $3D^{pol}$ elongation rate. Note that these data were obtained at 22.5 °C and pH 6.5 to minimize thermal inactivation of the polymerase, but faster rates of ≈70 nt/sec are obtained at higher temperature and pH values (59).

While the Trp5 mutants did not affect $3D^{pol}$ elongation rate, we did observe significant differences in the amplitudes of the elongation associated fluorescence signals from the various Trp5 mutants (Fig. 3.4A). The amplitude of the elongation dependent terminal fluorescence change decreased, particularly for the Trp5Ala mutant, although the data traces retained the expected lag phase behavior and maintained sufficient signal-to-noise to determine elongation rates (Fig. 3.4B). During the experiments, we also observed that the changes in anisotropy values consistently decreased during sequential replicate stopped-flow runs from the same pre-assembled +1 elongation complex mixture, and this effect was most pronounced with mutations to the smaller valine and alanine residues. Because the baseline fluorescence anisotropy signal is representative of the amount of RNA bound to polymerase and the amplitude of the signal change is dependent on the number of RNA molecules being elongated, these findings suggested that the mutations at Trp5 decreased the amount of active $3D^{pol}$ elongation complex in the reactions.

Table 3.2. Enzymatic parameters of 3D^{pol} elongation complexes.

3D^{pol}	RNA K_d (μM)	Elongation rate V_{max} (nt/s)	NTP K_m (μM)	Elongation complex stability (min)
wild-type	8.6 ± 0.6	2.1 ± 0.1	18 ± 3	186 ± 4
Trp5Tyr	ND[a]	ND	ND	56 ± 3
Trp5Phe	9.7 ± 2.4	1.8 ± 0.2	10 ± 3	26 ± 1
Trp5Leu	ND	1.9 ± 0.2	17 ± 3	4.4 ± 0.4
Trp5Val	7.2 ± 0.5	3.0 ± 0.3	22 ± 7	5.3 ± 0.5
Trp5Ala	ND	2.0 ± 0.1	17 ± 2	5.3 ± 0.2

[a] ND, not determined

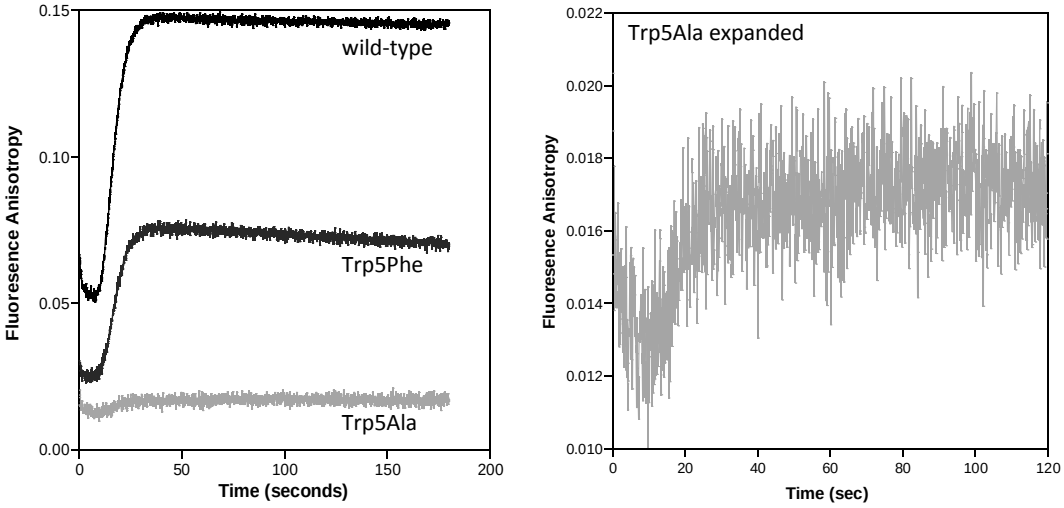

FIG. 3.4 D E. 3D^{pol} elongation stability. (A) Raw stopped-flow data showing the elongation curves of wild-type, Trp5Phe, and Trp5Ala 3D^{pol} at 40 μM NTPs. The difference in amplitude change and the decrease in starting baseline value indicates that there are fewer complexes being elongated for Trp5Phe and Trp5Ala mutants compared to the wild-type enzyme. (B) Expansion of Trp5Ala data from panel A illustrating that the signal for Trp5Ala retains the expected shape and an accurate elongation rate can be determined despite its low signal amplitude.

3.2.4 Residue 5 mutations have significant effects on elongation complex stability

To more specifically determine the effects of Trp5 mutations on elongation complex stability we designed an experiment, described in Chapter 2, Section 2.7, to first form stalled +2 elongation complexes and then measure, as a function of incubation time, how efficiently the +2 RNA could be elongated to the longer +20 product by the addition of the remaining NTPs. The 9+2-24 RNA was used to generate +2 complexes in the presence of ATP and GTP for 5-15 minutes (to reach >95% complex formation based on rates listed in Table 3.1) and the reactions were then diluted 10-fold with buffer containing either 300 mM NaCl or 75 mM NaCl. The 10+1-12 RNA was also added at this point to serve as a degradation and reinitiation control. At various time points post-dilution, small samples of the reaction were tested for their ability to rapidly incorporate additional nucleotides in 3 minutes and the products were analyzed by denaturing PAGE and quantitation of the IRdye labeled RNAs.

As shown by the gels in Fig. 3.5A, wild-type $3D^{pol}$ forms a very stable elongation complex that efficiently chases the +2 RNA into +20 product even after several hours of incubation at room temperature in 300 mM NaCl. The various Trp5 mutants, on the other hand, exhibited a rapid loss of elongation ability that ranked according to the size and hydrophobicity of the mutant residue; tyrosine and phenylalanine had the smallest effects (3 to 7-fold) while leucine, valine, and alanine reduced complex stability more than 35-fold. Quantitation of the gel bands and plotting of the data as a fraction of the +2 RNA that could be elongated, i.e. [+20 band] ÷ [sum of +2 and +20 bands], showed that the loss of competent elongation complexes exhibited single exponential decay behavior (Fig. 3.5B). Curve fitting of the data revealed that the wild-type $3D^{pol}$ elongation

A

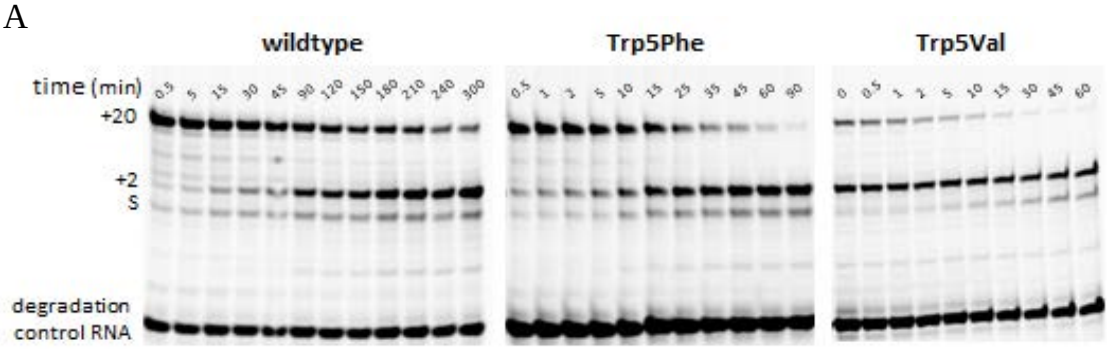

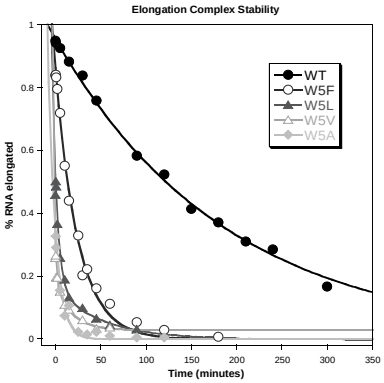

FIG. 3.5. Elongation complex stability. (A) Denaturing PAGE showing +2 ECs can be chased to +20 product after various incubation times. ECs were formed by the pre-incubation of 1 µM 9+2-24 PETE RNA, 15 µM $3D^{pol}$, and 40 µM ATP and GTP to form the +2 elongation complex from the starting RNA [S], diluted 10x in 300 mM NaCl and then chased at indicated times by addition of NTPs for 3 minutes prior to quenching the samples. The stability is determined by calculating the fraction of RNA able to chase from the +2 band to the +20 band. (B) Plot of data obtained from PAGE analysis showing single exponential loss of $3D^{pol}$ elongation complex stability.

complex has a decay constant of about three hours; this is reduced to ≈55 and ≈25 minutes for the Trp5Tyr and Trp5Phe mutants, and to as little as ≈5 minutes for the leucine, valine and alanine mutants (Table 3.2). No elongation of the control RNA 10+1-12 was observed, confirming that the +20 products arise only from the pre-formed elongation complexes.

We did see evidence of RNA release and reinitiation during the incubation period when the elongation complexes were diluted in 75 mM NaCl without heparin (Fig. 6.3A), as opposed to 75 mM NaCl with heparin or 300 mM NaCl without heparin. In this case the elongation complex decay curves showed biphasic characteristics, with a fast phase matching that seen in the presence of higher salt and a slow phase whose amplitude was dependent on the post-dilution protein concentration, as determined by changing the dilution factor between the complex formation and incubation steps from 2- to 5- to 10-fold (Figs. 3.6 B and C). We interpret this slow phase formation of the +20 product as being due to reinitiation on RNA that has been released during the extended incubation step. This suggests that the polymerase dissociates from the RNA upon inactivation, allowing the RNA to be rebound and elongated by another polymerase molecule.

To verify that the mutant polymerases remained soluble during the elongation complex stability assays, we repeated the experiments and centrifuged the sample to pellet any precipitated protein and then analyzed the supernatant by SDS-PAGE, methods described in Chapter 2, Section 2.8. These experiments were performed on Trp5Tyr and Trp5Ala mutants and no loss of soluble $3D^{pol}$ was observed for either mutant with assay done at room temperature (Fig 3.7). However, we did observe loss of soluble protein in samples that were incubated at 37 °C (≈80% in 75 mM NaCl and ≈20% in 300 mM

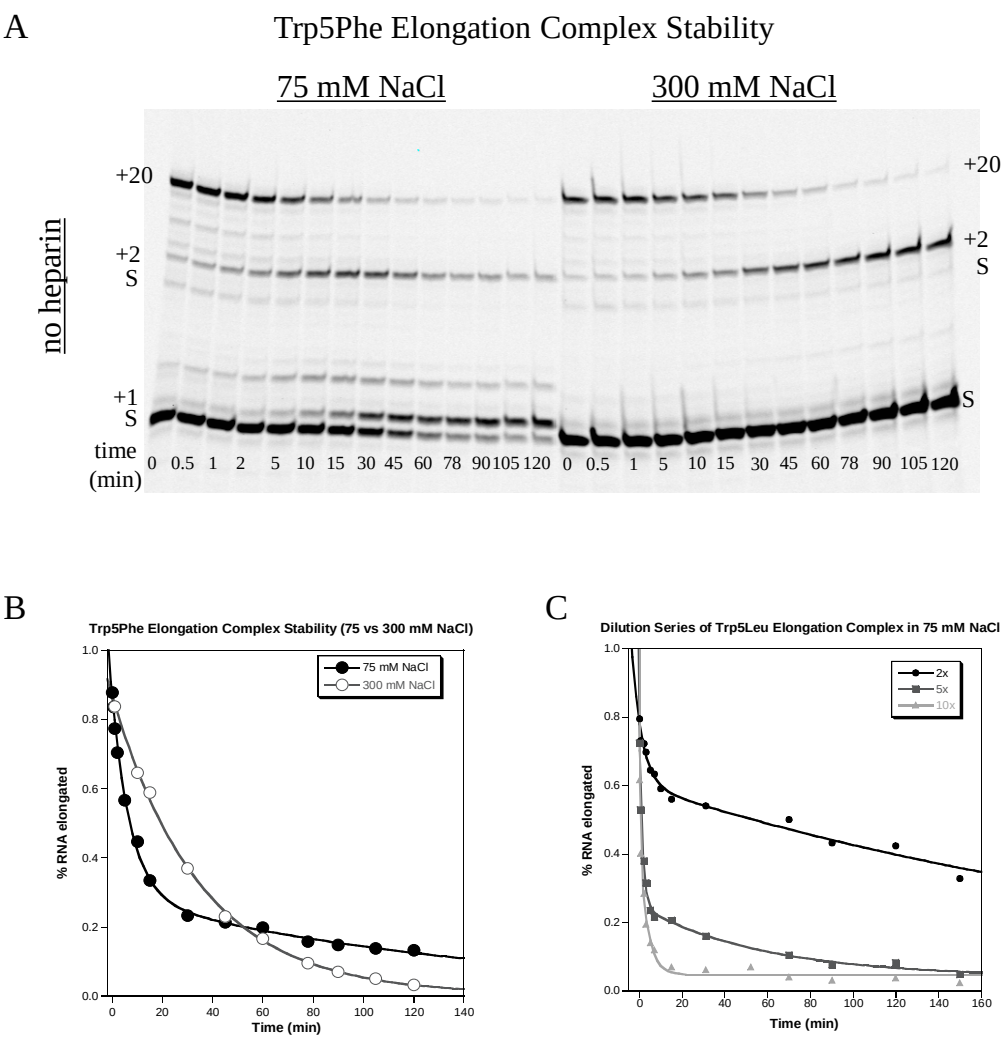

FIG. 3.6. Salt effects on elongation complex stability. (A) Denaturing PAGE showing Trp5Phe +2 ECs chased to +20 product in 75 mM (*left*) or 300 mM (*right*) NaCl after various incubation times. (B) Data comparing stability of Trp5Phe elongation complexes in 75 mM and 300 mM NaCl. The 75 mM NaCl decay curve exhibits biphasic behavior. The first phase is indicative of EC stability and the second rate is protein concentration dependent and indicative of $3D^{pol}$ rebinding and reinitiating on released RNA. (C) Plot of Trp5Leu elongation complex stability in 75 mM NaCl after 2, 5, and 10-fold dilutions of the +2 complex (resulting in 7.5, 3, and 1.5 μM final $3D^{pol}$) to show that the second rate of the biphasic curve is protein concentration dependent.

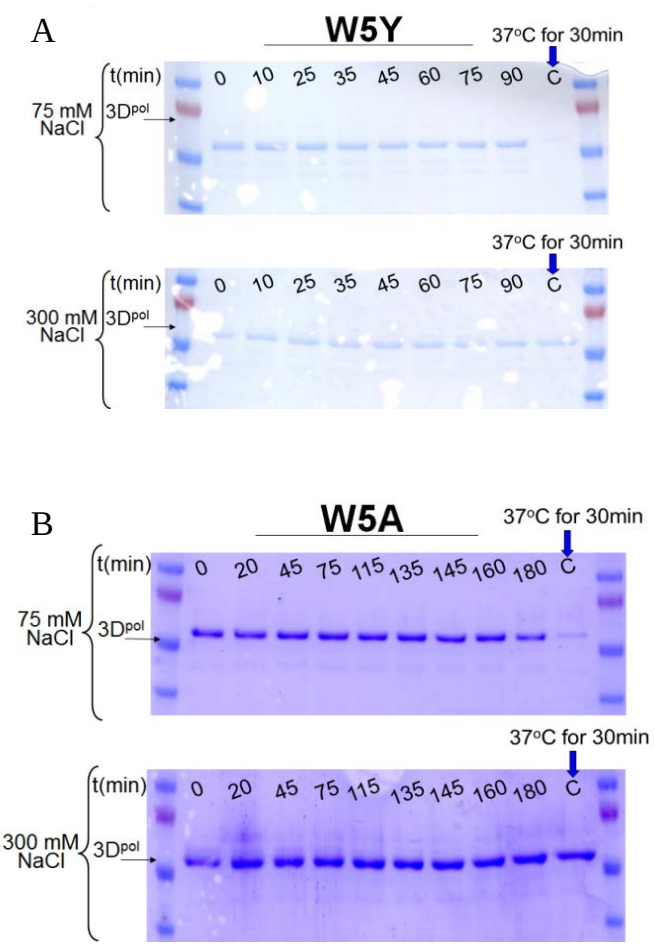

FIG 3.7. Solubility of 3D^{pol} during stability assays. Assays were performed exactly as elongation complex stability assays but instead of chasing at indicated times 14 µl samples were removed, centrifuged and supernatant was analyzed by SDS-PAGE. **(A)** W5Y and (**B**) W5A stability at 75 mM (*top*) and 300 mM (*bottom*) NaCl. All samples indicate 3D^{pol} is able to stay soluble entirety of stability assays. Lane C, is an insoluble control made by incubating 3D^{pol} at 37°C for 30 min. Control remained soluble in 300 mM NaCl.

NaCl), consistent with the ≈40 °C melting point of $3D^{pol}$ (151). These results indicate that the polymerase remains soluble throughout the stability assays done at room temperature.

3.3 Discussion

The crystal structures of the polio, coxsackie, rhino, and foot-and-mouth disease virus polymerases show a conserved structural motif whereby the very N-terminus of the protein is buried in a pocket at the base of the fingers domain. This conformation is essential for polymerase activity and can only be formed after the proteolytic processing of $3CD^{pro}$ to generate the native $3D^{pol}$ N-terminus. When solving the structure of coxsackievirus B3 polymerase, we also noticed the structural conservation of a distortion in the β-strand composed of residues 1-9 that resulted in the usually hydrophobic residue 5 being exposed on the surface of the protein (Fig. 3.1A) (32). Through mutational analysis we found that residue 5 was indeed important for coxsackievirus $3D^{pol}$ function; mutations of the native phenylalanine to smaller residues greatly decreased polymerase activity while mutation to a larger tryptophan increased polymerase activity as determined by product formation in a poly-A template activity assay. The $3D^{pol}$ structures lead us to propose that residue 5 could flip into an adjacent hydrophobic pocket during the catalytic cycle, providing a driving force for NTP positioning prior to catalysis.

In this work we further elucidate the function of residue 5 and the role it plays in the molecular mechanisms of $3D^{pol}$ initiation and elongation. Formation of an active $3D^{pol}$ elongation complex is a multi-step process that has been well characterized for poliovirus (9) and foot-and-mouth disease virus (6) polymerases. Overall, the process consists of *a*) RNA binding followed by an initial conformational change to generate a catalytically competent complex, *b*) a second conformational change associated with

incorporation of the first NTP to generate the elongation complex, and *c*) processive replication of the entire viral genome. Mutations at residue 5 could affect $3D^{pol}$ activity by altering the initiation steps, by altering the elongation rate of the enzyme, or by altering the stability of the elongation complex.

To determine if residue 5 was involved in initial RNA binding we utilized a solution based fluorescence polarization assay to measure the affinity of a short hairpin RNA in 75 mM NaCl (99). The data collected from mutations that introduce either a planar phenylalanine or a smaller branched valine showed no significant effects on RNA affinity as compared to the wild-type enzyme, indicating that $3D^{pol}$ residue 5 is not involved in RNA binding in the absence of nucleotides. To assess initiation and elongation complex formation we used two different length hairpin RNA substrates in the same reaction to simultaneously measure +1 product formation due to guanosine addition and +2 product formation due to adenosine and then guanosine addition. The RNAs were designed such that the resulting +1 and +2 complexes had exactly the same RNA sequence in the vicinity of the active site and differed only in the length of the remaining single stranded template sequence (Fig. 3.1B). The results show that all the Trp5 mutations slowed the rate of elongation complex formation, with smaller residues having slower complex formation rates (Fig. 3.2), but the effect of the mutations on the formation rate were at most only ≈3-fold (Table 3.1). While statistically significant, these changes in rate are not sufficient to be the sole contributor to the changes in activity we previously observed for the analogous mutations in coxsackievirus $3D^{pol}$ (32).

Using our PETE assay in a stopped-flow kinetic format (59), we also established that the mutations at Trp5 do not affect $3D^{pol}$ elongation rates, with all the mutations

having V_{max} and apparent NTP K_m values comparable to that of the wild-type enzyme (Fig. 3.3 & Table 3.2). We saw evidence during these elongation experiments that suggested residue 5 was involved in maintaining a stable elongation complex (Fig. 3.4). To show that residue 5 mutations have significant effects on the temporal stability of the competent $3D^{pol}$ elongation complex we designed an assay where the initial elongation complex is stalled after formation of the +2 product by omitting the next nucleotide triphosphate, and the ability of these stalled complexes to rapidly elongate the RNA by another 18 nucleotides was tested as a function of incubation time (Fig. 3.5).

Wild-type $3D^{pol}$ elongation complexes are quite stable and exhibit mono-exponential decay with a time constant of about three hours. The Trp5 mutations, on the other hand, show very rapid loss of elongation ability, with decay time constants of ≈55 and ≈25 minutes for tyrosine and phenylalanine mutants respectively, and only 5-15 minutes for the smaller leucine, valine, and alanine mutants (Table 3.2). All the proteins show mono-exponential loss of elongation ability in 300 mM NaCl or in 75 mM NaCl in the presence of heparin. However, in 75 mM NaCl without heparin we observe a biphasic decay curve whose second phase is dependent on protein concentration (Fig. 3.6C). This latter observation indicates that the loss of elongation complex competency is associated with a release of the RNA from the polymerase, allowing it to be rebound by another $3D^{pol}$ molecule for reinitiation in a secondary reaction whose rate is $3D^{pol}$ concentration dependent. Furthermore, the elongation complexes are slightly more stable in 300 mM than in 75 mM NaCl (Fig 3.6B); suggesting that maintaining the proper conformation of the complex may involve hydrophobic interactions that would be favored at the higher salt concentrations.

While our results show that residue 5 is important for the stability of the elongation complex, the molecular and structural details underlying this stabilization are not yet known. It may be that residue 5 interacts directly with the RNA template via base stacking interactions that are likely to be disrupted by mutations to small and non-planar amino acids, as shown by our data. While this could be the case for poliovirus and coxsackievirus polymerases that have tryptophan and phenylalanine residues at position 5, it is less likely for the structurally homologous rhinovirus enzyme having a small hydrophobic residue and foot-and-mount disease virus $3D^{pol}$ where residue 5 is an aspartic acid. Alternatively, residue 5 may play a role in maintaining $3D^{pol}$ in the proper conformation for processive elongation. For example, residue 5 could move into the hydrophobic pocket of the fingers domain as we suggested when describing the coxsackievirus $3D^{pol}$ structure (32); however, based on the new data resulting from this work we now expect this structural rearrangement to occur only once during elongation complex formation, fixing the hydrophobic residue within the nearby pocket rather than reiteratively flipping in and out of the pocket with each cycle of nucleotide addition. Notably, structures of $3D^{pol}$–RNA complexes from the homologous foot-and-mouth disease virus and Norwalk virus polymerases (53, 54, 163), as well as the PV $3D^{pol}$ elongation complex (60), indicate that residue 5 remains solvent exposed, suggesting that a structural rearrangement involving residue 5 may not occur. However, the RNA templates in the foot-and-mouth disease and Norwalk virus structures are not long enough to reveal whether or not the template strand interacts directly with the polymerase in the vicinity of residue 5 and the PV $3D^{pol}$-RNA elongation complex template is hindered by the crystal packing lattice (60). Thus, amino acid residue 5 could still

participate in structural rearrangements, interactions with template RNA or has some other function that we have yet to consider.

In conclusion, we have used poliovirus polymerase to further dissect the importance of residue 5 for $3D^{pol}$ function by generating a series of point mutations and measuring their effects on RNA binding, elongation complex formation, elongation rate, and the temporal stability of the elongation complex. The data show that while residue 5 plays a small role in elongation complex formation, the mutations have no effect on the elongation rate of the enzyme, and instead have significant effects on the stability of the elongation complex. These results indicate that the size and hydrophobicity of residue 5 are important for maintaining the $3D^{pol}$ elongation complex in a competent state.

Chapter 4

The Impact of Elongation Complex (In)Stability on Genome Replication

4.1 Introduction

*This chapter has been published as part of: Hobdey, S.E., Kempf, B.J., Steil, B.P., Barton, D.J., and Peersen, O.B. (2010) J Virol **84**,8072-8084.*

Authors contributing to this chapter: Hobdey, Figs 4.1 to 4.7 with Fig. 4.7 under the supervision of author Steil; Kempf, Figs 4.8 and 4.9 and Table 4.1. Authors Steil and Kempf were members of the Barton laboratory at the University of Colorado Health Sciences Center in Aurora, CO.

In Chapter 3 we discussed the effects PV $3D^{pol}$ residue 5 on the *in vitro* stability of stalled elongation complexes (ECs). In this chapter I will discuss the significance of EC stability on viral genome replication. Cell-free replication was completed by me under the instruction of Ben Steil in David Barton's laboratory at the University of Colorado's Health Sciences Center in Aurora, CO. For the infectious virus experiments I generated the $3D^{pol}$ cDNA mutations and sent plasmids to Brian Kempf of the Barton lab who carried out the infectious virus studies.

The formation of the picornavirus EC, $3D^{pol}$-RNA-NMP, is a rate limiting step in RNA replication that is required for the initiation of RNA replication initiation (7, 9, 11). This complex with the poliovirus (PV) wild-type $3D^{pol}$ has been shown to be very stable (9). As shown in Chapter 3, mutations to residue 5 of the PV $3D^{pol}$ have significant effects on EC stability; however, the significance of EC stability in viral replication was

not discussed. We hypothesized that an unstable EC would have significant effects on elongation with longer RNA templates; specifically, that the polymerase may fall off the RNA template during replication thus reducing polymerase processivity.

Polymerase processivity is defined as the average number of nucleotides incorporated into a primer before dissociation from the template. Processivity has been studied extensively for both RNA and DNA polymerases (76, 147). Highly processive DNA polymerases commonly require accessory proteins for processive DNA replication. For example, DNA polymerase III requires a sliding clamp that binds to the DNA polymerase and forms a ring-shaped structure around the DNA template to prevent polymerase dissociation (144, 145). The T7 bacteriophage DNA polymerase is controlled by an entirely different mechanism where the T7 polymerase has relatively low processivity alone, but it recruits the host protein thioredoxin to increase processivity about 80-fold by increasing the half-life of the DNA-polymerase complex from 1 second to 5 minutes (75, 76, 97, 146). Thioredoxin is an enzyme responsible for multiple redox reactions, including reduction of the ribonucleotide reductase, the enzyme required for the formation of DNA from RNA precursors (74). Thioredoxin has no DNA binding properties except when in complex with the T7 DNA polymerase (8). RNA polymerases, e.g. T7 RNA polymerase, have been found to be extremely processive as monomer (102) and affects to processivity have been found via point mutations within the polymerase protein itself (91). Interestingly, in all cases any change to polymerase processivity has been directly related to increasing or decreasing the polymerase-RNA dissociation constant (K_d) or RNA replication rate (74, 91, 145). Recently, a clamp-like structure has been found for the PV $3D^{pol}$ where the pinky and thumb of $3D^{pol}$ insert into the major and

minor groove, respectively, of the upstream dsRNA (60). However, it is not known if this clamp is required for processivity or affects the K_d of the polymerase-RNA complex.

Previous reports have shown that the PV $3D^{pol}$ is a highly processive polymerase with ~1 initiation event per genome replication (134); however, these experiments were completed on ~1.5 kb templates and only elongation products < 800 nucleotides were resolved, thus abortive products longer than 800 nucleotides would not have been observed (134). In this same report the authors did show that the K_d for the $3D^{pol}$-RNA complex and processivity of $3D^{pol}$ can be modulated independently, whereby the presence of PV protein 3AB decreased the $3D^{pol}$-RNA K_d but had no effect on $3D^{pol}$ processivity.

Here we used PV sub-genomic RNA (Fig. 4.1A) to show that residue 5 of the PV $3D^{pol}$ has significant effects on polymerase processivity. These mutations have negligible effects on K_d but have significant effects on EC stability (Table 3.2, Chapter 3). Also, we show that processivity plays a signification role in RNA replication in the context of viral replication centers via cell-free coupled translation-replication reactions; and furthermore affect virus propagation at the cellular level. Furthermore, we found that the 5'NTR, an element with extensive RNA structure (Fig 4.1D), has significant effects on $3D^{pol}$ processivity, especially for the residue 5 mutants.

4.2 Results

4.2.1 PV $3D^{pol}$ Residue 5 mutants affect replication processivity

Elongation processivity was determined by monitoring the amount of abortive products generated during replication of longer genomic RNAs by $3D^{pol}$. Poliovirus RNA templates were generated by T7 transcription from linearized pRNA2, resulting in 2201

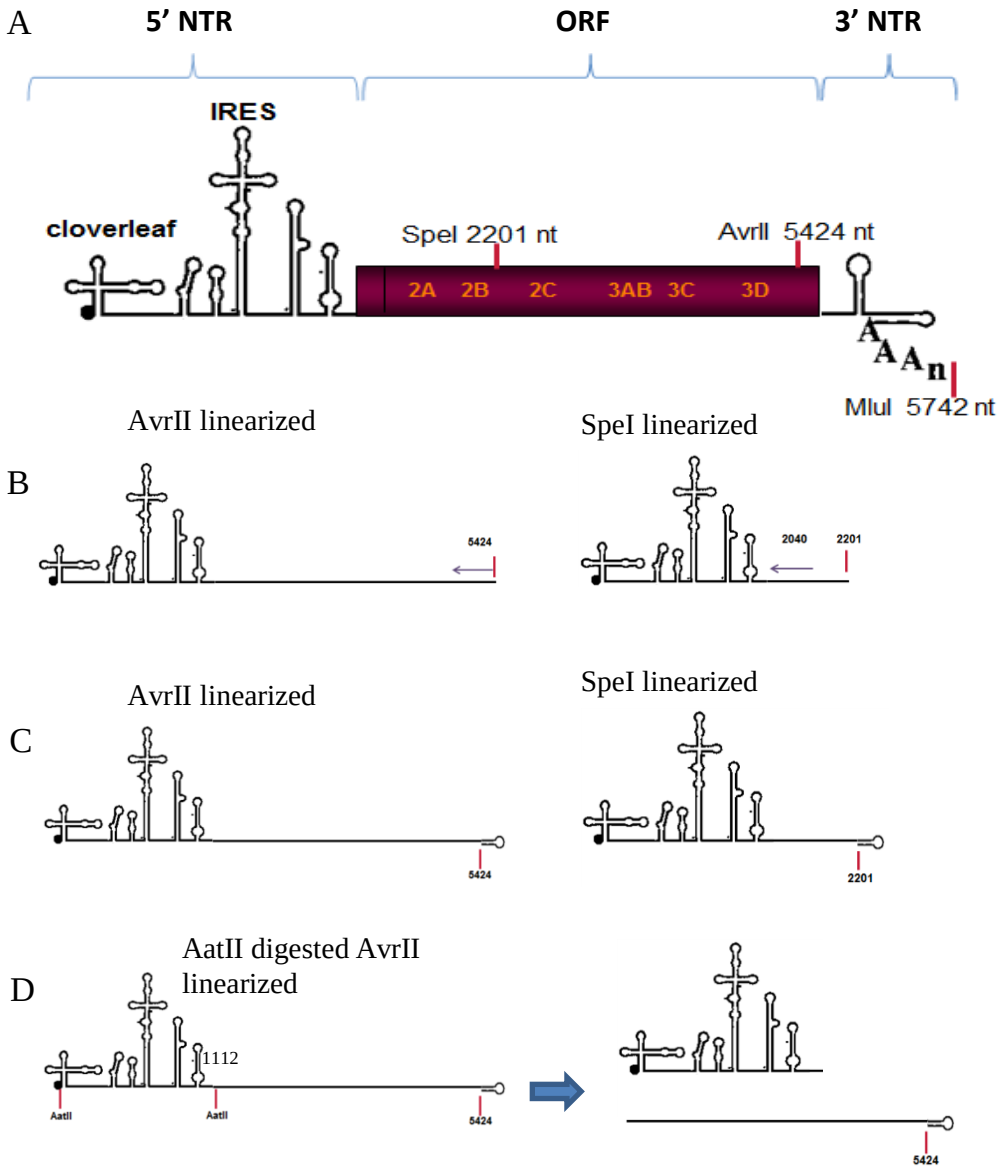

FIG. 4.1. Poliovirus RNA genome used for processivity experiments.
(A) Genomic RNA 5' UTR (non-translated region) with cloverleaf and IRES (internal ribosome entry site) RNA secondary structures. Followed by the ORF, missing the capsid domain, and 3' NTR. Bars indicated cut sites by restriction enzymes: SpeI, 2201 nt; AvrII, 5424 nt; MluI, 5742 nt. (B) RNA template used in primer extension assays. DNA primers are purple arrows. (C) Self-priming RNA. Hairpin forms at the 3' end. (D) Schematic of 5'NTR removal.

or 5424 nucleotide long RNA templates (Fig 4.1). These pRNA2 templated T7 transcription reactions also produced an additional 670 nucleotide fragment that corresponds to most of the poliovirus 5' NTR, including the IRES. This smaller fragment is due to the presence of a T7 polymerase abortive sequence, 5'-UAUCUGUU-3' (96), found shortly after the IRES element in the pRNA2 cDNA. This fragment is present in all the $3D^{pol}$ elongation reactions and provides additional elongation data from a shorter RNA template that is rich in structure.

Primer extension - My first attempt to characterize elongation processivity employed a primer extension assay by annealing an IRdye labeled DNA primer to a sub-genomic length RNA template replication, described in Chapter 2, Section 2.9.1. Primers were designed to anneal to the first $CUCU_n$ sequence after the linearization so that a locked elongation complex could be generated then chased. This required that the SpeI primer be 161 nts upstream of the SpeI linearization site while the AvrII primer annealed right at the linearization site (Fig. 4.1B). Experiments for agarose gel analysis were performed by annealing DNA primer to RNA template (see Materials and Methods in Chapter 2, section 2.7.1) then incubating 0.4 µM RNA/primer substrate, 10 µM $3D^{pol}$ an 40 µM each NTP in our standard 75 mM NaCl buffer. Pre-incubation for elongation complex formation step was omitted in this particular experiment. Experiments for PAGE analysis were performed by annealing the DNA primer to the RNA template then incubating 0.25 µM RNA/primer substrate with 20 µM $3D^{pol}$ and 500 µM each CTP and UTP for elongation complex formation, in 75 mM NaCl, 2.5 mM $MgCl_2$ and 50 mM HEPES pH 6.5. After 40 minutes of room temperature incubation, the reaction was diluted 5-fold into a high salt buffer containing all NTPs to a final concentration of 120

μM. The extended DNA primer was run on a non-denaturing agarose gel or denaturing PAGE to determine the elongation efficiency (Fig. 4.2). These experiments showed that the annealing (AvrII) or elongation (SpeI and AvrII) efficiency of the DNA primer to the RNA was low (Fig. 4.2A). Interestingly, the agarose gel shows that the presence of non-elongated, unannealed primer increased after elongation of the 2201 nt template, suggesting that the primer is being displaced during elongation. This effect was not so significant for the AvrII primer/template pair which annealed at the very 3' end of the template. The PAGE analysis of elongation of the AvrII template shows expected elongation at early time points with primer laddering indicating single nucleotide incorporations and later time points show accumulation of larger products near the well (Fig. 4.2B). Attempts to repeat this experiment were unsuccessful. Figure 4.3 shows the IR and UV image of an elongation experiment of SpeI primer/RNA. The experiment was performed as described above and images show the differences between the IR-dye labeled primer and the total RNA population. The annealed primer is displaced from the RNA template as during elongation and very little primer extension can be seen. The UV image indicates that more RNA is being elongated than is seen in the IR image and shows that the IRES element (the 5' 660 nts) is able to self-prime and be elongated.

Self-priming extension - To initiate RNA elongation we utilized the fact that the 3' ends of single stranded RNA transcripts often form localized snap-back structures that create self-priming hairpins for RNA elongation by $3D^{pol}$ (35). Experiments were performed by pre-incubating 0.4 μM RNA, 20 μM polymerase and 500 μM each of all four NTPs for 7-15 minutes at room temperature to form elongation complexes, mimicking the locked complex formation step used in the polymerase rate and stability

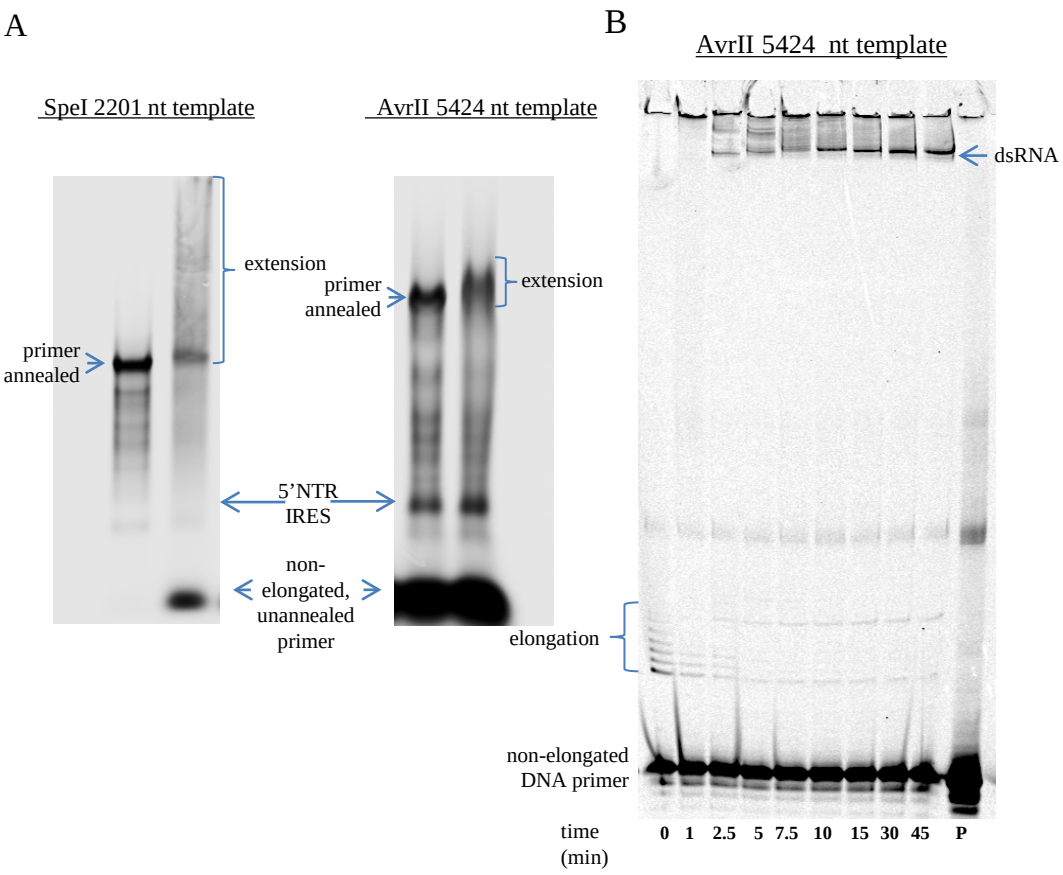

FIG. 4.2. DNA primer extension assay. (A) Infrared image of agarose gel showing annealing and elongation efficiency of SpeI primer on the 2201 nt template *(left)* and AvrII primer on 5424 nt template *(right)*. Primers were annealed by heating 75 µM RNA template and primer in 16 mM NaCl 1.6 mM $MgCl_2$ at pH 7.5 to 90°C and slow cooling, 1 degree every 3 minutes to 30°C. Annealed RNA primers were extended by the incubation 0.25 µM template RNA, 100 µM each NTP and 4.0 µM $3D^{pol}$ in 75 mM NaCl and 2.5 mM $MgCl_2$. Elongation reactions were incubated for 20 min at room temperature. (B) Denaturing PAGE showing a time-course of AvrII primer extension. Lane P indicates control with no RNA template.

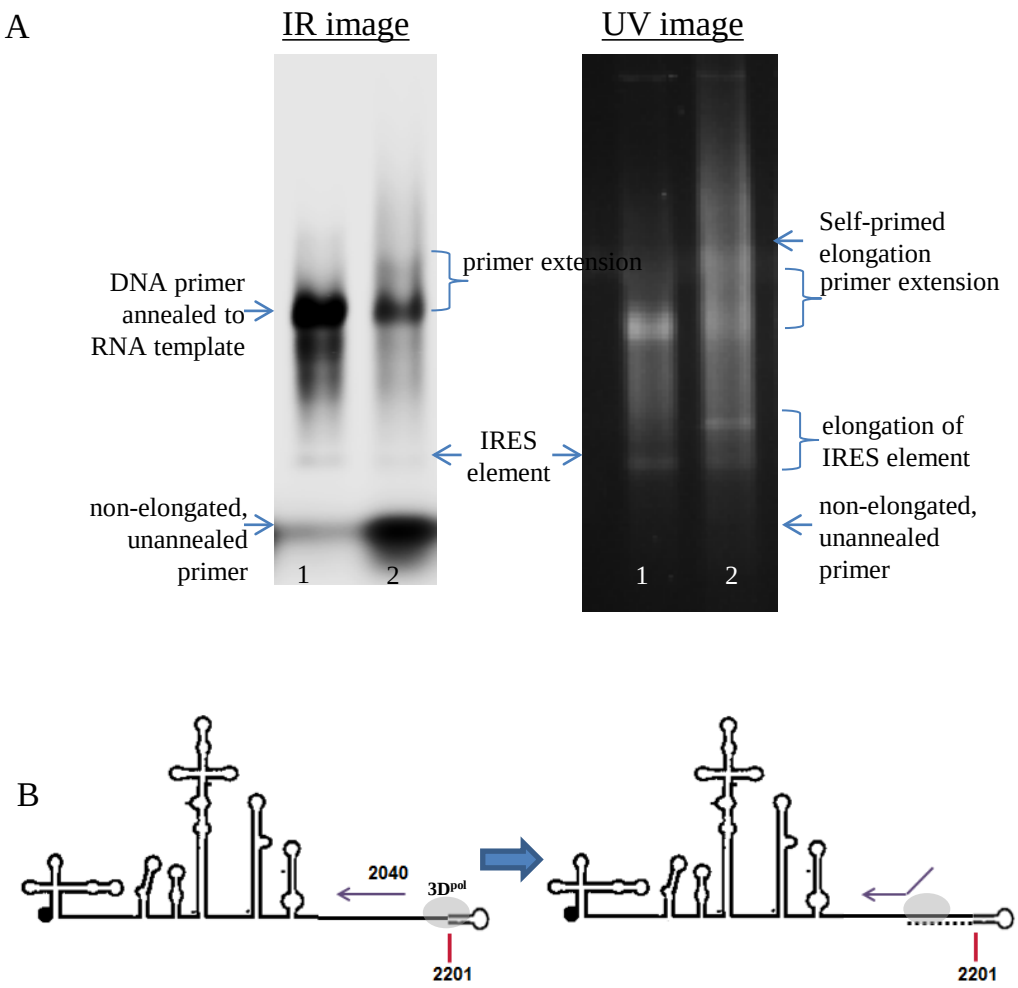

FIG. 4.3. Discovery of RNA self-priming. (A) Infrared image of agarose gel showing annealing and elongation of SpeI primer on the 2201 nt template *(left)* and UV image of EtBr stain of same gel *(right)*. Lanes 1 and 2 represent + or – $3D^{pol}$ respectively. IR-image shows only primer populations where increase in non-elongated, unannealed primer in lane 2 indicates the annealed primer (lane 1) is being displaced by the polymerase during elongation. The IRES element from the IR-image is likely due to non-specific interactions or primer trapping. The UV-image shows total RNA population including a larger RNA population that has not been extended from the primer (self-priming elongation). Also, elongation of the IRES element shows capability of self-priming. (B) Schematic of primer displacement by elongation (*right*) from 3' hairpin. DNA primer represented by purple arrows. Number represents nucleotide position.

assays. After this pre-incubation step, the complexes were diluted into high salt to prevent polymerase rebinding and additional initiation events during the elongation phase of the experiment, methods described in Chapter 2, Section 2.9.2. At indicated time points, reaction samples were quenched, phenol-chloroform extracted, and RNA content was analyzed by nondenaturing agarose gels stained with ethidium bromide.

Elongation of the 2201 (Fig. 4.4, *top*) and 5424 (Fig. 4.4, *bottom*) nucleotide long templates showed that the amount of full-length duplex RNA synthesized by $3D^{pol}$ was slightly reduced for the tyrosine and phenylalanine mutants as compared to the wild-type, and significantly reduced with the leucine, valine and alanine mutants. The elongation rate of wild-type and mutant polymerases was calculated to be ~0.4 nt/sec based on the ≈90 minutes needed to elongate the 2201 nt template. This is ≈5-fold slower than the rates observed in the PETE assay (Table 3.2, Chapter 3) and could be due to an increase in the NTP K_m^{app} due to the increased salt concentration during the elongation phase. In addition to a clear band that reflects full-length duplex RNA, the reactions with wild-type $3D^{pol}$ also show the time-dependent accumulation of very large and heterogeneous RNA products just below the sample wells. The amount of these large RNA products is reduced when Trp5 is mutated to phenylalanine or tyrosine and largely eliminated with the smaller leucine, valine, and alanine mutants (Fig. 4.5).

Elongation from self-primed templates also resulted in intermediate length RNA bands. Some of these RNAs continue to be elongated, suggesting there may be sites where the polymerase pauses, while other bands are no longer being elongated, indicating they are abortive products. Figure 4.5 shows a side-by-side comparison of products formed by wild-type and residue 5 mutant polymerases after 120 minutes of elongation

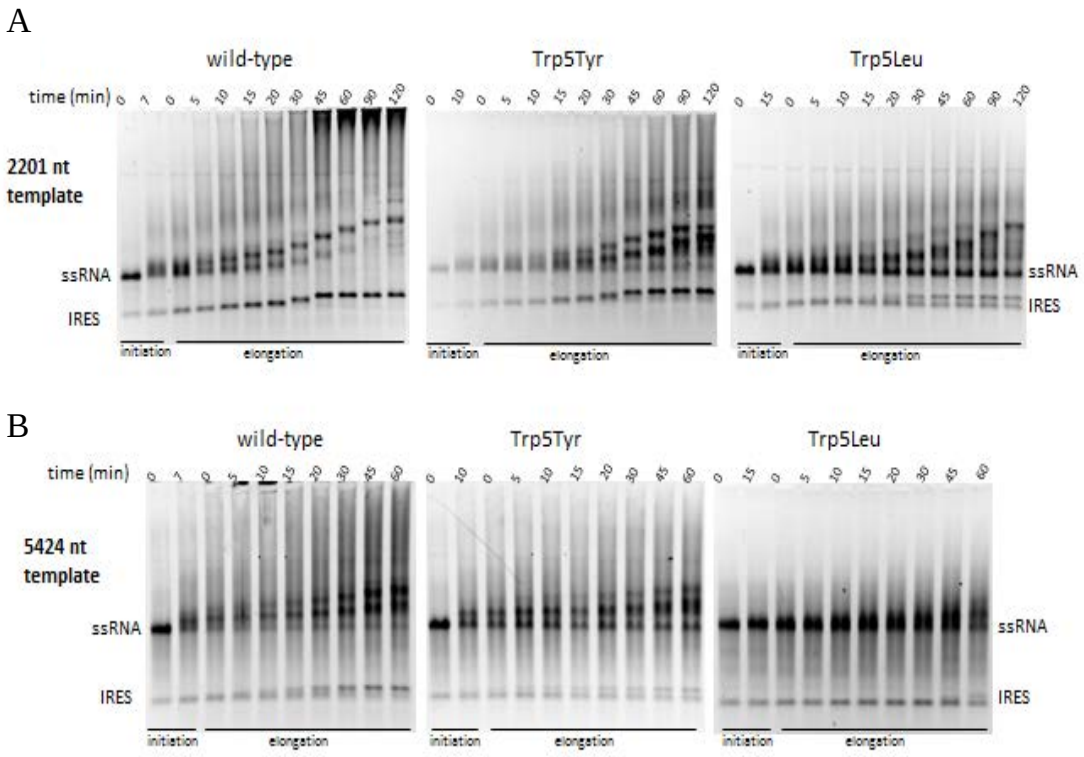

FIG. 4.4. Elongation processivity of self-primed poliovirus RNA. Ethidium bromide stained nondenaturing agarose gel electrophoresis showing a time course analysis of RNA elongation through (A) 2201 nt template and (B) 5424 nt template. RNA transcripts were pre-incubated with 20 µM $3D^{pol}$, 0.4 µM RNA and 0.5 mM NTPs in 75 mM NaCl for 7, 10 or 15 minutes to allow for initiation and the reactions were then diluted 5-fold into 300 mM NaCl and 260 µM NTPs. Reactions were quenched at indicated times. The IRES (internal ribosome entry site) band is from a T7 abortive sequence located just after the IRES in the poliovirus genome.

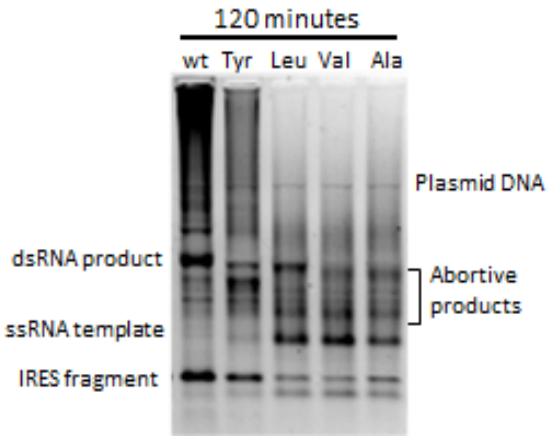

FIG. 4.5. Comparison of processivity from residue 5 mutants. Ethidium bromide stain of nondenaturing agarose gel electrophoresis directly comparing elongation of the 2201 nt RNA template by the different mutant polymerases after 120 minute reaction time.

on the 2201 nt template. The data show that wild-type $3D^{pol}$ produces few abortive products, the tyrosine mutant produced slightly more abortive products, and the leucine, valine and alanine mutants result in significantly more abortive products. For these smaller mutations, the abortive products represent a significant fraction of the final material when one considers that template utilization is also reduced by less efficient initiation.

The 670-nucleotide band resulting from the T7 abortive sequence in the 5'NTR is composed almost entirely of the internal ribosome entry site (IRES). This transcript can also self-prime and be elongated by the polymerase, albeit with reduced efficiency for the residue 5 mutants compared to wild-type. Interestingly, the alanine, valine and most of the leucine mutant never reach the 5' end of this short template. Although gels in Figure 4.4 and 4.5 do not have the resolution to show abortive products for the IRES band, it is apparent by the amount of elongation product that the mutant polymerases were extremely inhibited in replication of the IRES, and more so than for the full-length RNA elongation. These data suggest that replication through extensive RNA structure is more difficult for residue 5 mutants than for wild-type $3D^{pol}$, significantly slowing the polymerase and giving the unstable mutant polymerases time to dissociate from the template RNA. Consistent with this, the longer sub-genomic products generated by the mutants appear slightly shorter than those from the wild-type enzyme (Fig. 4.5), suggesting the mutants may not have replicated through the IRES that would be at the end of the negative-strand template.

When the 5' NTR, including the IRES element, was removed from the 5242 nt RNA template the processivity increased for all polymerases, but the efficiency of RNA

elongation was still lower for the mutants (Fig.4.6), indicating that downstream RNA structure may be having distant affects polymerase elongation. For wild-type and the Trp5Tyr mutant polymerase, two RNA populations can be seen with a lighter RNA band that runs about 1 kb above a more definite RNA product. The stronger band was the RNA product that was seen for all polymerase elongation reactions. Also, after removal of the 5'NTR there are less large RNA products that remained in the well when compared to replication of RNA with the 5' NTR (compare wells from Fig. 4.5 to Fig.4.6). The time course shows that there was no effect on elongation rate in the absence of the 5' NTR, where the 4339 nt template was replicated in ~180 minutes, or ~0.4 nt/sec.

4.2.2 Processivity effects caused by residue 5 mutations result in decreased RNA synthesis in a cell-free replication system

To ascertain the effects on the Trp5 mutations on viral genome synthesis we carried out cell-free coupled translation-replication reactions, described in Chapter 2, Section 2.10. Negative-strand RNA synthesis from sub-genomic poliovirus replicons harboring wild-type and Trp5Phe $3D^{pol}$ showed replication to the full-length negative-strand within 60 minutes, but the phenylalanine mutant had significantly lower yield than wild-type (Fig. 4.7A). Negative-strand RNA synthesis by the Trp5Ala mutant replicon was too faint to be detected after 60 minutes of replication, but a small amount of full-length negative-strand RNA product could be detected after 120 minutes of replication. In a time course experiment with wild-type and Trp5Phe $3D^{pol}$ we see that the two polymerases replicated poliovirus RNA at similar rates as both reached their maximal yield of negative-strand RNA after ≈45 minutes of incubation, but the Trp5Phe mutant yielded much less negative-strand RNA product (Fig. 4.7B). The reduced synthesis of

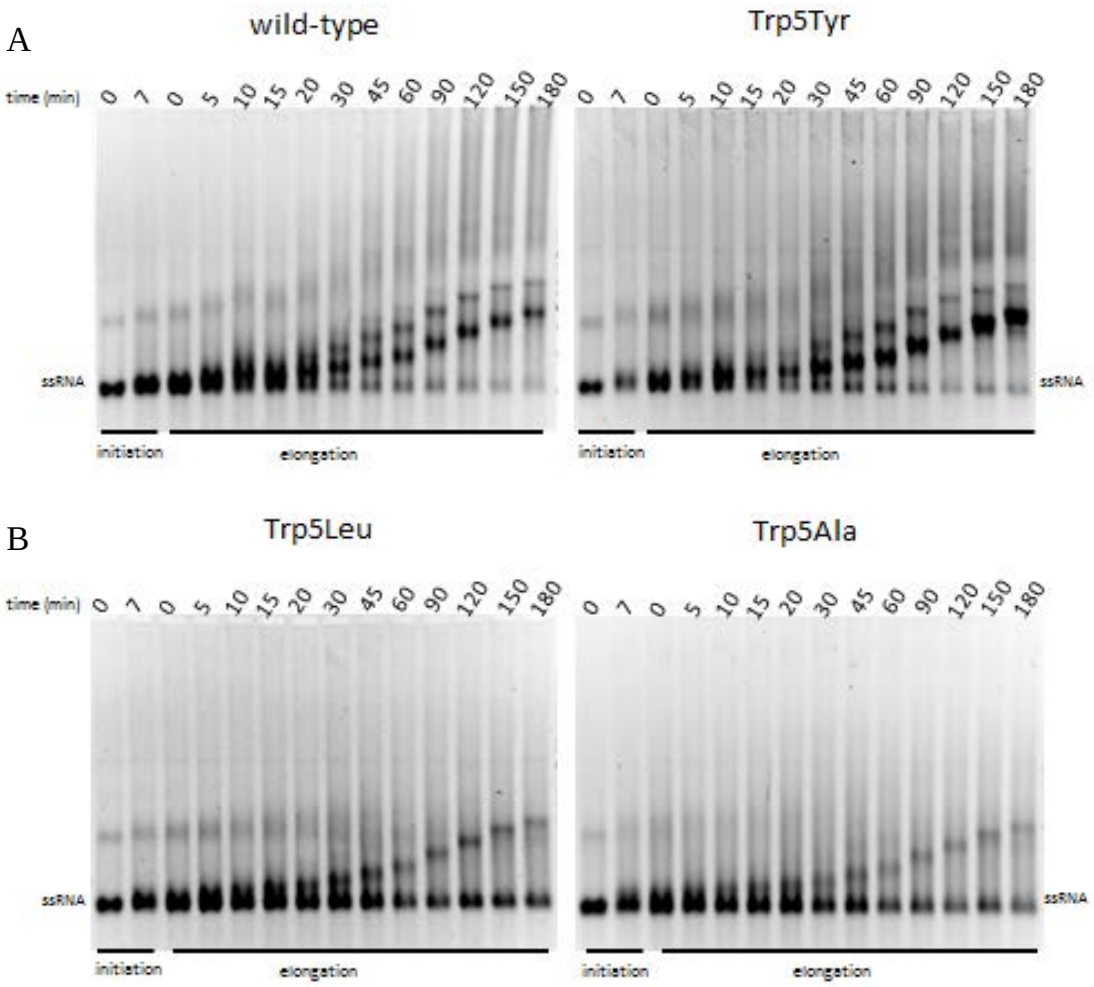

FIG. 4.6. Elongation processivity minus the 5' NTR. Ethidium bromide stained nondenaturing agarose gel electrophoresis showing a time course analysis of RNA elongation through a 4339 nt template with wild-type, Trp5Tyr (A) Trp5Leu and Trp5Ala (B). RNA transcripts were pre-incubated with 20 µM $3D^{pol}$, 0.4 µM RNA and 0.5 mM NTPs in 75 mM NaCl for 7, 10 or 15 minutes to allow for initiation and the reactions were then diluted 5-fold into 300 mM NaCl and 260 µM NTPs. Reactions were quenched at indicated times.

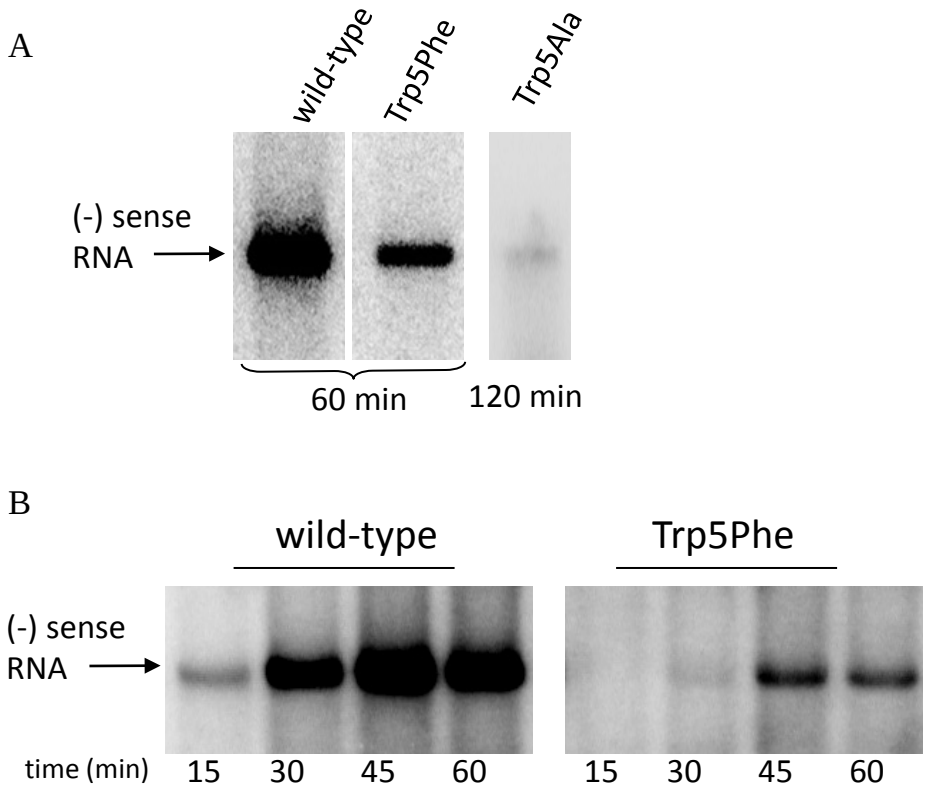

FIG. 4.7. Negative-strand RNA synthesis in a cell-free translation-replication system. (A) Endpoint analysis showing amounts of full-length negative-strand RNA produced by replicons containing wild-type, Trp5Phe (50% of wild-type) in 60 minutes. Product from the Trp5Ala (10% of wild-type) mutant was barely detectable after 120 minutes of replication. (B) Time course of product formation showing that both wild-type and Trp5Phe $3D^{pol}$ reach maximum RNA quantities after ≈45 minutes of replication, indicating that the polymerase mutations affect the yield of negative-strand RNA, but not the elongation rate, in the replication complex.

negative-strand RNA by Trp5Phe and Trp5Ala mutants is likely due to instability of the elongation complexes as a result of the residue 5 mutations. Importantly, these results indicate that in authentic RNA replication complexes the mutations to residue 5 do not affect the elongation rate itself, but rather the amount of full-length viral RNA produced.

4.2.3 A processive polymerase is required for viral propagation

To test the ability of the polymerase mutants to support virus growth we transfected HeLa cells with positive-strand genomic RNA containing the Trp5Phe and Trp5Leu mutations, described in Chapter 2, Section 2.11. Both mutants produced infectious virus (Table 4.1) and at 48 hours post transfection (hpt) the Trp5Phe mutant had only slightly lower viral titer than wild-type ($6.4x10^6$ vs. $2.5x10^7$ PFU/ml) while the Trp5Leu viral titer was significantly lower at $1.7x10^4$ PFU/ml. After 72 hours the titers of wild-type and Trp5Phe viruses were essentially equivalent at ~$5.0x10^7$ PFU/ml, although the phenylalanine mutant produced slightly smaller plaques (Fig. 4.8A). Sequencing confirmed that the Trp5Phe mutation was stable in the progeny virus population. Growth of the slow Trp5Leu virus, on the other hand, improved dramatically between 48 and 72 hours, producing plaques similar to the wild-type virus that suggested a reversion or acquisition of some compensatory mutation. This was confirmed by sequence analysis of the $3D^{pol}$ gene from progeny virus showing a mixed population of Leu5 and Trp5 residues at 48 hpt and complete reversion of the virus population to wild-type tryptophan at 72 hpt (Fig. 4.8B).

One-step growth curves of wild-type and the Trp5Phe $3D^{pol}$ mutant were performed by infection of HeLa cells (~10^6 cells per 35 mm well) with a multiplicity of infection (MOI) of 10 viruses per cell, described in Chapter 2, Section 2.12. 1 hour after

Table 4.1. Viability of poliovirus engineered to express $3D^{pol}$ residue 5

	48 hours post-transfection		72 hours post-transfection	
Virus	**Titer (PFU per ml)**	**Sequence**	**Titer (PFU per ml)**	**Sequence**
PV $A_{(80)}3D^{Pol}$ W5	$2.5x10^7$	Tryptophan	$5.0x10^7$	Tryptophan
PV $A_{(80)}3D^{Pol}$ W5F	$6.4x10^6$	Phenylalanine	$5.1x10^7$	Phenylalanine
PV $A_{(80)}3D^{Pol}$ W5L	$1.7x10^4$	Mixed*	$1.3x10^6$	Tryptophan

* Individual cDNA clones were sequenced. 13 out of 22 (59.1%) cDNA clones had a leucine (CUA) codon and 9 out of 22 (40.9%) cDNA clones had a tryptophan (UGG) codon.

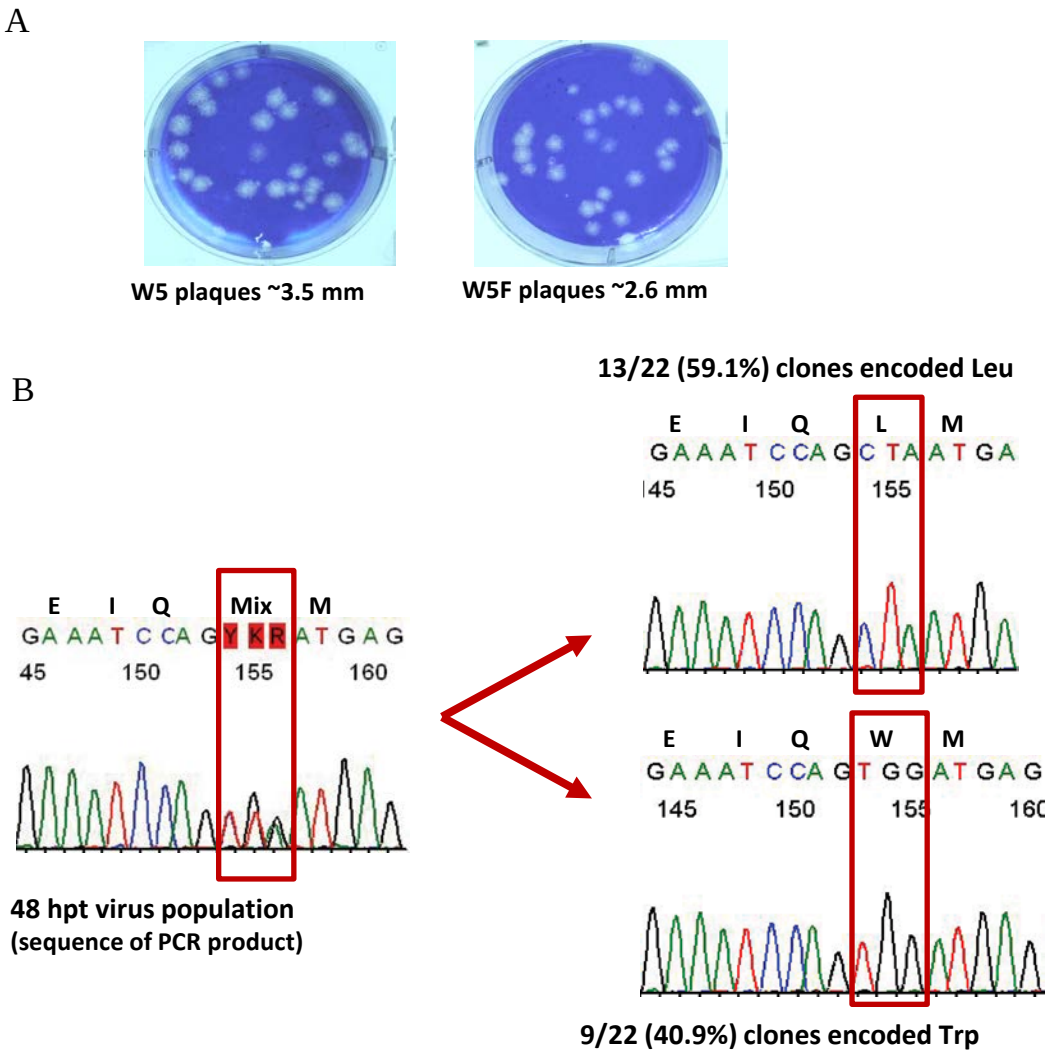

FIG. 4.8. Viability of poliovirus engineered to express residue 5 mutations. (A) Representative plaques from wild-type poliovirus and poliovirus with $3D^{pol}$ Trp5Phe mutation. (B) Sequence data of Trp5Leu cDNA PCR products from poliovirus at 48 hpt (*left*) and representative sequence data from individual cDNA clones (*right*).

adsorption virus inoculum was removed and replaced with 2 ml of culture medium and incubated at 37^{o}C for 1, 2, 3, 4, 6, 8 and 24 hours post-adsorption (hpa) before undergoing 3 freeze-thaw cycles to release virus. Growth curves were plotted as virus titer from plaque assays versus time (Fig. 4.9). In agreement with the prior transfection and plaque assay data, Trp5Phe 3D^{pol} produced viable virus with a growth rate that was only slightly slower than the wild-type virus and it reached the same end point of ~5.0x10^{9} PFU/ml at 24 hpa.

4.3 Discussion

PV 3D^{pol} residue 5 mutations have previously been shown to have significant effects on elongation complex stability, where there is a requirement for a large hydrophobic residue at this position to maintain a stable complex. Here we investigated the significance of a stable elongation complex in the context of genome replication. To do this we studied the ability of residue 5 mutations to replicate long, sub-genomic, PV RNA templates; as well as their ability to replicate in the cell-free system and in full virus. We found that mutations to residue 5 that reduced the elongation complex stability also had a significant reduction in polymerase processivity, or the number of nucleotides incorporated before dissociation. Also, the effects can be seen in the context of the cell-free replication where less RNA is generated from replication centers and in the full virus where severe processivity mutants were unable to maintain viral propagation.

My early attempts to study the ability of reside 5 mutations to replicate sub-genomic length PV RNA were unsuccessful due to inefficient substrate binding and elongation. The experimental design was to monitor primer extension from an IRdye labeled DNA primer annealed to a sub-genomic RNA template (Fig. 4.1B). Results

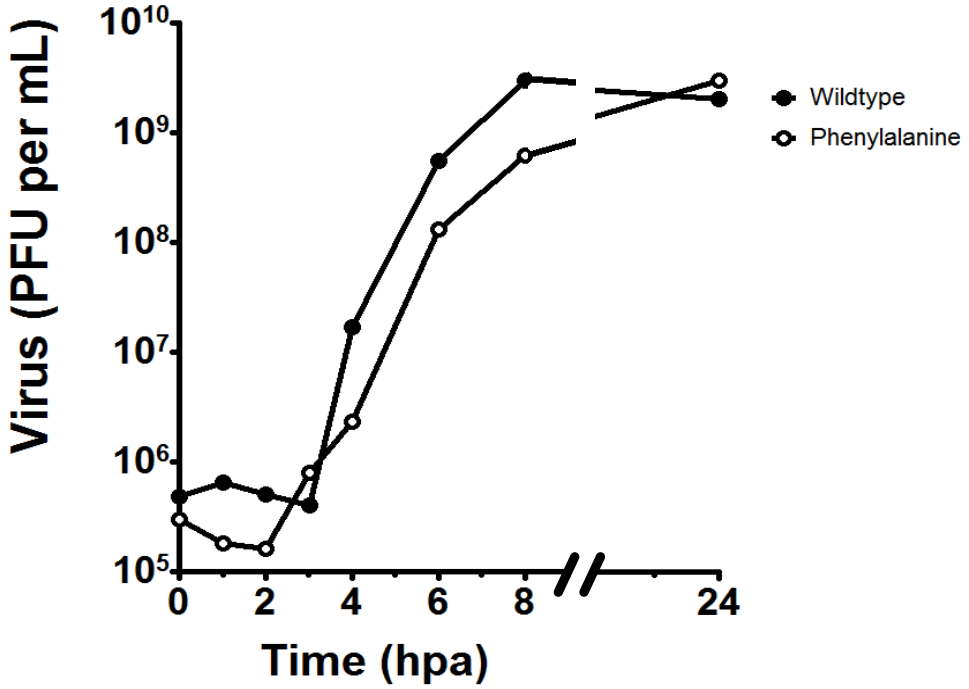

FIG. 4.9. One-step growth curve of wild-type and Trp5Phe poliovirus. HeLa cells (~10^6 cells per 35 mm well) were infected with 10 PFU per cell of wild-type or Trp5Phe poliovirus. After adsorption for 1 hour at room temperature, the virus inoculum was removed, the cells were given 2 ml of culture medium and incubated at 37°C. Cells were subjected to 3 cycles of freeze-thaw at 0,1,2,3,4,6,8 and 24 hours post-adsorption (hpa). Poliovirus titers were determined by plaque assay and plotted versus time.

showed that replication efficiency was low; it was difficult to get good resolution from long primer extensions (Fig. 4.2), and when I did see decent separation (Fig. 4.2B) the experiment was very difficult to repeat. However, displacement of the DNA primer during these experiments suggested that there was priming upstream of the oligo, possibly because the 3' end of the primed RNA template was folding back on itself to provide an RNA hairpin primer that was suitable for elongation (Fig. 4.3). We utilized this self-priming hairpin to carry out the rest of our sub-genomic length RNA replications (Fig 4.1C).

We found that the decreased elongation complex stability also reduced polymerase processivity during replication of longer RNA templates. Elongation of self-primed 2201 and 5424 nt RNA templates showed that mutation of Trp5 to smaller residues resulted in the accumulation of abortive intermediate length products and very little full-length product. These effects were dependent upon the mutation, with the smaller valine and alanine mutants having the most deleterious effects (Fig. 4.5). The mutants also showed a decrease in template utilization that is attributed to their reduced elongation complex formation rates (Table 3.1, Chapter 3). The abortive product bands, on the other hand, are attributed to elongation complexes that began during the low salt initiation step but failed to replicate to the very end of the template. These data indicate that the elongation complex stability is not only a characteristic of a stalled polymerase, but also of an actively elongating polymerase. The difference in processivity between the wild-type and mutant polymerases is also apparent from the amount of very large RNA produced in the reactions after long incubation times (Figure 4.4). The composition of these large RNAs was not determined, but they are presumably due to some form of

template switching or internal re-annealing during the elongation reactions. The lack of distinct initiation events during the elongation step of these reactions was confirmed by control reactions that did not show any observable product formation under high salt conditions.

The abortive products generated by the mutant polymerases also show several distinct bands that are suggestive of specific pause or dissociation sites along the template. Even the wild-type polymerase produces some abortive bands, something that has not been previously observed in studies showing that $3D^{pol}$ is quite processive and fully capable of elongation through secondary structures in the template (35). These bands are likely a result of our experimental conditions during the elongation phase of the reaction, where room temperature and high salt concentrations both act to stabilize RNA structures. RNA structures may be able to inhibit or stall polymerase movement along the template, allowing less stable polymerases to dissociate from the RNA template while more processive polymerases eventually elongate through the duplex section. In such a context, the increased banding seen with the smaller Trp5 mutants suggests that reduced elongation complex stability may be a particularly prominent defect when elongating through templates with double-stranded RNA structures. This is also consistent with how inefficiently these mutants replicate the separate 5' IRES fragment that is rich in RNA structure (Fig. 4.5). In contrast, the tyrosine mutant and wild-type $3D^{pol}$ containing a tryptophan at residue 5 produce few distinct abortive product bands and they elongated through the IRES template without difficulty. These results indicate that large hydrophobic amino acids at residue 5 may increase processivity by facilitating the unwinding of dsRNA structures in poliovirus RNA templates.

Interestingly, when the 5’ NTR, including cloverleaf and IRES elements, was removed from the 5424 nt RNA template, the processivity increased for all polymerases (Fig. 4.6). This suggests that residue 5 mutants are significantly affected by RNA structures that are thousands of nucleotides downstream. It has been shown that the PV 5’ NTR cloverleaf and IRES element are required for genome replication (104, 156); however, these assays were completed in the cell-free replication system where it is not clear whether host or other viral proteins could be binding the 5’ NTR to aid in RNA replication or if the 5’ NTR is involved in specific RNA-RNA interaction. However, direct RNA-RNA interactions of other virus genomes have been shown in the absence of other virus and host proteins (4, 37). In these reports the 5’ and 3’ NTRs come together to circularize the RNA genome and this circularization is required for negative-strand RNA synthesis (4, 37). It could be that the PV genome has similar direct RNA-RNA interactions in the reactions performed here, and removal of the 5’ NTR prevents these interactions. In such case the interaction could cause disruption of the elongating polymerase so that instable polymerases abort the RNA template while more stable polymerase are able plow through and complete genome replication. Then removal of the 5’NTR would allow more processive elongation from both stable and especially unstable polymerases. This idea is supported by the absence of the very large RNA products in the well when the 5’NTR is removed (compare wells in Fig. 4.4 and Fig. 4.6), where internal re-annealing could possibly be enhanced by a 5’NTR interaction with downstream RNA resulting in the formation of seemingly large RNA products.

The two RNA products generated by wild-type and Trp5Tyr polymerases (Fig. 4.6) are likely from two different priming sites caused by the non-specific fold-back and

are only visible for the polymerases that are able to make more stable ECs, Chapter 3 (Table 3.2). Conveniently, the increase in processivity coupled with the secondary priming shows that the downstream 5'NTR only affects processivity and has little to no effect on EC stability; however, a more detailed study would be required to determine actual effects of downstream RNA structure on the EC decay constant.

The effects of reduced elongation complex stability are also observed when the mutant polymerases are introduced into viral replication complexes using cell-free translation-replication reactions. The poliovirus cell-free replication system was used to compare negative-strand RNA synthesis by wild-type and mutant polymerase (Fig. 4.7). This system depends on *cis*-active elements within native viral RNA templates (25, 103) and reveals biochemical defects in RNA replication associated with mutations in $3D^{pol}$ (22). In these reactions, $3D^{pol}$ mutations result in detectable synthesis of full-length negative-strand RNA product at a timescale comparable to that observed for the wild-type enzyme, consistent with our biochemical finding that $3D^{pol}$ elongation rates are not affected by these mutations. However, the amount of full-length negative-strand product produced is significantly reduced, consistent with the reduced initiation rates of the mutant polymerases and the formation of unstable elongation complexes that dissociate prior to reaching the end of the ≈6 kb replicon genome.

Introduction of both the Trp5Phe and Trp5Leu $3D^{pol}$ mutations into poliovirus genomes resulted in virus growth after transfection into host cells. The phenylalanine mutation was stably maintained in the progeny virus with a slightly reduced plaque size but an essentially wild-type growth rate in a single step growth curve (Fig 4.9). In contrast, virus containing the more deleterious leucine mutant grew very slowly with

titers at 48 hpt that were ≈1000-fold less than those of the wild-type virus. The leucine mutation was not stable and sequencing of the progeny virus pool revealed a mixed population of leucine and tryptophan at residue 5 after 48 hours and completes reversion to the wild-type tryptophan by 72 hours post transfection (Table 4.1 and Fig. 4.8B). The loss of the leucine codon is not unexpected given the instability of its elongation complexes on the PETE RNAs and its inefficient synthesis of genomic size RNA *in vitro*, but it is a bit surprising that only a triple mutation (CUA to UGG) reversion to the wild-type tryptophan was observed, rather than two mutations to generate a phenylalanine (CUA to $UU^{U}/_{C}$) that has essentially wild-type growth characteristics. These results demonstrate that poliovirus propagation is dependent upon processive RNA replication and that poliovirus $3D^{pol}$ can tolerate a small decrease in elongation complex stability and processivity and maintain the ability to propagate. The emergence of the Leu5Trp reversion and the genetic stability of the Phe5 mutant may also point to a requirement for a planar residue 5 in order to get optimal viral growth.

In conclusion, we further dissected the importance of PV $3D^{pol}$ residue 5 function in context of genome replication by measuring the effect of residue 5 mutations in processivity. The results indicate that the size and hydrophobicity, and possibly the planarity, of residue 5 are important to maintain the $3D^{pol}$ in an elongation-competent state. Consistent with this, viral genomes containing Trp5 $3D^{pol}$ mutations show reduced levels of RNA synthesis in cell-free translation-replication reactions and impaired growth of infectious virus that results in the rapid emergence of revertant virus. Interestingly, downstream RNA structure, such as the IRES, enhanced the processivity defects seen with the mutant polymerases in a reconstituted replication system; however, we were

unable to study these effects in the cell-free system or *in vivo* due to the requirement of the 5’ NTR for translation and replication.

Chapter 5

Poliovirus 3D^{pol} Downstream RNA Interactions and Elongation Complex Lock Length

5.1 Introduction

My work in this chapter is currently being written for journal publication. Authorship from publication of this chapter will included Hobdey, SE and Peersen, OB.

The poliovirus (PV) genome is comprised of a single strand of positive-sense RNA whose replication is dependent upon regions of higher RNA structure (160). In order for the virus to multiply in the host cell, numerous copies of the viral genome must be generated by the virally encoded RNA dependent RNA polymerase (RdRP). As the PV genome is of positive-polarity, 3D^{pol} must first generate a negative-sense RNA intermediate that serves as a template for the generation of multiple positive-sense genomic RNA strands. *In vivo*, the complementary positive and negative- strands of RNA are mostly single-stranded, suggesting that the complementary strands are melted by either a host or viral protein (132). In order to synthesize positive-sense RNA from the newly made negative-sense RNA, the complementary segments must be unwound and displaced during or prior to replication. *In vitro*, PV 3D^{pol} has been shown to be capable of unwinding long stretches of dsRNA, (~1000 nts), independent of a distinct helicase domain and in the absence of other viral or host proteins (35); thus, it is believed that 3D^{pol} is able to unwind large segments of dsRNA on its own. Also, the crystal structure of the PV 3D^{pol} elongation complex (EC) indicates that strand separation can take place

as the dsRNA enters the polymerase, where a conserved cleft between the index and pinky fingers allows the template strand to enter the active site and the non-template strand continues across the fingers domain (Fig. 5.1) (60).

In Chapters 3 and 4, I showed that the wild-type PV $3D^{pol}$ was able to efficiently replicate through the 5' NTR, a segment of RNA with extensive structure, and that mutations to residue 5 of the PV $3D^{pol}$ significantly effected this efficiency (71). However, when the 5' NTR was removed polymerase processivity increased for wild-type polymerase and especially for residue 5 mutants, indicating that distant downstream RNA structures have significant effects on $3D^{pol}$ processivity and EC stability. When looking at the PV $3D^{pol}$-RNA EC structure it is possible that the template or downstream duplex could come in direct contact with residue 5 and these contacts could be required for EC stability or strand separation (Fig. 5.1A) (60). RNA structures can induce more downstream secondary or tertiary structures by folding back upon itself to have RNA-RNA interaction, as has been seen with the Flavivirus genome (Fig. 5.1B) (4), a family of RNA viruses similar to the Picornavirus family of viruses.

Here I report the effects of immediate downstream duplex RNA on polymerase EC formation and stability, as well as test the stabilities of ECs after formation with 1, 4 or 7 nucleotide long lock sequences. For these assays we will use the nomenclature EC_{+1}, EC_{+4} or EC_{+7} to represent EC formation with 1, 4 or 7 nucleotides, respectively. I also investigate the interaction of downstream RNA with the $3D^{pol}$ ssRNA templates that contain 2-aminopurine (2AP), a fluorescent nucleotide analogue that is sensitive to stacking interactions with either adjacent bases or aromatic amino acids (141). Thus, when 2AP is incorporated into a nucleotide oligo its fluorescence can be used to report on

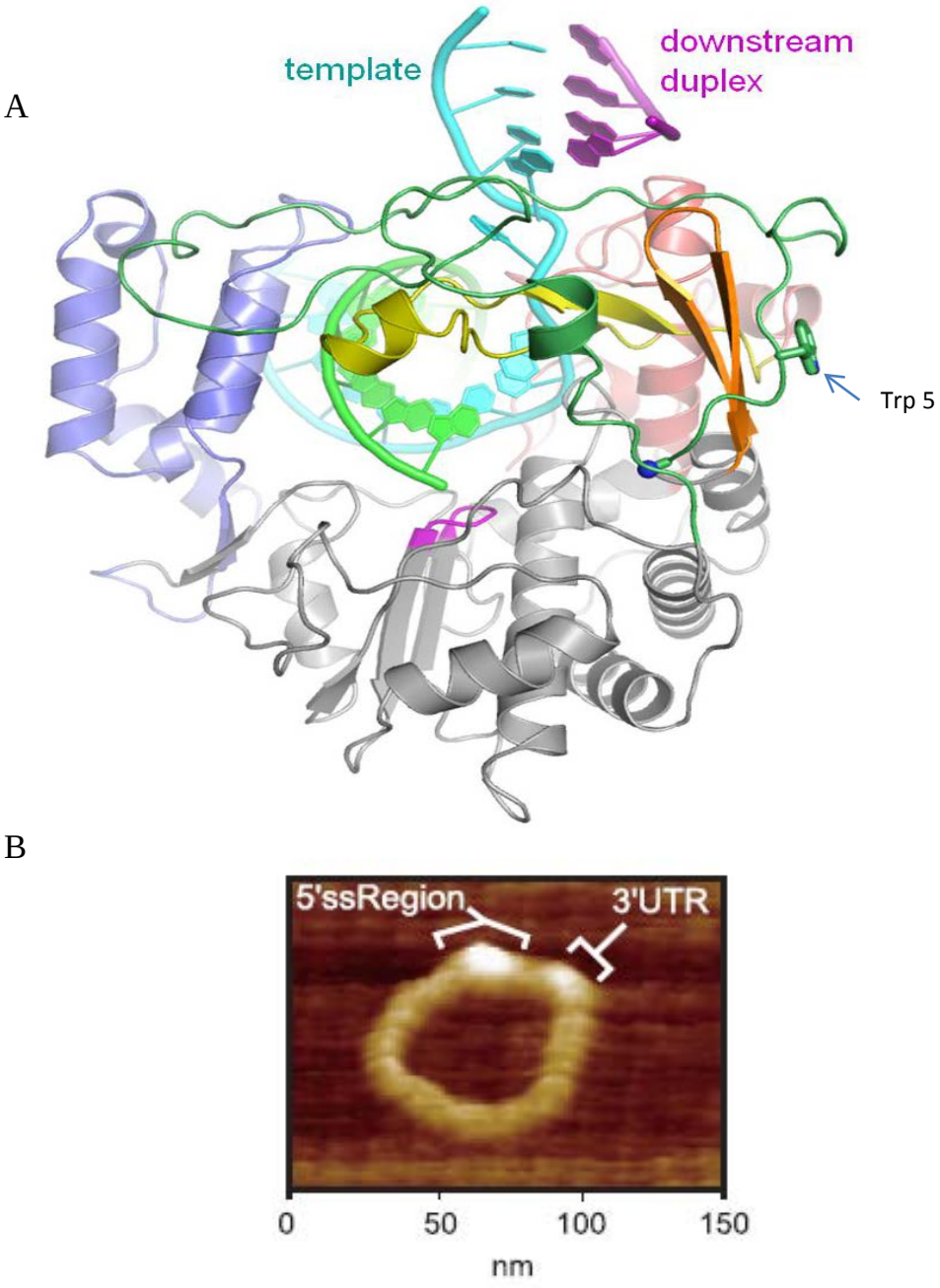

FIG. 5.1. Possible PV RNA interactions. (A) PV $3D^{pol}$ elongation complex. back view showing Trp 5 in relation to the downstream dsRNA, the RNA template is in cyan and the non-template is in magenta. The polymerase thumb domain is in blue, palm domain, grey, and fingers domain is in green, orange, yellow and pink. (B) Atomic force microscopy showing circularization of Flavivirus genome through RNA-RNA contacts at the 5' and 3' NTRs (or UTRs meaning un-translated region). 5'ssRegion is single-stranded RNA that has a significant amount of structure, like the 5' end of the PV RNA. *Alvarez et al. 2005. J. Virol.* (4)

specific base conformations (42, 43). When RNA templates containing 2AP are replicated, the fluorescence signal can be used as a real time kinetic reporter, indicating various RNA conformations during elongation (149). Given this kinetic data we could then potentially fit the data using modeling software, to an algebraic equation describing the amplitude and rate associated with fluorescence changes related to 2AP threading through the active site. Once the 2AP fluorescence change was determined for each nucleotide binding site as it enters and exits the polymerase active site, we could then monitor fluorescence changes, based on the kinetic fit, that are not associated with the amplitudes related to active site. For example, if downstream nucleotides had stacking interaction to residue 5 we would see 2AP fluorescence quenched by the aromatic residue at position 5; alternatively if the polymerase interacted with the phosphate backbone the 2AP would exhibit higher fluorescence intensity.

The results show that there are significant stabilizing affects from the presence of a downstream RNA duplex and, separately, an EC_{+4} is more stabilizing than EC_{+1}. Also, while kinetic modeling of 2AP data was unsuccessful, using the fluorescence intensities alone the data indicated intermittent interactions with downstream ssRNA. However, in both cases it remains unclear whether these downstream RNA interactions were affected by residue 5 mutations.

5.2 Results

5.2.1 Downstream duplex has no effect on elongation complex formation and replication

To determine the effects of a downstream RNA duplex on EC formation we employed RNA templates called dblPETE 8+4_0+9 and dblPETE 8+4_3+8, both of which are 8 base pair hairpin primed RNA templates, with a 4-nucleotide, CUCU, lock

sequence (EC_{+4}) and a downstream duplex (Fig. 2.3B). The dblPETE 8+4_0+9 has a 9 bp downstream duplex in which the 5' end is base paired with nucleotide 8 in the RNA template. Based on the PV $3D^{pol}$-RNA co-crystal structure, this should result in the 5' end just coming in contact with $3D^{pol}$ after EC formation but not undergoing any strand separation. The dblPETE 8+4_3+8 has a 8 bp downstream duplex with a 3-base fray at the 5' end, and thus the 3 unpaired bases of this template can contact the polymerase remote to the template entry site. PETE 8+4_3_3 RNA template was used as a control RNA that has the same sequence and EC_{+4} lock but no downstream duplex. EC were formed and the formation rates were determined by PAGE analysis of the quenched samples followed by band quantitation of the IRdye labeled RNAs to determine relative amounts of RNA formed, as previously described in Chapter 3. The EC_{+4} formation rates were determined for wild-type and residue 5 mutations W5A and W5Y as described in Chapter 2, Section 2.5.2. All polymerases exhibited single exponential kinetic rates that were consistently ~1.5 fold faster than the EC_{+1} and EC_{+2} formation rates described in Chapter 3 and exhibited the same trend seen for residue 5 mutations where large aromatic residue (wild-type and W5Y) were slightly faster at EC formation than smaller residue W5A (Fig. 5.2 and Table 5.1).

After EC_{+4} formation rates were determined, we wanted to verify the efficiency of wild-type and residue 5 mutants (W5A, W5L and W5Y) $3D^{pol}$ replication through downstream RNA duplex. This was determined by first forming the stable EC_{+4} then diluting the reaction 20-fold into a high NaCl buffer to prevent reinitiation in the presence of 20 μM each GTP, ATP UTP and CTP. Small aliquots of the reaction were quenched at 0.5, 1, 1.5, 2, and 2.5 minutes and analyzed by PAGE (Fig. 5.3). Results show that

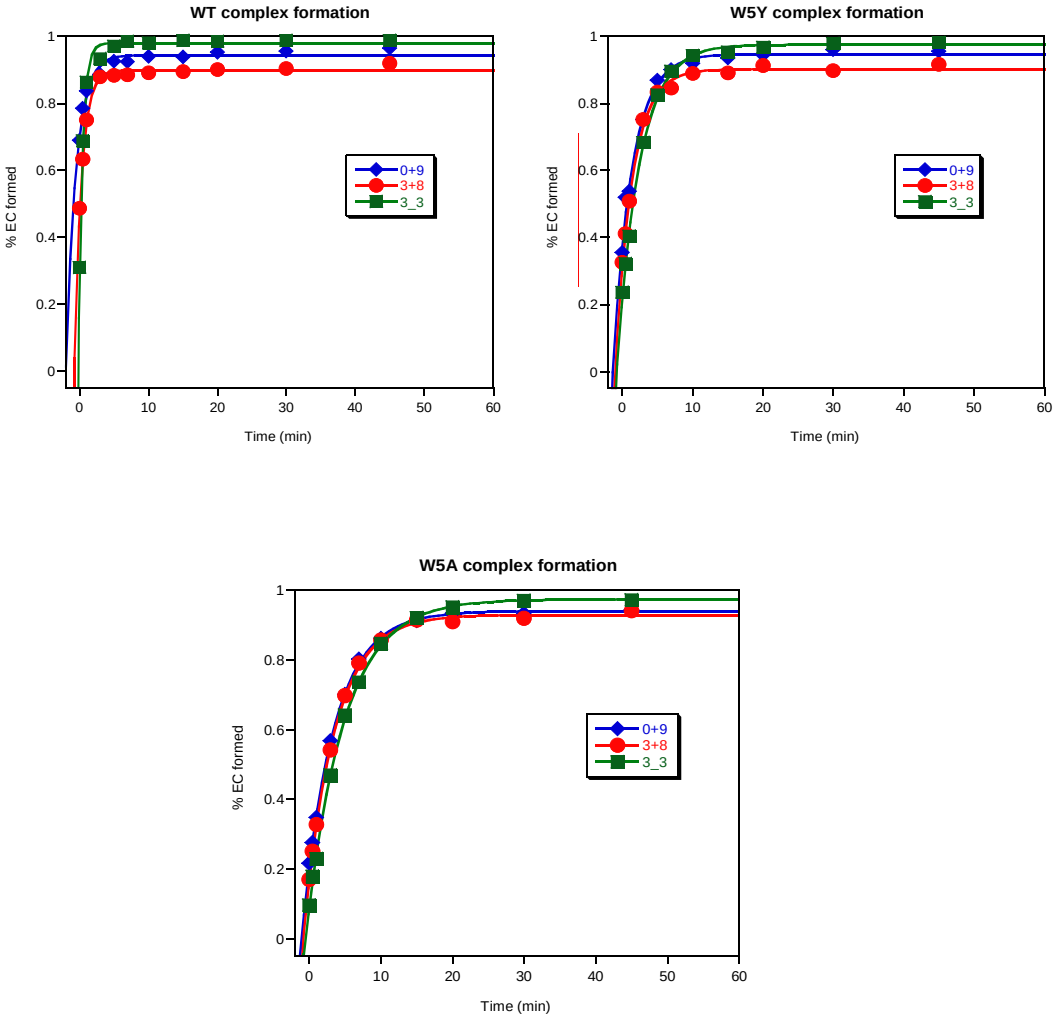

FIG 5.2. Elongation complex formation kinetics. (A) Wild-type, (B) W5Y, and C) W5A EC formation for dblPETE 8+4_0+9 (blue), dblPETE 8+4_3+8 (red) and PETE 8+4_3_3 (green). Data was fit to a single exponential with a significant initial offset because the 0 min time point was not subtracted from the data, specifically because some the formation is able to take place on ice during equilibration. Data are representative of the cleanest data from three replicates

Table 5.1. Elongation complex (EC) formation on PETE RNA templates with downstream duplex.

EC_{+4} formation rates (minutes)				
RNA template	EC_{+n}	Wild-type	W5Y	W5A
8+4_0+9	4	1.4 ± 0.2	2.7 ± 0.2	4.3 ± 0.1
8+4_3+8_3	4	1.02 ± 0.07	2.4 ± 0.1	4.2 ± 0.1
8+4_3_3	4	0.59 ± 0.01	3.2 ± 0.1	5.2 ± 0.1
9+2_24	2	3.0 ± 0.2	4.5 ± 0.5	7.5 ± 0.5
10+1_12	1	2.0 ± 0.1	4.2 ± 0.5	6.6 ± 0.7

errors based on curve fits of the data

A

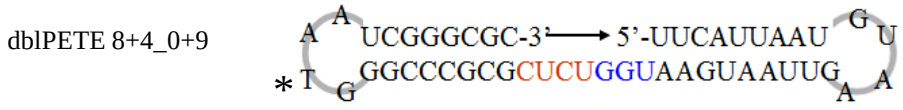

B

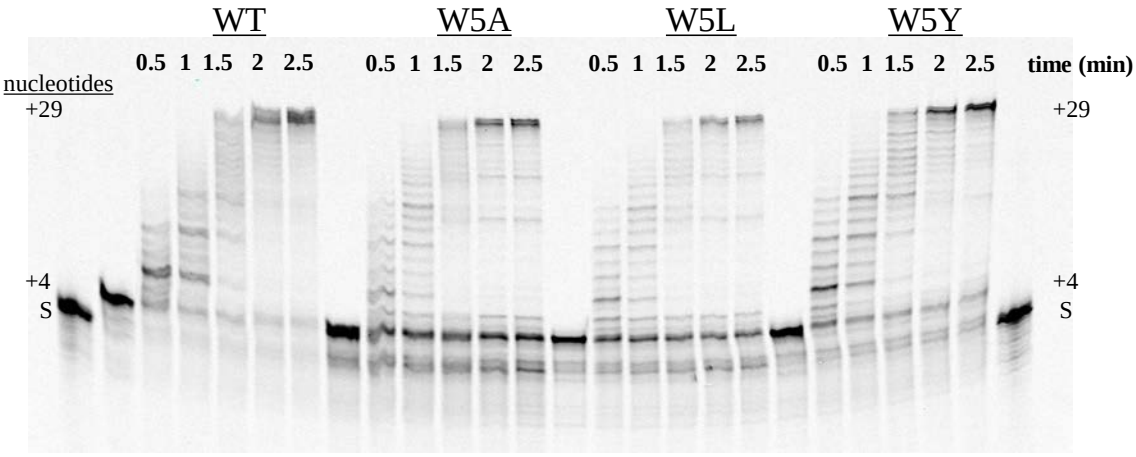

FIG 5.3. Elongation of through duplex RNA. (A) Cartoon representation of dblPETE 8+4_0+9 RNA used in this experiment. (B) Denaturing PAGE showing efficient replication of dblPETE 8+4_0+9 RNA by wild-type, W5A, W5L and W5Y $3D^{pol}$ mutants. EC_{+4}s were formed, as previously described where S represents the starting material and +4 represents the formation of EC_{+4}, for 15 minutes then chased with 40 µM NTPs and quench by 10 mM EDTA at indicated time points.

wild-type and all residue 5 mutants replicated through duplex RNA at essentially the same rate, taking between 1.5 and 2 minutes to replicate through 25 nucleotides.

5.2.2 Downstream duplex has stabilizing effects on the elongation complex

To determine the effects of downstream RNA duplex on EC stability, we performed stability experiments as previously described in Chapter 2, Section 2.7, on dblPETE 8+4_0+9, 8+4_3+8_3 and PETE 8+4_3_3 RNA templates. EC_{+4}s were incubated at room temperature for 15 minutes before being diluted 10-fold into a high [NaCl] buffer. Diluted reactions were incubated from 0-300 minutes for wild-type, 0-240 minutes for W5Y and W5F, and 0-120 minutes for W5A (time points were dictated by the previously reported EC decay constants (71)). Reactions were analyzed by PAGE and bands were quantitated to determine EC_{+4} stability by comparing the relative amounts of +4 and fully elongated products (Fig. 5.4). The results show that a downstream duplex significantly increases the stability of the EC for W5Y and W5F polymerases (Fig. 5.5 and Table 5.2). EC stability of wild-type was difficult to determine since all complexes were very stable, past 300 minutes. Downstream duplex seems to have a smaller effect on the W5A polymerase, where the PETE 8+4_3_3 RNA was only 2.1-fold less stable than the dblPETE 8+4_0+9 RNA, rather than the 5.4 and 9.1-fold seen with the W5Y and W5F mutants, respectively. Also, there is significant increase in EC stability for the W5A mutant when using ssRNA PETE 8+4_3_3 compared to the ssRNA PETE 9+2_24 RNA that was previously reported (Table 5.2).

5.2.3 Nucleotide lock length on elongation complex stability: +4>+1>+7

To compare the effects of the number of nucleotides added in EC formation on EC stability, we performed stability assays, described in Chapter 2, Section 2.7, on ECs

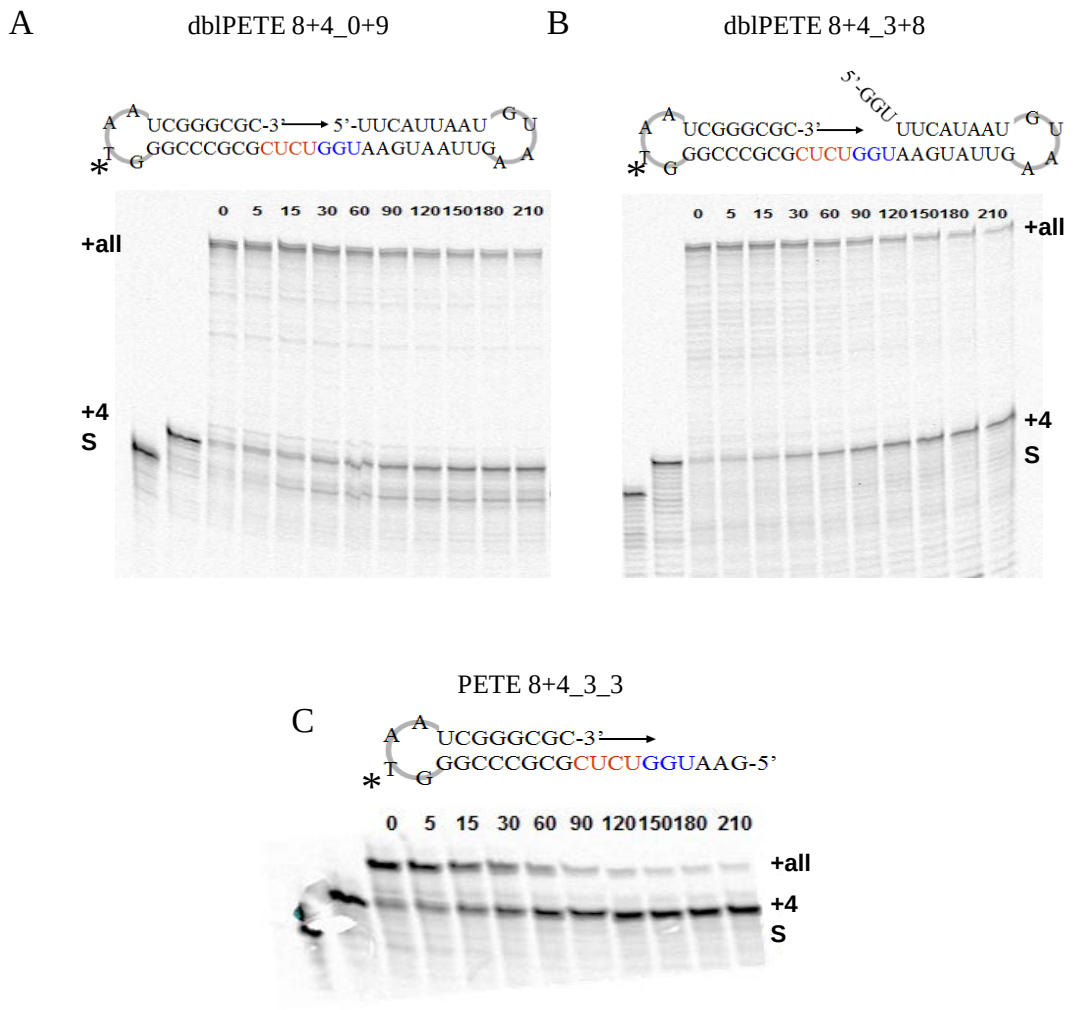

FIG 5.4. EC_{+4} stability. PAGE analysis of W5F EC_{+4} stability on (A) dblPETE 8+4_0+9, (B) dblPETE 8+4_3+8 and (C) PETE 8+4_3_3 RNA. EC_{+4} were formed as previously described for 15 minutes then chased by the addition of 40 μM NTPs for 5 minutes.

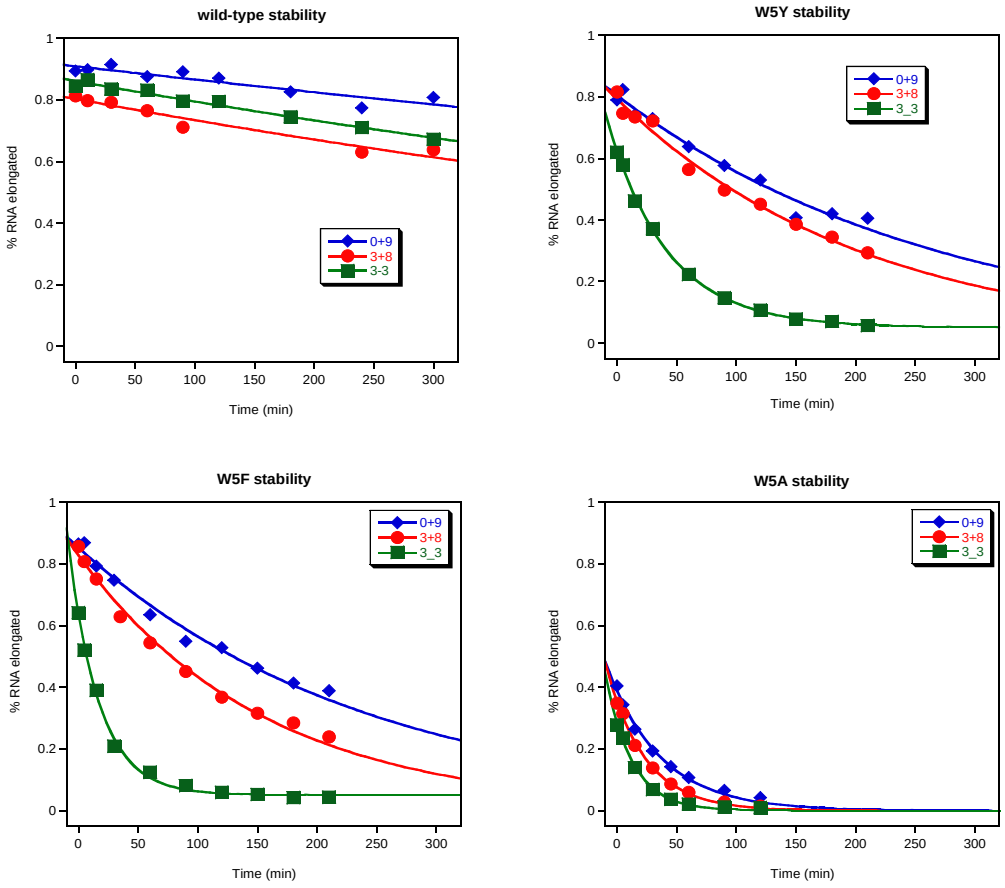

FIG 5.5. EC_{+4} stability kinetics. Plot of data obtained from PAGE analysis showing single exponential loss of $3D^{pol}$ EC_{+4} stability. Data indicate that downstream duplex aids in EC stability. Data represents the best data set from three replicates, determined by fit.

Table 5.2. EC stability on PETE and dblPETE RNA templates.

A. EC_{+4} stability decay constant (minutes)				
RNA template	wild-type	W5Y	W5F	W5A
8+4_0+9	2100 ±400	271 ±17	242 ± 12	45.1 ±2.4
8+4_3+8	1110 ±130	210 ± 10	154 ± 6	32.2 ±1.2
8+4_3_3	1250 ± 70	50.1 ± 1.9*	25.5 ± 1.6*	21.9 ±1.0
9+2_24	186 ± 4	56.0 ±3.0	26.0 ± 1.0	5.3 ±0.2
B. EC_{+4} stability fold decrease normalized to wild-type				
RNA template	wild-type	W5Y	W5F	W5A
8+4_0+9	1.0 ± 0.2	7.6 ± 1.4**	9.1 ± 1.6**	45 ± 8.1**
8+4_3+8	1.0 ± 0.2	5.4 ± 0.6**	7.2 ± 0.9**	35 ± 4.1**
8+4_3_3	1.0 ± 0.1	24 ± 9**	49 ± 4.1**	57 ± 4.1**
9+2_24	1.0 ± 0.03	3.3 ± 0.2**	7.1 ± 0.3**	35 ± 1.5**
C. EC_{+4} stability fold decrease normalized to 8+4_0+9 EC complex				
RNA template	wild-type	W5Y	W5F	W5A
8+4_0+9	1.0 ± 0.2	1.0 ± 0.1	1.0 ± 0.1	1.0 ± 0.1
8+4_3+8	1.8 ± 0.4	1.3 ± 0.1	1.5 ± 0.1	1.4 ± 0.1
8+4_3_3	1.6 ± 0.3	5.4 ± 0.4**	9.1 ± 0.7**	2.1 ± 0.1**
9+2_24	11 ± 1.9**	4.8 ± 0.4**	9.3 ± 0.6**	8.5 ± 0.6**

* values required an offset because they did not reach 0% elongation
** values that differed significantly from the normalized value
Fold errors were propagated by $(\Delta A/A)^2+(\Delta B/B)^2=(\Delta Z/Z)^2$

that were formed with either +1, +4 or +7 nucleotides on dblPETE 8+4_0+9, 8+4_3+8 and PETE 8+4_3_3 RNA templates, resulting in the final states shown in Figure 5.6. The results of this experiment showed that for most polymerase-RNA complexes, an EC_{+4} was more stable than EC_{+1} and EC_{+7} (Fig. 5.7 and Table 5.3). Figure 5.7 shows an example of W5Y stability data, notice that the EC_{+7} on the 0+9 template produces a curve with a very small amplitude and low starting value, indicative of a polymerase more unstable than the curve fit reports. The 0+9 template EC_{+7} gel (Fig. 5.7A) shows that after 15 minutes of pre-incubation most of the RNA is elongated by 7 nucleotides but the chases are very inefficient. The most severe stability effects are from the EC_{+7} on the PETE 8+4_3_3 RNA, where there are only three template nucleotides left after the EC formation.

5.2.4 There is a detectable 2-aminopurine florescence change associated with elongation complex formation

Since $3D^{pol}$ appears to interact with downstream RNA, we designed a fluorescence based assay that would allow us to more precisely determine where along the downstream RNA template the polymerase-RNA interaction was occurring. We designed a set of PETE RNAs that contained 2-aminopurine (2AP) at downstream positions +3, +5, +7 and +9 after EC_{+4} formation (Fig. 5.8). 2AP is an adenine base analog with strong fluorescence signal that is extremely sensitive to stacking interactions, where the signal is strongest when 2AP is completely un-stacked and is weak when quenched by stacking. The RNAs were named using a 9+4ap*N*_13, where 9 is the number of base pairs in the self-priming hairpin, +4 is the number of nucleotides adding during EC formation, ap*N* is the position of the 2AP (3, 5, 7, or 9) after EC_{+4} formation and _13

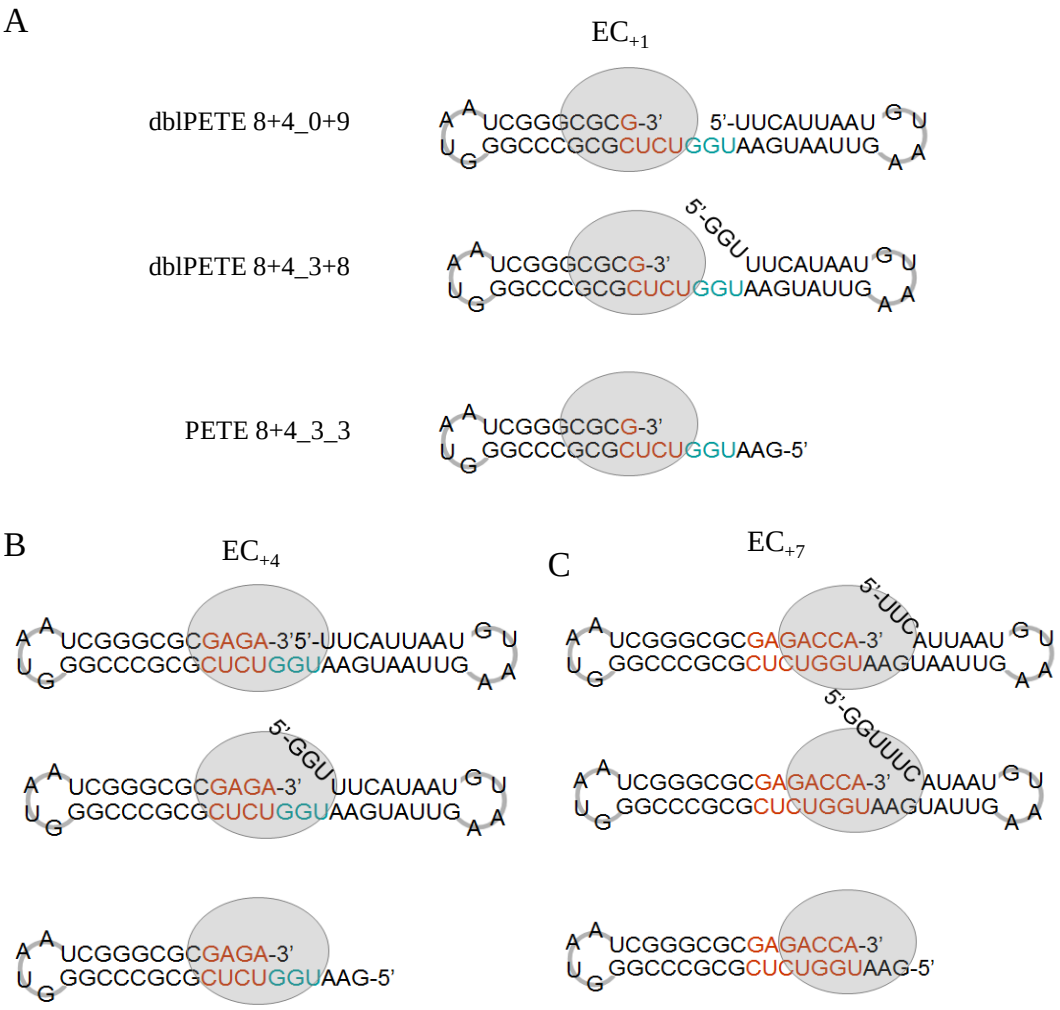

FIG 5.6. Cartoon models of expected $EC_{+1,+4}$ and$_{+7}$ formations. (A) EC_{+1} (B) EC_{+4} and (C) EC_{+7} for dblPETE 8+4_0+9 (*top*), dblPETE 8+4_3+8 (*middle*) and PETE 8+4_3_3 (*bottom*).

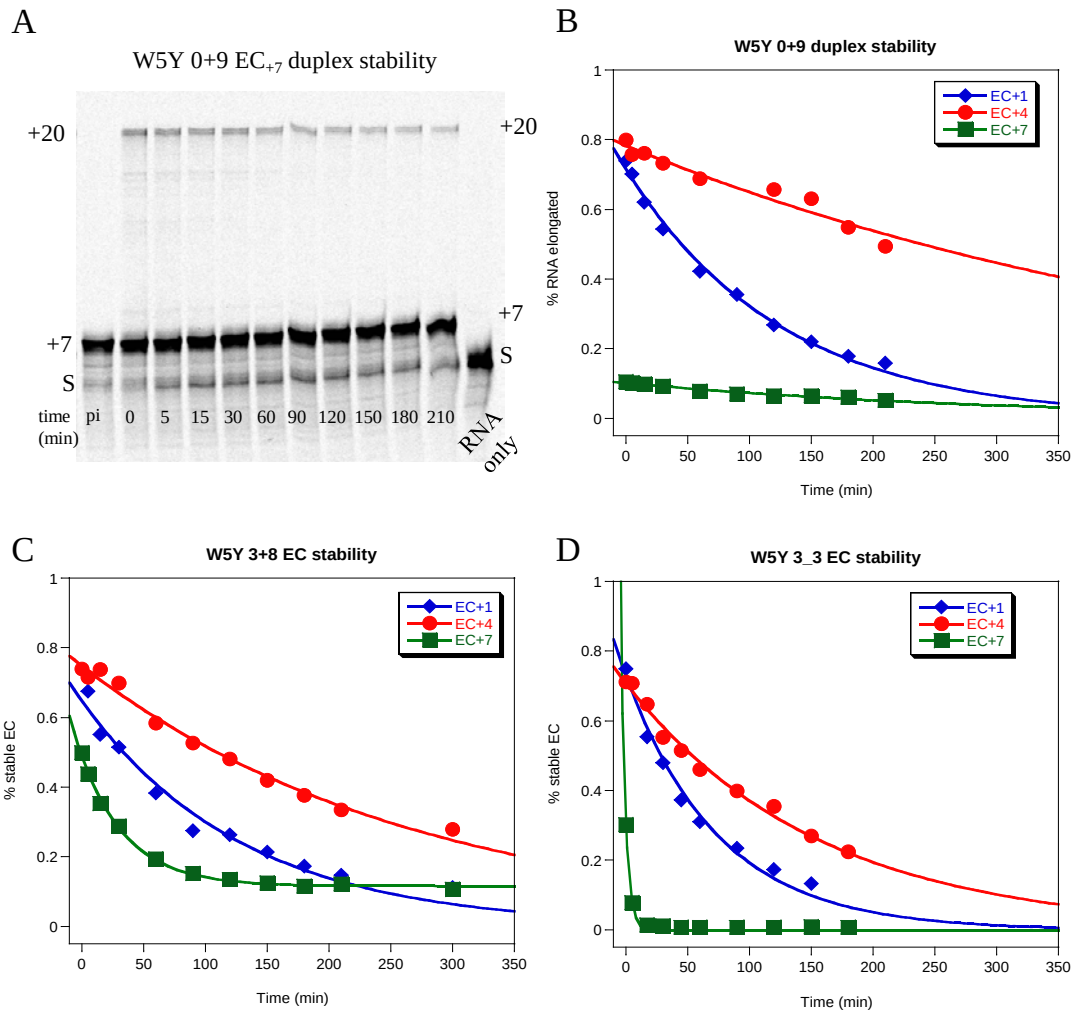

FIG 5.7. Kinetics of $EC_{+1,+4}$ and$_{+7}$ stability. .(A) PAGE analysis of W5Y EC_{+7} stability on dblPETE 8+4_0+9. Plotted data from PAGE analysis of EC_{+1} (blue), EC_{+4} (red) and EC_{+7} (green) from W5Y on (B) dlbPETE 8+4_0+9, (C) dblPETE 8+4_3+8, and (D) PETE 8+4_3_3 RNA templates. Decay constants are found in Table 5.3. Data represent the best fit from two experimental repeats

Table 5.3. EC stability lock length.

A. $EC_{+1,+4,+7}$ stability (minutes)					
RNA template	EC_n	wild-type	W5Y	W5F	W5A
	+1	276 ± 33*	125 ± 4.5	51.4 ± 4.9	18.6± 2.2
8+4_0+9	+4	2039 ± 555	534 ± 51	226 ± 13	49.3 ± 3.0
	+7	248 ± 33*	301 ± 22*	24.9 ± 3.6*	1.0 ± 0.1*
	+1	360 ± 157	130 ± 11	44.4± 5.1	16.4 ± 1.2
8+4_3+8	+4	1082 ± 124	271 ± 12**	107 ± 6.9	30 ± 3.0
	+7	529 ± 49	37 ± 1.8	16.3 ± 2.0	11 ± 3.1
	+1	299 ± 22**	75 ± 4.2	40.0 ± 2.0	9.9 ± 0.6
8+4_3_3	+4	532 ± 27**	154 ± 6.9	82.8 ± 4.8	22 ±0.9
	+7	4.4 ± 0.4	3.8 ± 0.3	3.4 ± 0.5	5.0 ±1.5

B. $EC_{+1,+4,+7}$ stability fold decrease normalized to EC_{+4}					
RNA template	EC_n	wild-type	W5Y	W5F	W5A
	+1	7.4 ± 2.3	4.2 ± 0.4	4.4 ± 0.5	2.6 ± 0.3
8+4_0+9	+4	1.0 ± 0.4	1.0 ± 0.1	1.0 ± 0.1	1.0 ± 0.1
	+7	8.2 ± 2.5*	1.8 ± 0.2*	9.1 ± 1.4*	48 ± 0.4*
	+1	3.0 ± 1.4	2.1 ± 0.2	2.4 ± 0.3	1.8 ± 0.2
8+4_3+8	+4	1.0 ± 0.2	1.0 ± 0.1	1.0 ± 0.1	1.0 ± 0.1
	+7	2.1 ± 0.3	7.3 ± 0.5	6.6 ± 0.9	2.7 ± 0.8
	+1	1.8 ± 0.2	2.1 ± 0.1	5.1 ± 0.7	2.2 ± 0.2
8+4_3_3	+4	1.0 ± 0.1	1.0 ± 0.1	1.0 ± 0.1	1.0 ± 0.1
	+7	121 ± 13	41 ± 4	24 ± 4	4.4 ± 1.3

* stability not accurate: amplitude <0.3% and when x = 0 is y = <10%)
** values required an offset
Fold errors were propagated by $(\Delta A/A)^2+(\Delta B/B)^2=(\Delta Z/Z)^2$

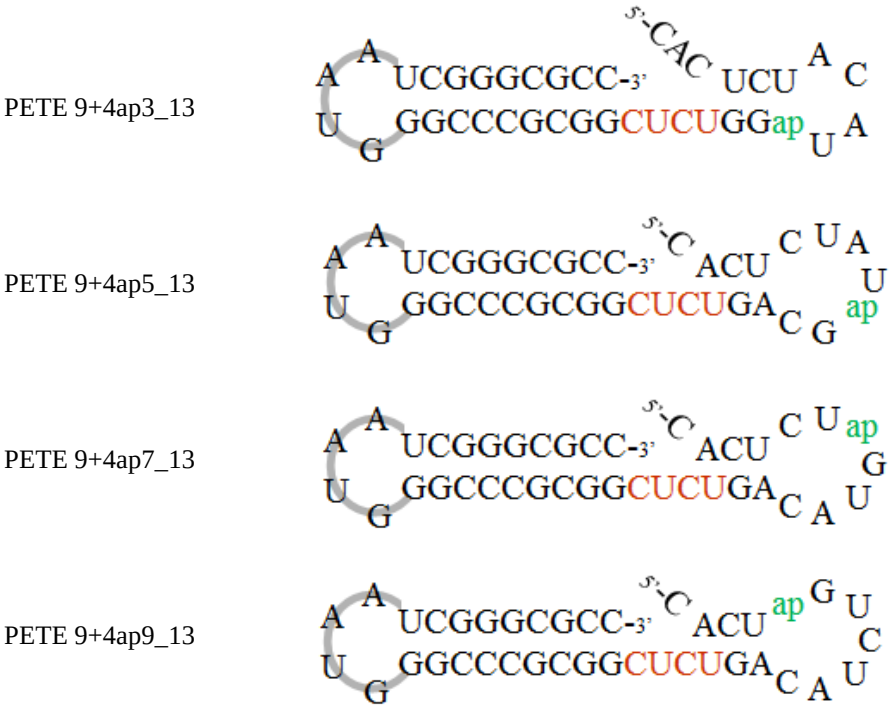

Fig. 5.8. UNAfold predicted RNA secondary structure of 2AP templates before EC formation. Using the older mfold program predicted only a single 9-base pair hairpin ΔG = -24 kcal/mol such as those modeled in Fig. 2.3. After the software update to UNAfold a second 3-base pair hairpin ΔG = -5 kcal/mol was predicted at 37°C in 1M NaCl . http://mfold.rna.albany.edu/

is the number of total nucleotides in the single stranded template after EC_{+4} formation. See Figure 5.9 for EC formation model.

It has been shown biochemically that $3D^{pol}$ has two conformational changes upon formation of the stable EC (9). This conformational change may have some effect on how the polymerase contacts the downstream RNA template. To determine if there is a change in downstream RNA interactions during EC formation we utilized 2AP RNA templates in a stopped-flow format to monitor 2AP fluorescence, described in Chapter 2, Section 2.5.3. The four PETE templates, ap3, ap5, ap7 and ap9, used in this experiment indicate the final position of 2AP after a EC_{+4} lock, rather than the starting position. Mixing the preformed $3D^{pol}$-RNA complexes with a mock NTP mix containing no NTPs showed a slight single exponential increase in fluorescence with an average time constant of 9.5 seconds for all the RNA templates (Fig. 5.10), which may be related to k_{off}, or k_{-1} illustrated in Figure 5.9. For wild-type $3D^{pol}$ formation, the baseline signal when no nucleotides were added exhibited single exponential behavior with a time constant of ~9 seconds with the exception of ap5 which fit the sum of two exponentials and had a slow second exponential of 192 seconds, values reported in Table 5.4.

In the presence of 40 μM NTPs, EC_{+4} formation on ap3, ap5, ap7 and ap9 templates also resulted in an exponential increase in fluorescence signal. ap3 and ap5 fit the sum of two exponentials with fast time constants for the first exponential followed by slower second exponential. ap7 and ap9 fit a single exponential with time constants 6.0 and 4.8 seconds, respectively (Table 5.4). The fluorescence traces from ap3 and ap9 templates started at the same intensity as the 0 μM NTP control but increased exponentially with a time constant of ~4 seconds for the first exponential, ~2.5 fold faster

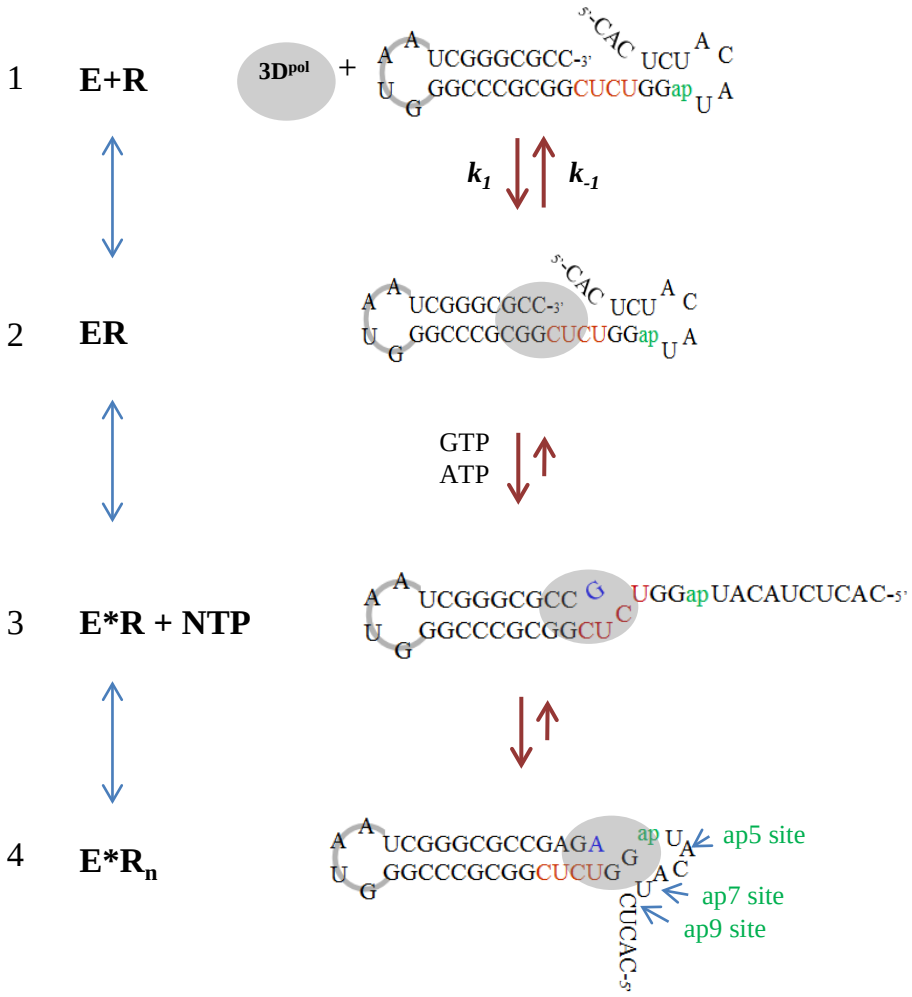

FIG. 5.9. Model of EC formation on 2AP templates. EC formation is broken down into four states requiring three steps, as previously reported. States 1 and 2 polymerase-RNA binding. Upon NTP addition there is a conformational change, state 3, (E*) before incorporation of the first NTP. Blue letter represents incoming NTP. State 4 shows hypothesized downstream RNA rearrangement associated with the E* conformational change and incorporation of the first NTP. After the stable EC_{+4} processive elongation of RNA templates can occur upon the addition of all NTPs.

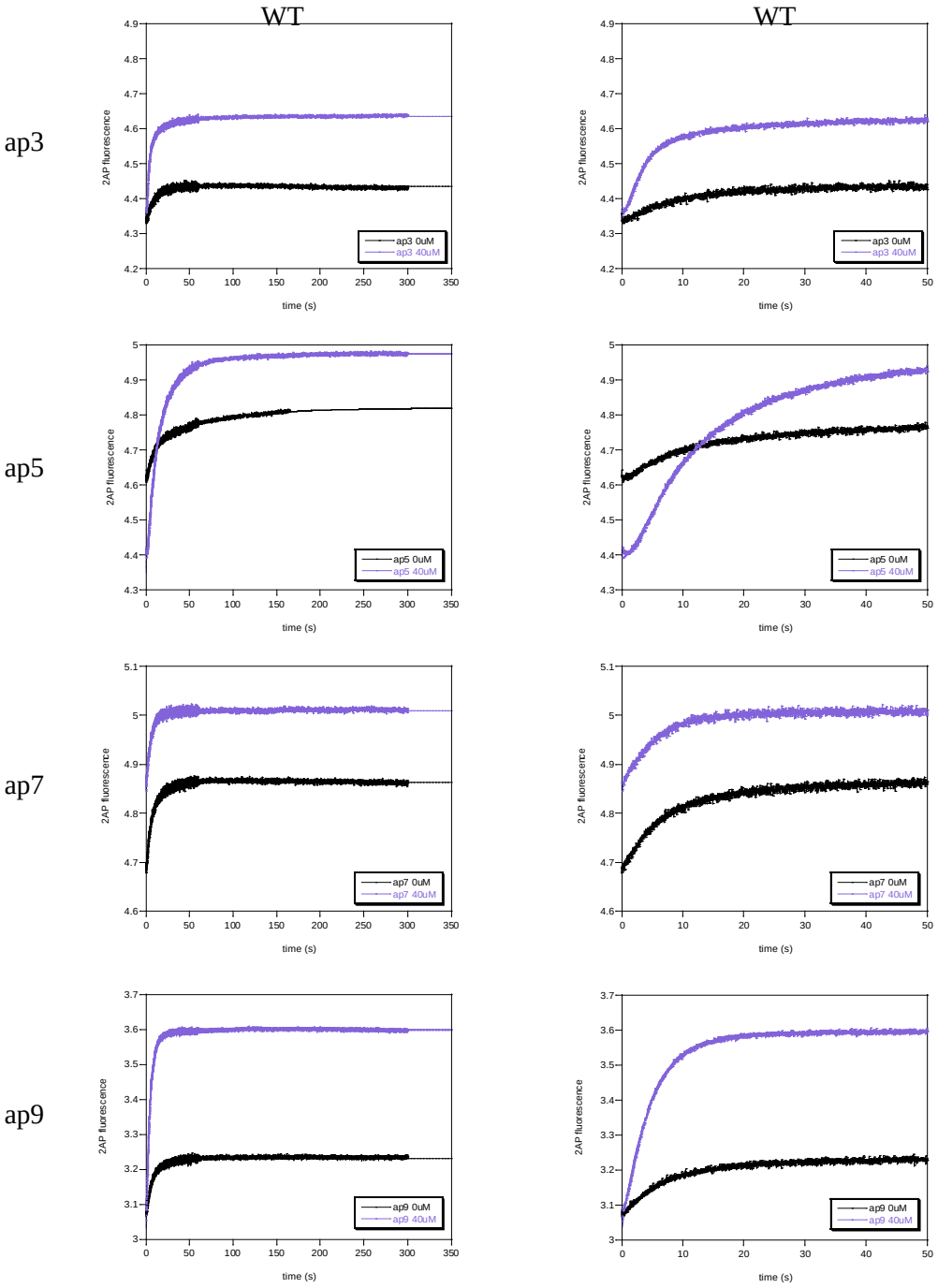

FIG 5.10. 2AP fluorescence during wild-type EC_{+4} formation. Graphs show wild-type $3D^{pol}$-RNA + (purple) or – (black) NTPs. Data was collected by injecting equal volumes of +/- NTP solution and preformed $3D^{pol}$-RNA complex via rapid stopped flow. Reactions were monitored for 300 s (*left*). Early exponential characteristics can be seen in the first 50 s (*right*). Data were fit to a single or sum of two exponentials. Exponents and their amplitudes are recorded in Table 5.4. Each experiment was done in triplicate or greater.

Table 5.4. 2AP wild-type EC_{+4} formation kinetics

	2AP template EC formation by wild-type $3D^{pol}$					
	RNA	**curve**	**1st exp (sec)**	**1st amp**	**2nd exp (sec)**	**2nd amp**
0 µM NTPs	ap3	single	9.8	0.10	n.a.	n.a.
	ap5	double	10.2	0.12	192	0.13
	ap7	single	9.0	0.17	n.a.	n.a.
	ap9	single	9.3	0.15	n.a.	n.a.
	RNA	**curve**	**1st exp**	**1st amp**	**2nd exp[a]**	**2nd amp[a]**
40 µM NTPs	ap3	double	3.8	0.25	30.5	0.06
	ap5	double	12.6	0.53	52.1	0.09
	ap7	single	6.0	0.15	n.a.	n.a.
	ap9	single	4.8	0.56	n.a.	n.a.

[a] dissociation modeled in Fig. 5.14. n.a. not applicable

than the 0 μM NTP control. The ap5 RNA fluorescence signal started below baseline with a lag of ~1 second followed by an exponential increase that has an early time constant of 12.6 seconds. The ap7 template exhibited no change in overall amplitude and trace characteristics compared to the 0 μM control, but had a small difference time constant (Table 5.4). No fluorescence changes were seen when the polymerase was omitted from the assay in either the absence or presence of NTPs.

When this experiment was repeated with $3D^{pol}$ W5L there was only insignificant changes from baseline for all of the 2AP RNA templates (Fig. 5.11). All data fit to the sum of two exponentials but this is more likely due to data inconsistency and scatter than with some specific trend as seen for wild-type. The fluorescence change associated with 0 μM, indicating k_{-1}, was between scattered between 7 and 16 seconds for each RNA template and 8 to 12 seconds for EC_{+4} formation (Table 5.5).

5.2.5 There is a detectable fluorescence change associated with 2-aminopurine treading through the active site of $3D^{pol}$

Using rapid stopped-flow, I monitored the change in 2AP fluorescence during elongation of PETE RNA. Experiments were completed similarly to the stopped-flow elongation rate experiments in Chapter 3 where EC_{+4}s were preformed, diluted 10-fold, and then mixed via rapid stopped-flow with various NTP concentrations. Upon the addition of NTPs, all data traces showed a signal increase as 2AP becomes un-stacked moving, giving off its maximal fluorescence signal, followed by a decrease as 2AP becomes completely base stacked and base paired giving off its minimal signal (Fig. 5.12). When comparing the data traces from each RNA template, the ap3 data trace showed an immediate increase, suggesting that at the +2 position 2AP mostly or

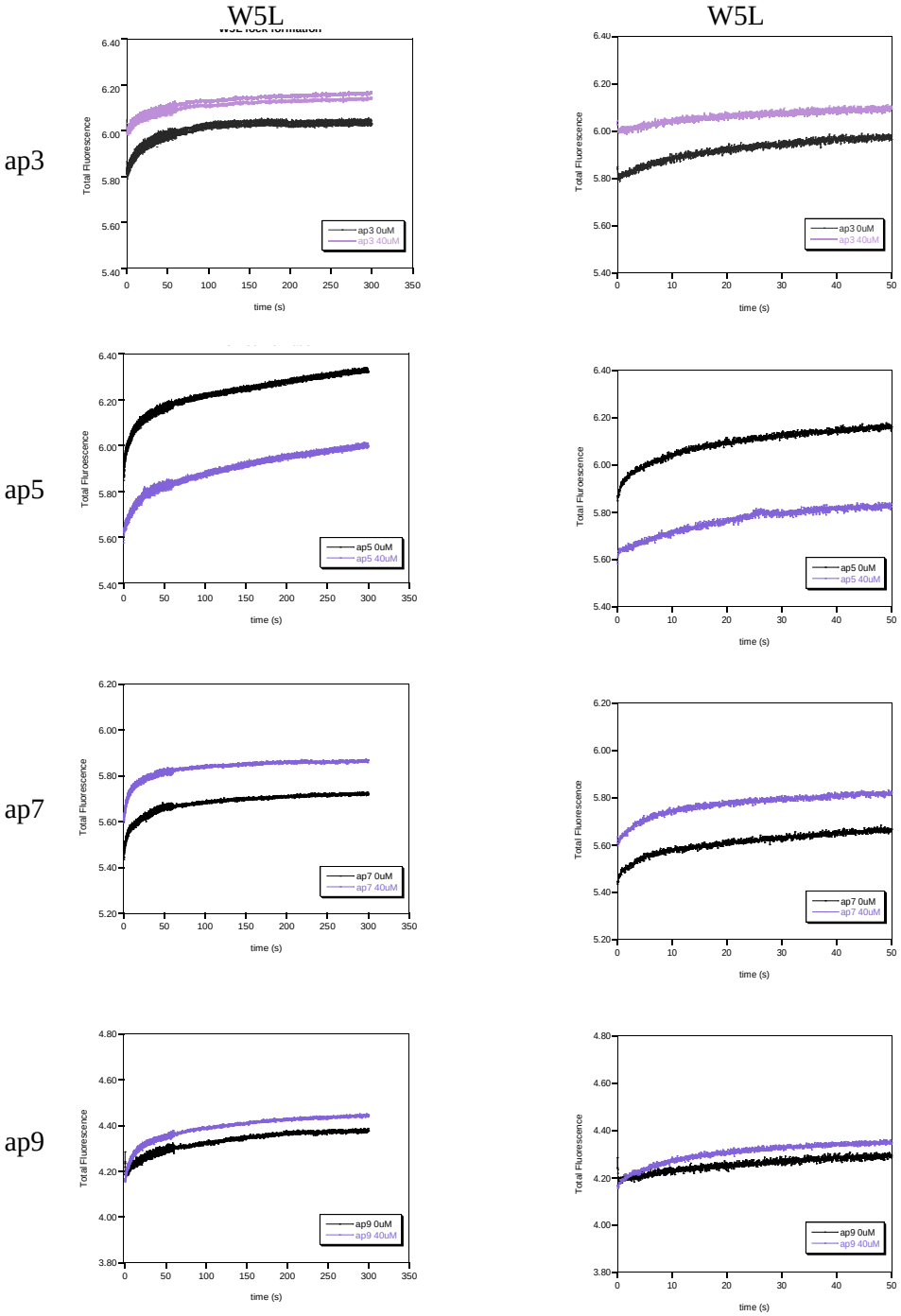

FIG 5.11. 2AP fluorescence during W5L EC_{+4} formation. Graphs show W5L $3D^{pol}$-RNA + (purple) or – (black) NTPs Data was collected by injecting equal volumes of +/- NTP solution and preformed $3D^{pol}$-RNA complex via rapid stopped flow. Reactions were monitored for 200 s (*left*). Early characteristics can be seen in the first 50 s (*right*). Each experiment was done in triplicate or greater

Table 5.5 2AP W5L EC_{+4} formation kinetics

2AP template EC formation by W5L $3D^{pol}$					
RNA	**curve**	**1st exp**	**1st amp**	**2nd exp**	**2nd amp**
0 µM NTPs					
ap3	double	7.1	0.06	48.9	0.16
ap5	double	11.3	0.19	243	0.31
ap7	double	11.8	0.12	100	0.11
ap9	double	16.6	0.06	137	0.14
RNA	**curve**	**1st exp**	**1st amp**	**2nd exp[a]**	**2nd amp[a]**
40 µM NTPs					
ap3	double	12.1	0.05	89.6	0.10
ap5	double	12.9	0.15	278	0.35
ap7	double	5.7	0.13	58.7	0.11
ap9	double	8.7	0.17	110.6	0.16

[a] dissociation modeled in Fig. 5.14

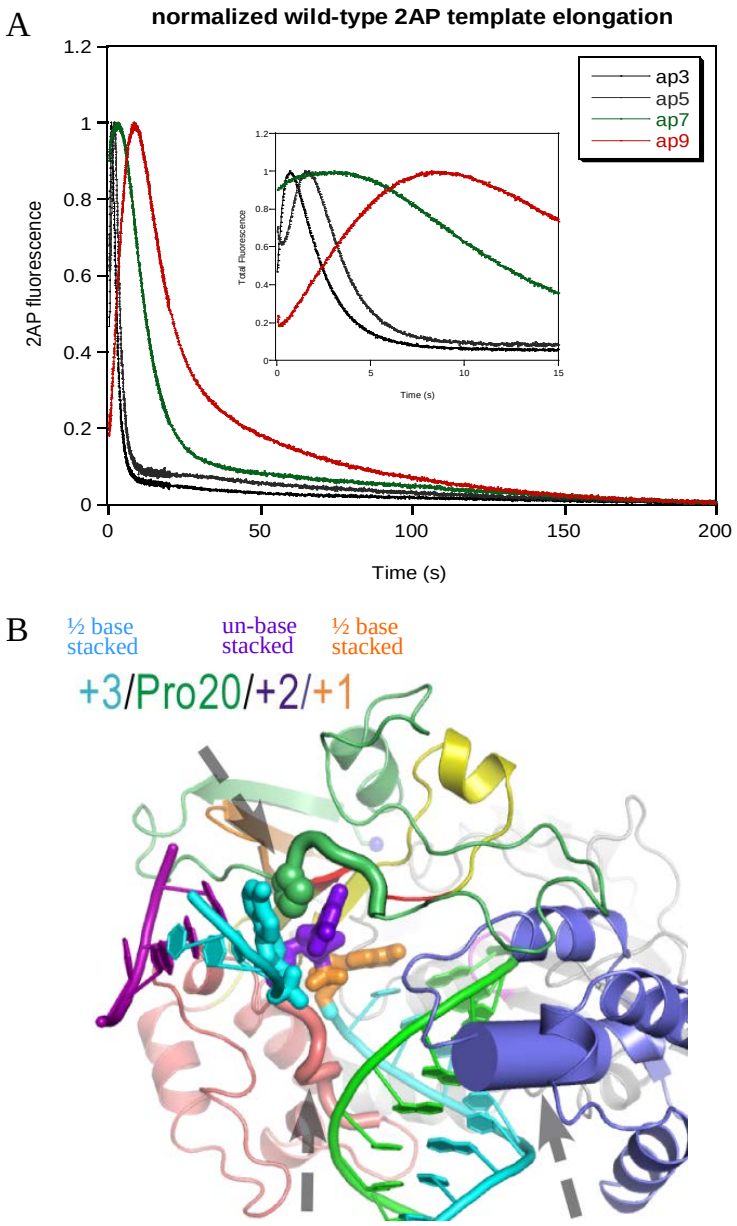

FIG 5.12. 2AP fluorescence associated with 3D^{pol} elongation. (A) Fluorescence signal from each 2AP RNA template (Fig 2.3) by wild-type 3D^{pol}. Elongation was initiated by the addition 5 µM NTPs to preformed EC_{+4}s in rapid stopped-flow format. Elongation was monitored for 200 seconds. Inset shows first 15 seconds for comparison of peak fluorescence intensities: ap3, ~0.7 s; ap5, ~1.7 s; ap7, ~3.1 s; ap9, ~8.2 s, for an overall rate of ~1.5 nts/second (B) Crystal structure of PV 3D^{pol} EC showing the single stranded RNA template threading through the active site. +3 (cyan), +2 (purple), and +1 (orange) nucleotides are shown in thick stick representation. Structure from *Gong and Peersen. 2010. PNAS.* (60)

completely un-stacked. ap5, ap7 and ap9 traces show a lag phase indicative of time for the 2AP to reach the +2 position (Fig. 5.12A). The replication rate on each template can be calculated by dividing the 2AP-2 starting position by the time it takes to reach maximum fluorescence, resulting in an elongation rate of ~1.5 nt/sec (Fig. 5.12A inset). The peak intensities broaden for templates where the 2AP starting position is further from the active site, indicating a larger distribution of states in the elongating population. A direct comparison between wild-type and W5Y mutant shows that there is very little difference between elongations of any of the templates with the exception of ap7 which has a smaller amplitude for the increase compared to the other RNA templates (Fig. 5.13).

Data traces of an NTP series on the ap9 template with wild-type, W5Y and W5L were subtracted by the terminal value and show that the lag phase shortens as NTP concentrations increase until a V_{max} is reached between 80 and 120 μM NTPs. Overall, the signal to noise was significantly lower for W5Y and W5L mutants, due to EC instability (Fig. 5.14). With these data and data shown in Fig. 5.12 I attempted to design a mathematical equation that could model the data based on discrete fluorescence intensities for each downstream NTP position. However, kinetic modeling of data traces was unsuccessful due to difficulty in associating each nucleotide position with the relative to the active site +3 → +2 → +1 → -1 with a specific amplitude, or vice versa. Because I could not model an absolute value for elongation through the active site, it was impossible to mathematically elucidate mutation-induced changes in signal due to interactions outside the active site, so data can only be analyzed by visually.

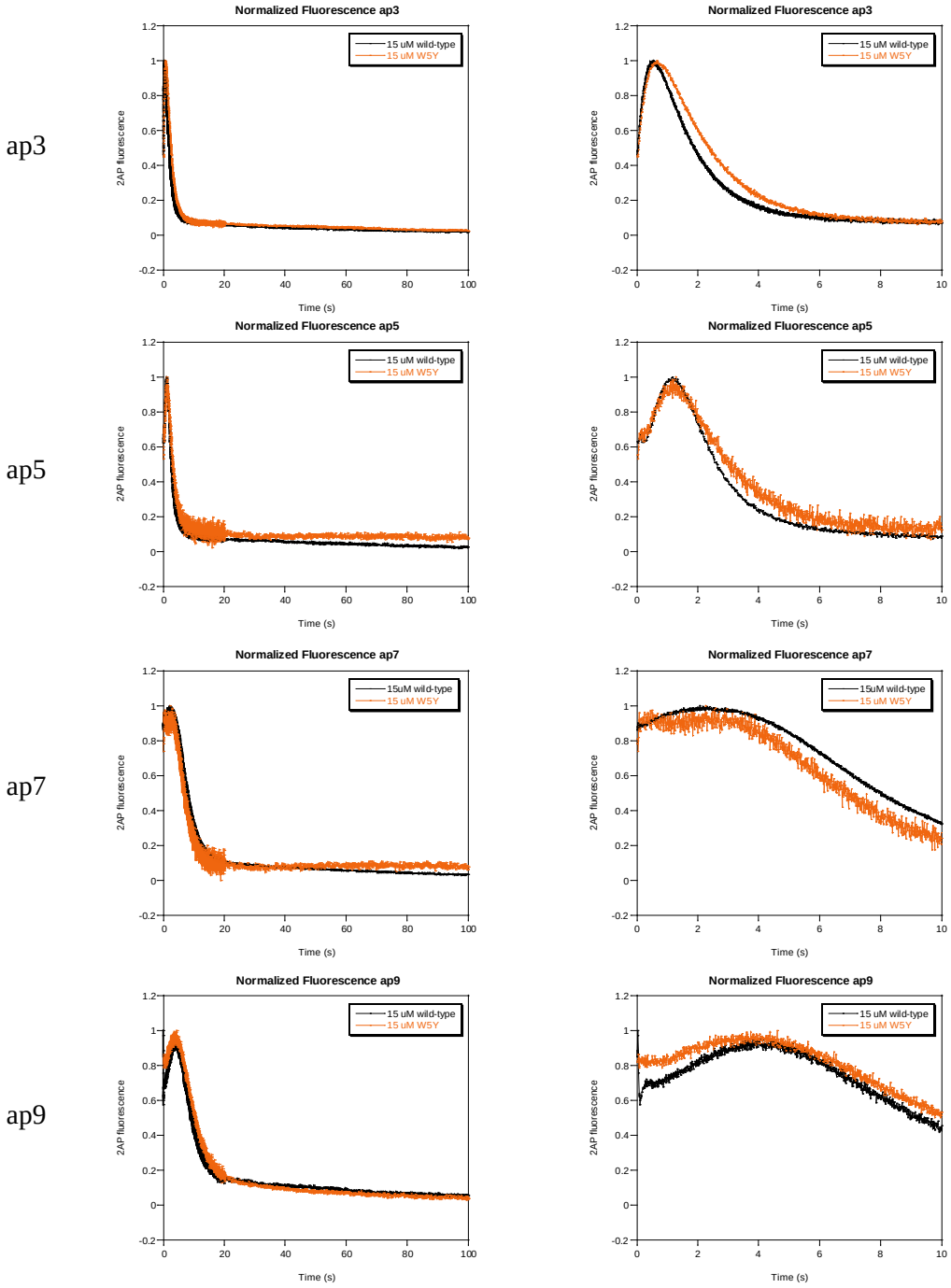

FIG. 5.13. Comparison of normalized 2AP signals during elongation. Graphs show 2AP template by wild-type (*black*) and W5Y (*orange*) in the presence of 15 µM NTPs. Data was collected by injecting equal volumes of +/- NTP solution and preformed EC_{+4} via rapid stopped-flow. Reactions were monitored for 100 s (*left*). Early 2AP characteristics can be seen in the first 10 s (*right*) and show peak intensities relative to 2AP position in the RNA template.

wild-type

W5Y

W5L

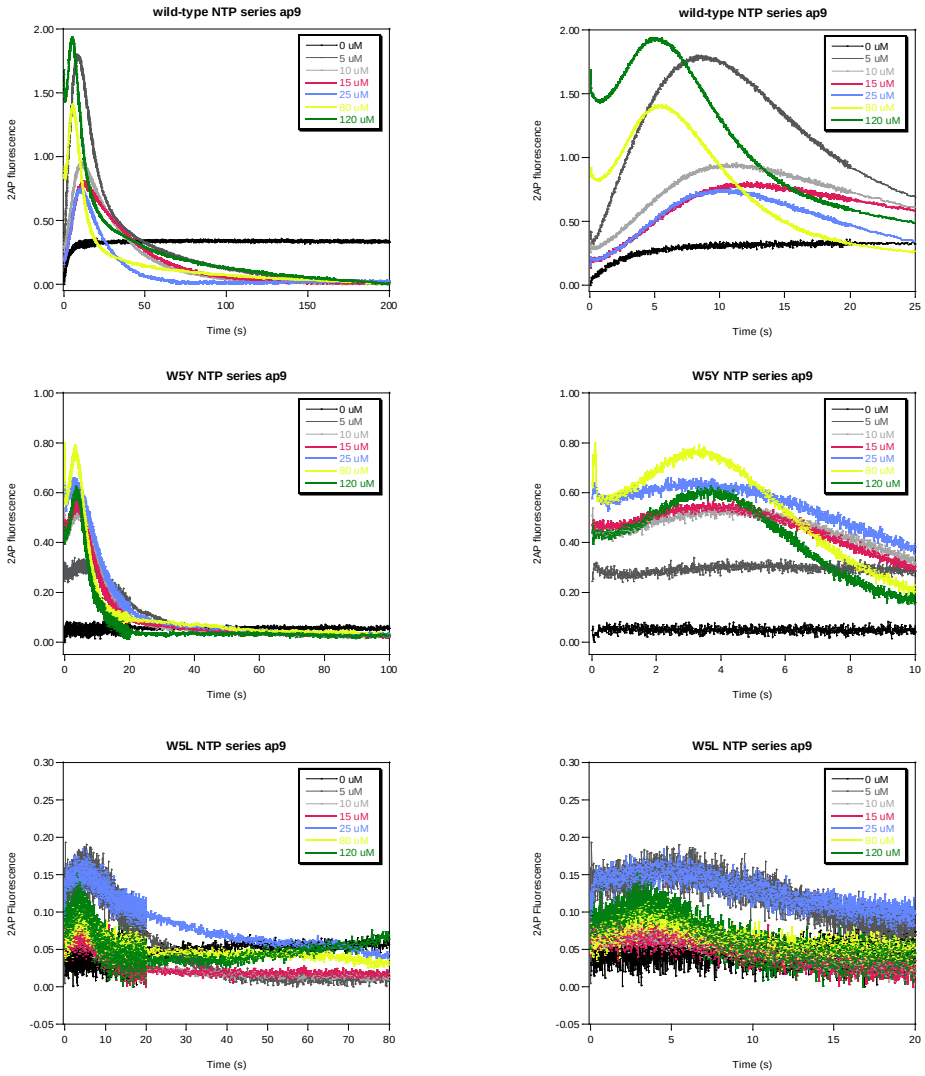

FIG 5.14. NTP series on ap9 template by wild-type and residue 5 mutnats. EC_{+4} were formed as previously described for 15 minutes, diluted 10-fold for sample loading then 2 fold upon injection with NTPs. Data collected by rapid stopped-flow for 80-200 s (*right*) and show elongation of ap9 RNA templates by (A) wild-type, (B) W5Y and (C)W5L. Date demonstrate expected increase and decrease for elongation by all polymerases but peak intensities are difficult to discern for the very instable W5L mutant ECs.

5.3 Discussion

In vivo, picornavirus genome replication requires a processive RNA-dependent RNA polymerase (RdRP) that is able to replicate through extensive RNA structures (89). Currently, the structural aspects that enable the polymerase to replicate through extensive RNA structure are unknown. Some reports speculate viral protein 2C may act as a helicase to aid in dsRNA unwinding (135, 136) while other reports show that $3D^{pol}$ is able to unwind large segments of dsRNA single-handedly (35). In Chapters 3 and 4 we illustrated that mutations at PV $3D^{pol}$ residue 5 have significant effects on elongation complex (EC) stability and replication processivity. In this work, we have investigated the modulation of EC stability by interactions of the PV $3D^{pol}$ with downstream RNA and the number of nucleotides incorporated during EC lock formation. We saw in Chapter 4 that downstream 5' NTR, an element of extensive RNA structures, had significant effects on polymerase processivity. Also, the PV $3D^{pol}$-RNA co-crystal structure shows that residue 5 is in a position that could potentially interact with the RNA template or downstream duplex (Fig. 5.1) (60).

To determine the effects of downstream duplex on EC formation, replication rate and EC stability, we utilized double hairpin RNA templates where one hairpin provided the 3'OH primer and the other hairpin provided a downstream duplex to simulate RNA structures (Fig. 2.3). The EC_{+4} formation assays showed that downstream duplex had very little effect on EC formation (Table 5.1). When stable ECs were chased, after 15 minutes of formation, wild-type and residue 5 mutants were able to efficiently replicate through the duplex at similar rates, about 15 nts/min (Fig. 5.3). These rates were slightly slower than the replication rates through a ssRNA template that was analyzed by PAGE

in similar conditions, likely due to high NaCl concentrations favoring RNA structure requiring more energy to replicate through duplex.

In Chapter 4, I found that replication of the PV genome was severely impaired for residue 5 mutants by the presence of multiple abortive products during RNA replication in high salt. I hypothesized that this was due to extensive RNA structure and showed that when we remove the 5' NTR including the IRES (an element of highly structured RNA,) replication through the genome was much more efficient, while EC stability was not changed. Stability assays performed on smaller RNA templates with downstream duplex RNA showed that the presence of a downstream duplex significantly enhanced the stability for W5Yand W5F but not for wild-type and W5A (Fig. 5.5 and Table 5.2). However, the wild-type stability was difficult to determine because the polymerase was so stable after a +4 lock that only very small amplitudes were curve fit (Fig 5.5). As history has shown, it is most likely that the wild-type polymerase would behave like the W5Y and W5F polymerases when taken out to longer time points. The fact that the W5A mutant was not significantly affected by the presence of a downstream duplex suggests that residue 5 has stability effects on $3D^{pol}$ interactions with the downstream RNA or downstream duplex. Also interesting was the significant increase in W5A EC_{+4} stability when comparing the single-stranded control RNA used in this experiment to the ssRNA template (PETE 9+2_24) that was used previously (Chapter 3) to determine EC_{+2} stability. This result indicates that EC_{+4} is more stabilizing that EC_{+2}, which can somewhat overcome the devastating effects a residue 5 mutation has on polymerase stability.

To more directly compare how the number of nucleotides incorporated upon EC formation affected stability, we used the dblPETE RNA templates (8+4_3+8_3 and 8+4_0+9) and the ssRNA PETE control (8+4_3_3) to vary the nucleotides incorporated by +1, +4, or +7 depending on a pre-incubation with ATP, ATP and GTP, or ATP, GTP and UTP, respectively. These experiments showed that for all $3D^{pol}$-ECs the EC_{+4} was 2-3 fold more stable than the EC_{+1} and 2-120 fold more stable than the EC_{+7} (Fig. 5.7 and Table 5.3). The most unstable complexes for all polymerases were generated by EC_{+7} on the ssRNA control, where after the incorporation of 7 nucleotides there are only 3 template nucleotides remaining. This suggests a requirement for significant downstream RNA contacts to maintain a stable complex. This was not surprising as a previous report from our lab showed that the PV $3D^{pol}$ on a similar ssRNA template, 5' end labeled with a fluorescein, the polymerase came into contact with the fluorescein when the polymerase was positioned 5 nucleotides from the end (59). The result that the EC_{+7} was less stable than either EC_{+4} or EC_{+1} on the longer dblPETE templates was surprising because the downstream contacts should still be intact and able to contribute the stabilizing effects. Even if the downstream duplex was no longer intact, we would expect the EC_{+7} to be at least as stable as the EC_{+4} on the ssRNA control; instead, it was significantly less stable. The fact that the EC_{+7} is much less stable than EC_{+4} is either due to a conformational change in the polymerase or differences in RNA contacts or sequence. For example, it could be that there are conformational changes associated with strand displacement that make the polymerase less stable. In support of this is the comparison of EC_{+7} on dblPETE 8+4_0+9 and EC_{+4} on dblPETE 8+4_3+8, which should be nearly identical in polymerase-RNA contacts; the only differences are the number of nucleotides

incorporated (+4 vs. +7) and the nucleotide composition at the +1, +2 and +3 positions, which are shown in the PV $3D^{pol}$ EC to interact with the polymerase (60). However, the results showed EC_{+7} was significantly less stable than EC_{+4}; therefore, either the act of displacing 3 RNA bases, during formation of EC_{+7}, or the composition of nucleotides in positions +1, +2, and +3 determines EC stability. In this experiment the three single stranded template nucleotides threading through the active site are 3'-AAG-5' for EC_{+7} and 3'-GGU-5' for EC_{+4}. There has been evidence of abortive sequences for other polymerases, for example, T7 has an abortive sequence 5'-TATCTGTT-3' (96). However, no such data exists for the PV $3D^{pol}$ nor other related RdRPs. Therefore, further biochemical studies are needed to determine if sequence specific effects are responsible for the EC stability differences. The importance of template nucleotide sequence could be tested by repeating stability experiments on RNA designed to look have different template sequences after the same lock length.

To further investigate $3D^{pol}$-RNA interactions we incorporated 2-aminopurine (2AP), a fluorescent adenine analog whose signal can be quenched by stacking interactions, into our PETE RNA at various positions (ap3, ap5, ap7 or ap9). Our rationale was if downstream nucleotides had a stacking interaction with residue 5, then we would see 2AP fluorescence quenched by aromatic residue at position 5; alternatively if the polymerase interacted with the phosphate backbone this could result in a more solvent exposed 2AP we would see higher fluorescence intensity.

It has been shown for both PV and FMDV picornavirus polymerases that EC formation is a rate limiting event associated with a conformational change in the polymerase resulting in a very stable complex (7, 9). This conformational change could

create or change the interaction between $3D^{pol}$ and the RNA which could be detected by monitoring EC formation with the 2AP RNA templates. Since, EC formation on these templates was designed to be the addition of the first four nucleotides, the data traces from this experiment show the movement through 4 nucleotides before being stalled. The movement, described by the starting and ending position of 2AP for each template is as follows: ap3, 7→3; ap5, 9→5; ap7, 11→7; ap9, 13→9. The secondary structure predictions based on the new UNAfold program show that for each of the 2AP RNA templates there are two possible hairpins, the designed 9 bp priming hairpin and a second 3 bp downstream hairpin that is unable to exist after the lock because the bases are interacting with the polymerase (Fig. 5.8). Thus, ap3 and ap9 could have a somewhat quenched fluorescence signal upon $3D^{pol}$ binding, but should increase upon formation of EC_{+4}, while ap5 and ap7 templates should have no change in fluorescence unless a 2AP interacts with the polymerase.

Upon addition of NTPs the results showed the expected fluorescence increase for ap3, ap7 and ap9 RNA templates indicating formation of the EC (Fig. 5.10). Interestingly, the 2AP fluorescence from the ap5 template was quenched compared to the addition of 0 μM, indicating an alternative RNA conformation upon EC formation that can be detected by the ap5 template (Fig. 5.15 states 3 and 4). Since it is known that there are conformational changes associated with EC formation (9) it is likely that the 2AP at position 5 is sampling different environments caused by a conformational change within the polymerase upon addition of NTP. Curve fits of the fluorescence data showed that ap3 and ap5 exhibited the sum of two exponentials, indicating that there are two events taking place (Table 5.4). The first exponential for all these data is likely the EC_{+4}

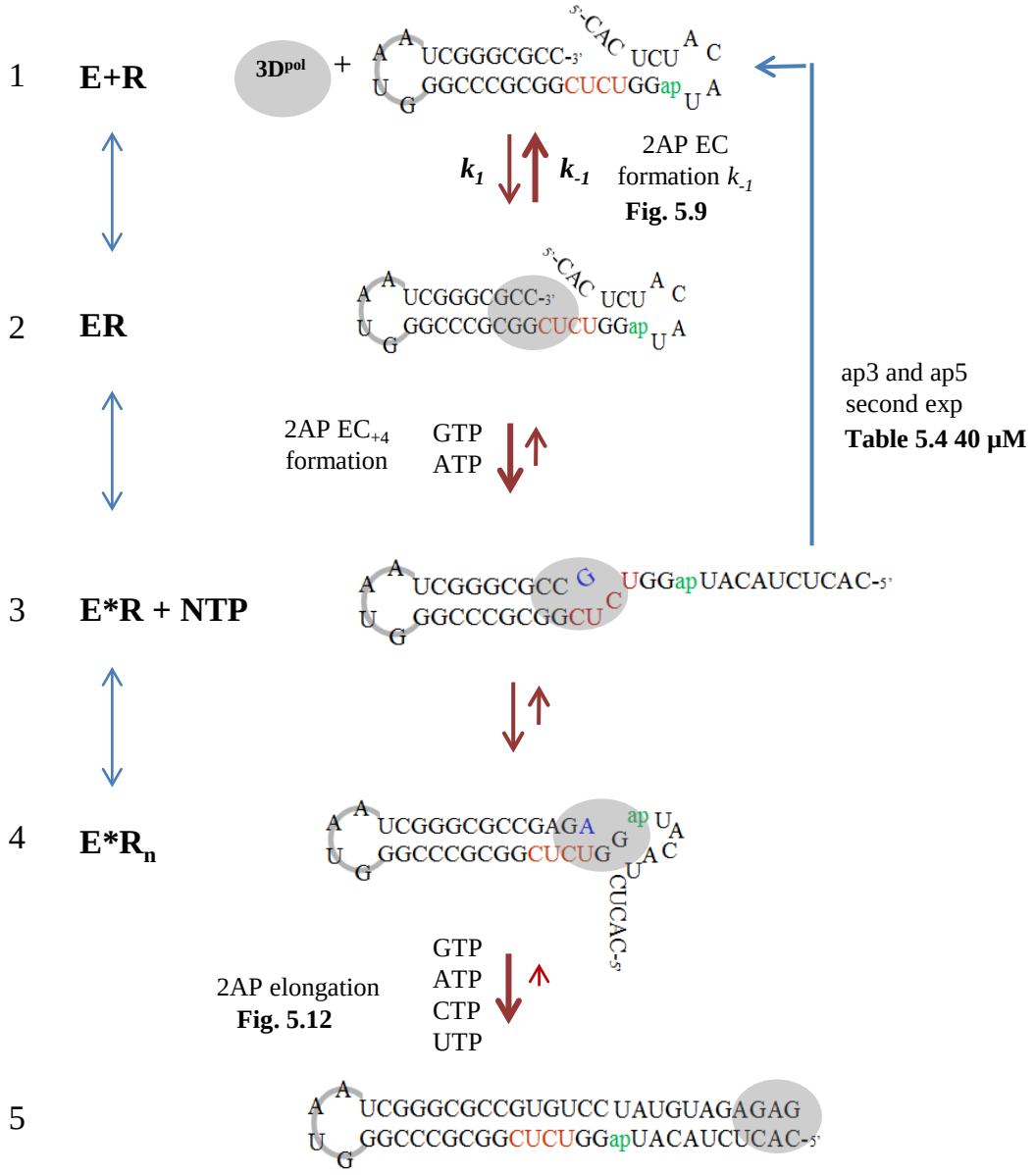

FIG. 5.15. Final model of EC formation with data adaptations. The EC formation model from Fig. 5.9 has been adapted to correlated data from this chapter associated with each step or state. The added state 5 is associated with RNA elongation.

formation rates while the second rate for ap3 and ap5 are the dissociation rate of the EC_{+4} which is ~3-5 fold slower than the dissociation rate of the RNA-$3D^{pol}$ complex alone, which is similar to previous reports (9). This second exponential was not seen for the ap7 and ap9 templates most likely because the 2AP is too distant to show these interactions. When these experiments were repeated with the W5L mutant there was no significant change in 2AP signal compared to the 0 μM NTP control (Fig. 5.11 and Table 5.5). This could indicate a loss of interaction between the RNA and residue 5, or residue 5 could be providing some structural maintenance of $3D^{pol}$ required for RNA interactions elsewhere on the polymerase. However, I cannot rule out that this polymerase may just be too unstable to monitor formation EC_{+4} in the stopped-flow format.

As 2AP RNA templates are elongated, the predicted fluorescent traces of 2AP movement through the active site were seen, based on the PV EC crystal structure showing +3, +2 and +1 nucleotides in a stacked, un-stacked, stacked orientation, respectively (Fig. 5.12) (60). I attempted to fit these data traces, particularly ap3 since the interactions of the nucleotide at position 3 are known (60), to a kinetic equation that reported on 2AP threading through the active site. The reason being that if I could determine the amplitude and kinetics of 2AP at positions +3, +2, +1 and -1 then I could monitor changes in data traces that were independent of the active site fluorescence changes. Specifically, I expected to see early, unpredicted, fluorescence changes that suggested $3D^{pol}$-RNA interactions beyond the active site and that these may be changed by the W5 mutations, indicating this residue was contributing to downstream RNA contacts. The traces from elongation by the wild-type polymerase on all four RNA templates (ap3, ap5, ap7 and ap9) showed the predicted fluorescence increase and

decrease as the template RNA moved through the $3D^{pol}$ active site. Replication rates, determined by the time to reach maximum fluorescence (2AP to reach position +2), was similar for each RNA template (Figure 5.12A). However, although the data were clean and repeatable, the kinetic modeling proved to be problematic in that a set of successive amplitude could not be fit to any two data traces. This was likely due to the fact that there are multiple intermediate RNA-polymerase interactions (see Fig. 5.15 step 3 for model). Since 2AP is very sensitive to environmental changes, we can only properly fit obvious changes from the data traces, making it difficult to model the more comprehensive analysis we had hoped for.

Comparing the data traces of wild-type and W5Y from the four RNA templates, we found very little evidence of alternative interactions between the two polymerases (Fig. 5.13). However, for both polymerases the ap7 template seems to have smaller amplitude associated with the increase. This could indicate that when $3D^{pol}$ is stalled on the ap7 template after EC_{+4} formation, the nucleotide at the +7 position has fewer stacking interactions than when at the +3, +5 or +9 positions. Alternatively this could be a characteristic of this particular RNA construct. To determine such interactions more RNA templates would need to be synthesized with 2AP at alternative positions and examined for elongation.

To elucidate whether fluorescence changes were dependent upon residue 5, I monitored elongation of ap9 with various NTP concentrations for wild-type, W5Y and W5L $3D^{pol}$ enzymes. The 2AP fluorescence data in Figure 5.14 show that the signal to noise was too low to determine the peak signal intensity for most of the W5L data traces,

making it difficult to elucidate any differences in early interactions. Thus, it remains unclear whether interactions with wild-type and W5Y would be affected by residue 5.

In conclusion, these data show that $3D^{pol}$ EC stability can be modulated by downstream RNA interactions and EC lock length. Some of these interactions are stabilizing, as seen by with the downstream duplex, and some are destabilizing, such as the interaction when the dblPETE template EC_{+7}. I have also shown some evidence for structural rearrangement of RNA during EC formation via RNA-$3D^{pol}$ interactions on 2AP RNA templates. In any case, it is not exactly clear whether downstream RNA interactions or rearrangements are *directly* with or affected by residue 5 or with some other area on the polymerase. In all, these are the first reported data that indicate $3D^{pol}$ interactions exist with the downstream RNA template beyond the polymerase active site.

.

Chapter 6

Discussion and Future Directions

6.1 Introduction

RNA viruses are responsible for many acute and chronic diseases in humans, plants and animals. The enzyme responsible for replication of viral RNA genomes is the RNA-dependent RNA polymerase. Due to its uniqueness to the virus and requirement for viral multiplication, the RdRP is considered an ideal enzyme for a drug target and has therefore, been the subject of much antiviral research. As novel RNA viruses are continually emerging (128) and more information is being discovered about the RdRP, the poliovirus (PV) RdRP has proven to be an important model enzyme for elucidating structure-function relationships in all RNA virus RdRPs.

Results presented in Chapters 3-5 have advanced the field in the area of structure-function relationships of the picornavirus RdRP. Experiments have demonstrated that residue 5 of the poliovirus (PV) RdRP is required for elongation complex (EC) stability and processive elongation of the PV RNA genome. Furthermore, I showed evidence of PV polymerase interactions with downstream RNA and show that EC lock length and downstream duplex also a role in EC stability. In this chapter I will discuss how these findings have filled in some gaps within the field and touch on some future directions that will be important for further elucidation of structure-function relationships of $3D^{pol}$.

6.2 The Picornavirus Replication Complex Stability and Processivity

In the host cell, PV replication is extremely robust, reaching upwards of $5.0x10^5$ copies of the positive-strand genome within six hours post infection (112). This level of replication requires that the polymerase be highly active and processive. In 2000 Arnold and Cameron described the assembly of the PV $3D^{pol}$ stable elongation-competent complex as the enzyme-RNA-1^{st} NTP complex (9). The incorporation of the first nucleotide is a rate-limiting step in replication that results in a complex that is >4 fold more stable than the enzyme-RNA complex before nucleotide incorporation. This step of initiation is required for processive elongation (9). However, to date there has been very little data collected on the processivity of the PV $3D^{pol}$. In 2001, Rodriguez-Wells *et al* (134) described a study where the processivity of PV $3D^{pol}$ was directly measured via primer extension. The authors reported that the $3D^{pol}$ was a highly processive polymerase based on the observation that the primer extended to a final product of 1388 nucleotides (134). However, the resolution obtained from the denaturing PAGE where the replication products were analyzed was <800 nucleotides, so abortive products between ~700-1388 nucleotides could not be resolved (Fig. 6.1). This is not to say that the PV polymerase is not processive, but it could be that the polymerase only replicates about 1000 nucleotides on average before dissociation rather than the one initiation event per genome replication proposed by the authors of this study. An earlier report, that investigated the unwinding capabilities of PV $3D^{pol}$, indirectly reported on the processivity of the polymerase using a method similar to 3' self-priming method I used in Chapter 4 (35). In that study the authors transcribed a long (nucleotides 4600-7500 of the positive-strand genome) RNA template from PV cDNA using T7 RNA polymerase and showed that when the template

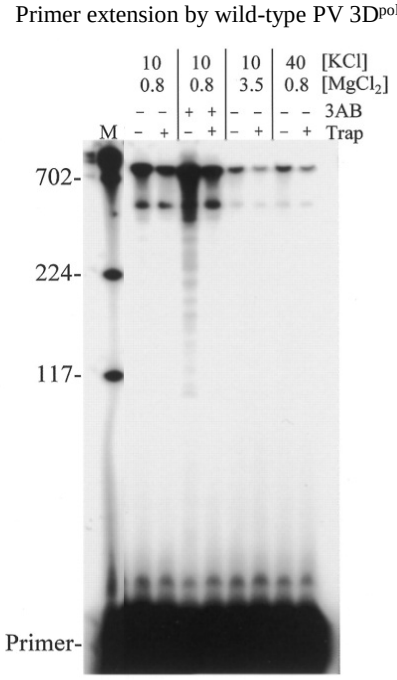

FIG. 6.1. Analysis of primer extension by wild-type PV 3D^{pol}.
PAGE of primer extension used to show that PV 3D^{pol} is a processive polymerase. Reactions were performed by incubation of 13 nM 3D^{pol}, 5 nM template/primer, 50 µM NTPs for 1 hour at 30^{o}C Reactions used a 1499 nucleotide template and a 20 nucleotide 5'-^{32}P-labeled RNA primer. Full primer extension results in 1388 nucleotide product. PV protein 3AB was added in some cases to monitor changes in processivity. A heparin trap was added in some cases to prevent reinitiation. Reaction products were analyzed by 6% denaturing PAGE. Figure adapted from *Rodrigues-Wells et al 2001*. *Nucleic Acids Res*. (134)

alone was incubated with $3D^{pol}$ and NTPs a predominant product roughly twice the size of the template was made suggesting that the 3' end of the template was snapping back to form a hairpin primer (35). The products of these reactions were very homologous, suggesting that the snap-back was very specific, whereas in the similar experiment I performed I had two initiation sites, represented by the tow bands shown in Fig. 6.2B. However, this can likely be explained by different reaction conditions, where my reactions were completed in high NaCl concentrations favoring RNA structures and possibly alternative snap-back structure.

The significance of my data is that a residue at the N-terminus of the poliovirus polymerase is required for processive elongation. I showed that PV residue 5 was involved in the stability of the elongation complex and that EC stability had directed effects on processivity. My results presented in Chapter 4 showed that the wild-type $3D^{pol}$ was very processive, having only a few abortive sites during replication of the first 2201 and 5424 nts of the RNA genome and that residue 5 of the polymerase has significant involvement in its processivity. Also, in collaboration with the Barton lab in Denver, we showed that the less processive mutants greatly affect the ability of the infectious virus to replicate in a cell-based assay. To my knowledge, this is the first report directly characterizing a specific residue of the PV $3D^{pol}$ involved in processivity based on assays complete with sub-genomic RNA templates. Also novel, was the finding that removal of the 5' non-translated region (NTR) of the genome (nucleotides 15-1123), which contains areas of extensive RNA structure, increased processivity of the wild-type and residue 5 $3D^{pol}$ mutants.

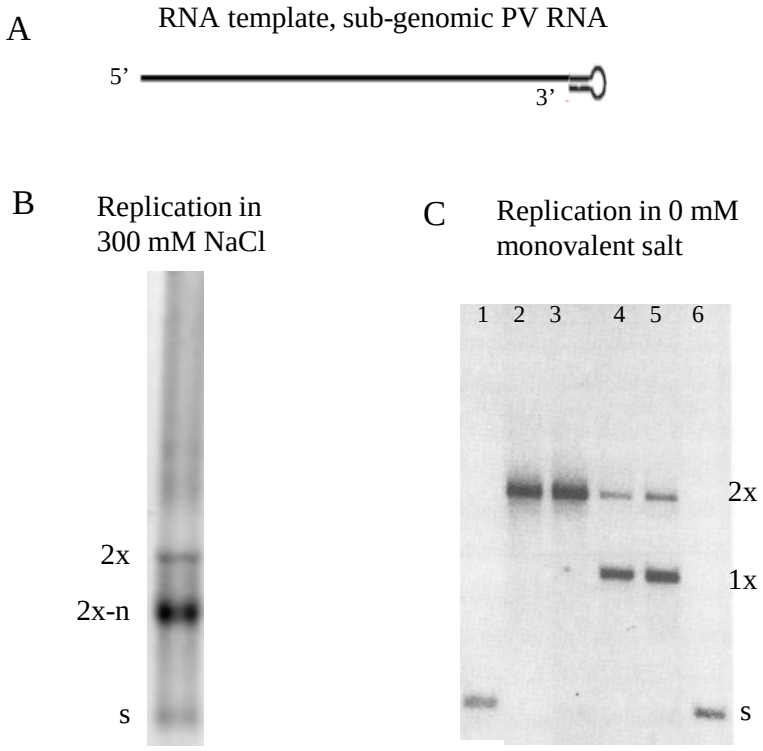

FIG. 6.2. Snap-back/self-primed RNA template elongation. (A) Schematic of PV sub-genomic RNA used in self-priming elongation experiments, analyzed by gels in B and C. 5’ NTR and 3’ poly(A) tailwas removed and 3’ end forms snap-back has hairpin structure. (B) Alternative priming from two different snap-back structures, adapted from Fig. 4.6, showing that in high NaCl there can be multiple priming sites. In this gel there are two bands one (2x) represents the larger product that is likely twice the size of the starting material (S). The second band (2x-n) is from an alternative priming sight that primes upstream (n) of the 2x band and is more abundant in this particular experiment. (C) Agarose gel showing elongation of single snap-back priming site. Adapted from *Cho et al. 1993. J. Virol*. Lanes 1 and 6 marker, 2 and 3 elongation, and 3 and 4 marker are repeats. 2x is a product twice the size of the starting material (S). 2x-n is twice S minus some *n* number of nucleotides from alternative snap-back structure. (35, 71)

In Chapter 5, I investigated the reactions with downstream RNA and found that PV $3D^{pol}$ does interact with downstream RNA but the extent to which residue 5 is involved remains unclear. This is likely due to the fact that downstream interactions are transient and thus difficult to discern for polymerases that are non-processive and unstable in a stalled complex. These intermittent interactions could be due to a conformational change with in the polymerase which changes the orientation of the RNA in the entry channel. This is the first evidence for PV RNA-$3D^{pol}$ interactions outside of the RNA binding site (31), but would not be the first report of a conformational change for the reorganization of the viral RNA (9, 26). Beckman and Kirkegaard (26) were the first to describe a conformational change in the polymerase upon RNA binding, determined by changes in IC_{50}s when binding RNA oligos of different lengths. Later Arnold and Cameron (9) used AMP incorporation into a primer/template to determine the rate of the conformational change to be ~0.08 s^{-1}, similar to the off rate described by my 2AP EC formation assays of ~0.1 s^{-1}.

6.3 Future Directions

6.3.1 Effects of Zn^{++} on EC stability

PV $3D^{pol}$ residue 5 has significant effects on viral replication processivity via aiding in the stability of the elongation complex. However, the structural details as to how residue 5 is affecting polymerase stability are still unknown. The crystal structures of the coxsackievirus and poliovirus polymerases show that there is a conserved β-strand distortion and large hydrophobic residue at position 5 (32, 152). Adjacent to residue 5 there is a hydrophobic pocket into which residue 5 could possible rotate in to, burying the hydrophobic residue and resolving the β-strand distortion into a β-sheet with the middle

finger. However, we have seen no evidence of such structural changes even after the solving the structure of a $3D^{pol}$ elongation complex (60). However, also adjacent to this β-strand distortion at position 5 is a group of amino acid side chains presented on the middle finger that have possible metal binding geometries, specifically to Zn^{++} (148) having two histidine (residues H270 and H272) and a cysteine and possibly glutamine (residue 4) (Fig. 6.3). Zn^{++} binding sites such as these commonly play a role in the structural stability of a protein (148). In this case, mutations to residue 5 of the polymerase could change or affect the geometries of the adjacent metal binding site affecting the overall structural stability of the polymerase. However, most reports show that higher concentrations of Zn^{++} in the cell inhibit picornavirus replication but it is not clear if these increased Zn^{++} concentrations have any direct effect on the polymerase (82, 87, 126). More recently Zn^{++} has been shown to bind, directly to and inhibit the Coronavirus RdRP to prevent RNA binding (150), however, these assay did not investigate possible effects the RdRP after binding. It could be that Zn^{++} aids the polymerase some structural rigidity that inhibits binding but could be beneficial after RNA binding to form a stable elongation complex.

6.3.2 Abortive elongation "hot-spots"

When investigating polymerase processivity in Chapter 4, I pointed out a few abortive "hot-spots" during replication of the sub-genomic RNA. It would be interesting and novel to investigate the sequence or RNA structure of these "hot-spots". There are currently no reports of RNA sequences that are abortive for any RNA virus polymerases. However, there are such sites for the T7 DNA-dependent RNA polymerase (96). As very little is known about RdRP processivity it is reasonable to imagine that abortive

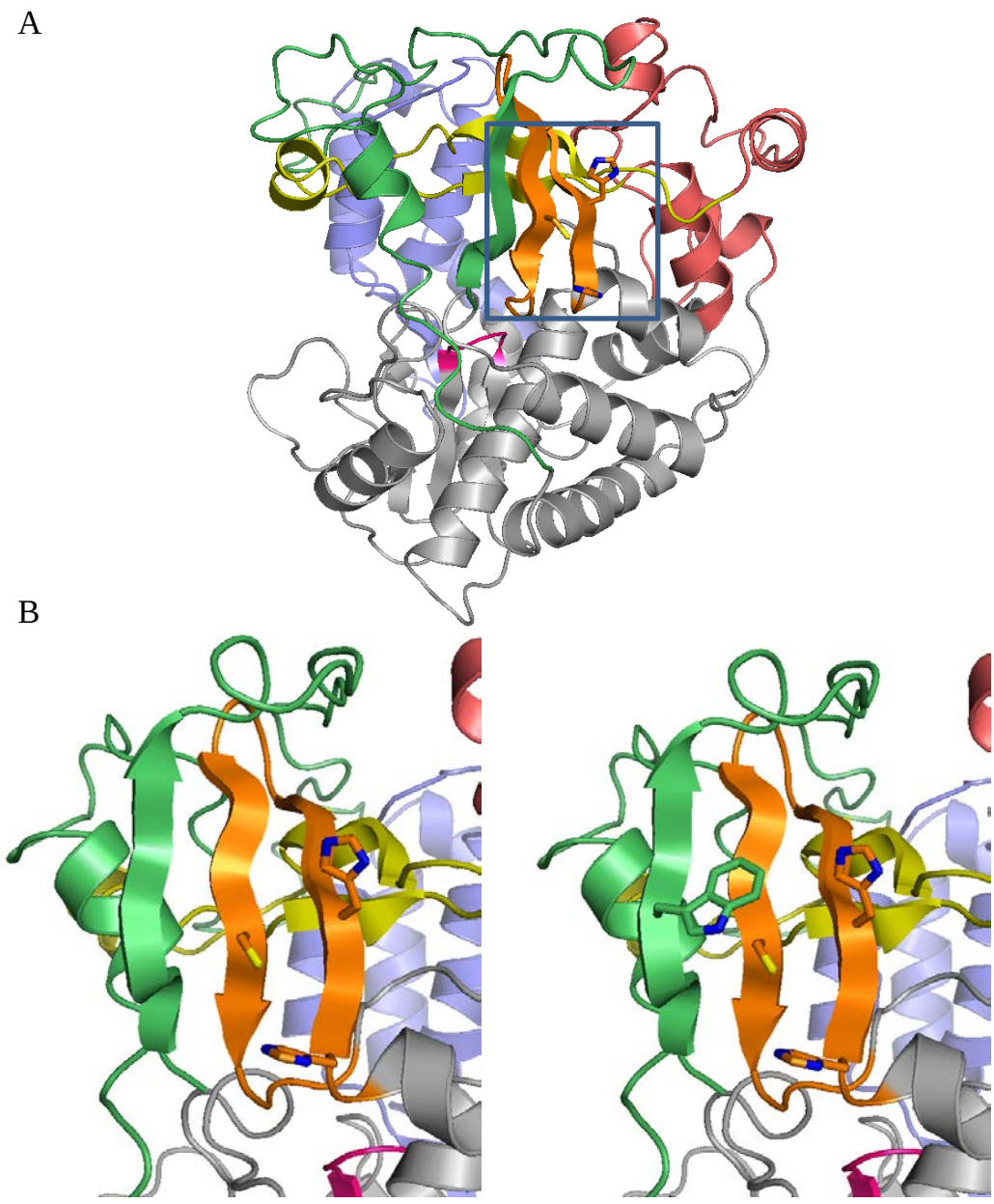

FIG. 6.3. 3D^{pol} crystal structure showing potential Zn^{++} binding site. (A) complete PV 3D^{pol} structure showing rotated slightly from back view to show potential Zn^{++} binding residues on middle finger (*orange*). Residues H270, H272 and C281 are shown as sticks, with nitrogen atoms in blue and sulfur in yellow. (B) close-up of potential Zn^{++} binding site without (*left*) and with (*right*) residue 5 stick modeled.

sequences may exist but are currently undetected. Or these abortive hot-spots could be related to areas of significant RNA structure. Such assays could be performed by generating cDNA copies of abortive products from gel purified RNA bands that can be transformed in to bacteria for plasmid purification. Various bacterial isolates can then DNA prepared and cDNA sequences can be obtained (78). These results would show exactly where the abortive sites are then it could be determined whether or not these sites were sequence dependent or RNA structure dependent. Even though $3D^{pol}$ was able to elongate though extensive structures somewhat efficiently in my processivity assays, in the cell additional viral proteins may be required to relax the RNA for processive elongation, such as viral protein 2C, a known ATPase that could have helicase like activity (136). Thus, smaller abortive products may not be observed incellular viral RNA isolates.

6.3.2 Fidelity of residue 5 mutants

Substantial amounts of research are currently underway to describe the structure-function relationships of the picornavirus $3D^{pol}$ related to fidelity (14, 109, 122, 162). As discussed in Chapter 1, $3D^{pol}$ has no exonuclease activity which results in the enzyme having relatively low fidelity (33). This is commonly thought to be advantageous to the virus as low replication fidelity increases the genetic diversity of the virus population promoting mechanisms of virus evolution generating what is known as quasispecies (73, 153). In 2003, Pfieffer and Kirkegaard found a single point mutation in the PV $3D^{pol}$ that causes resistance to the antiviral ribavirin via increased enzyme fidelity (G64S) (123). G64 is located in the palm domain of the polymerase but is remote to the catalytic active site. This mutation seems to have very little structural significance while having large

effects on enzyme fidelity (14). It could be that residue 5 has some similar effects in that it could affect fidelity while having no structural interaction with the residues involved in catalysis; therefore, it may be interesting to investigate the polymerase fidelity of various residue 5 mutants. It is known that misincorporation decreases the rate of incorporation for the single nucleotide (81); therefore, any extra time spent in a stalled complex during misincorporation increase the chances of dissociation especially by mutants that are unstable. In this case, it would be interesting and novel to correlate polymerase processivity effects on fidelity. Since I have already generated infectious virus with residue 5 mutations, it would be straightforward to perform a comparative fidelity screen using the guanidine-resistance assay (39, 123). As previously described, guanidine HCl is commonly used to inhibit negative-strand RNA synthesis (21) and this can be overcome by single point mutations in viral protein 2C resulting in guanidine resistance (15, 125). These experiments are performed by using high titer stocks to infect cells in the presence of low molar guanidine, if the fidelity of the polymerase increases fewer point mutations will be generate decreasing the frequency of guanidine resistant populations in respect to the wild-type frequency (123). Alternatively, if the fidelity is decreased the frequency of guanidine resistant populations will increase. If different error frequencies were found it might then be interesting to obtain and actual error rate, for which RT PCR and sequence of cDNA could be looked at and/or *in vitro* fidelity could be examined by monitoring misincorporation on our fluorescence PETE RNA by the addition of increasing concentrations of the incorrect nucleotide. Using the PETE assay higher fidelity mutants would require higher concentrations of the incorrect nucleotide to drive misincorporation,

where lower fidelity mutants would incorporate the incorrect nucleotide when present at low concentrations.

6.4 Conclusion

In all, a more complete understanding of the structure-functional relationships of viral polymerases facilitates in the design of specific enzyme inhibitors that could eventually serve as antivirals to aid in restriction of virus-caused diseases and their transmission; therefore, understanding the differences between these viral and cellular enzymes is crucial. The work presented in this dissertation further elucidates structure-function relationships of the PV $3D^{pol}$, the enzyme required for genome replication. Although eradicated in most developed countries, PV is still a medical heath concern in less developed countries causing potentially debilitating poliomyelitis; also, PV $3D^{pol}$ serves as a good model RNA-dependent RNA polymerase for many RNA viruses.

References

1. 1988. Global Polio Eradication Initiative. www.polioeradication.org.

2. **Agol, V. I.** 2002. Picornavirus Genome: an Overview. *In* B. L. Semler and E. Wimmer (ed.), Molecular Biology of Picornaviruses. ASM Press, Washington, D.C.

3. **Agol, V. I., G. A. Belov, K. Bienz, D. Egger, M. S. Kolesnikova, N. T. Raikhlin, L. I. Romanova, E. A. Smirnova, and E. A. Tolskaya.** 1998. Two types of death of poliovirus-infected cells: caspase involvement in the apoptosis but not cytopathic effect. Virology **252:**343-53.

4. **Alvarez, D. E., M. F. Lodeiro, S. J. Luduena, L. I. Pietrasanta, and A. V. Gamarnik.** 2005. Long-range RNA-RNA interactions circularize the dengue virus genome. J Virol **79:**6631-43.

5. **Ambros, V., R. F. Pettersson, and D. Baltimore.** 1978. An enzymatic activity in uninfected cells that cleaves the linkage between poliovirion RNA and the 5' terminal protein. Cell **15:**1439-46.

6. **Arias, A., J. J. Arnold, M. Sierra, E. Smidansky, E. Domingo, and C. E. Cameron.** 2008. Determinants of RNA-dependent RNA polymerase (in)fidelity revealed by kinetic analysis of the polymerase encoded by a foot-and-mouth disease virus mutant with reduced sensitivity to ribavirin. J Virol.

7. **Arias, A., J. J. Arnold, M. Sierra, E. D. Smidansky, E. Domingo, and C. E. Cameron.** 2008. Determinants of RNA-dependent RNA polymerase (in)fidelity revealed by kinetic analysis of the polymerase encoded by a foot-and-mouth disease virus mutant with reduced sensitivity to ribavirin. J Virol **82:**12346-55.

8. **Arner, E. S., and A. Holmgren.** 2000. Physiological functions of thioredoxin and thioredoxin reductase. Eur J Biochem **267:**6102-9.

9. **Arnold, J. J., and C. E. Cameron.** 2000. Poliovirus RNA-dependent RNA polymerase (3D(pol)). Assembly of stable, elongation-competent complexes by using a symmetrical primer-template substrate (sym/sub). J Biol Chem **275:**5329-36.

10. **Arnold, J. J., and C. E. Cameron.** 1999. Poliovirus RNA-dependent RNA polymerase (3Dpol) is sufficient for template switching in vitro. J Biol Chem **274:**2706-16.

11. **Arnold, J. J., and C. E. Cameron.** 2004. Poliovirus RNA-dependent RNA polymerase (3Dpol): pre-steady-state kinetic analysis of ribonucleotide incorporation in the presence of Mg2+. Biochemistry **43:**5126-37.

12. **Arnold, J. J., S. K. Ghosh, and C. E. Cameron.** 1999. Poliovirus RNA-dependent RNA polymerase (3D(pol)). Divalent cation modulation of primer, template, and nucleotide selection. J Biol Chem **274:**37060-9.

13. **Arnold, J. J., D. W. Gohara, and C. E. Cameron.** 2004. Poliovirus RNA-dependent RNA polymerase (3Dpol): pre-steady-state kinetic analysis of ribonucleotide incorporation in the presence of Mn2+. Biochemistry **43:**5138-48.

14. **Arnold, J. J., M. Vignuzzi, J. K. Stone, R. Andino, and C. E. Cameron.** 2005. Remote site control of an active site fidelity checkpoint in a viral RNA-dependent RNA polymerase. J Biol Chem **280:**25706-16.

15. **Baltera, R. F., Jr., and D. R. Tershak.** 1989. Guanidine-resistant mutants of poliovirus have distinct mutations in peptide 2C. J Virol **63:**4441-4.

16. **Baltimore, D.** 1964. In Vitro Synthesis of Viral Rna by the Poliovirus Rna Polymerase. Proc Natl Acad Sci U S A **51:**450-6.

17. **Baltimore, D., Y. Becker, and J. E. Darnell.** 1964. Virus-Specific Double-Stranded Rna in Poliovirus-Infected Cells. Science **143:**1034-6.

18. **Baltimore, D., H. J. Eggers, R. M. Franklin, and I. Tamm.** 1963. Poliovirus-induced RNA polymerase and the effects of virus-specific inhibitors on its production. Proc Natl Acad Sci U S A **49:**843-9.

19. **Baltimore, D., and M. Girard.** 1966. An intermediate in the synthesis of poliovirus RNA. Proc Natl Acad Sci U S A **56:**741-8.

20. **Barton, D. J.** 2002. Poliovirus RNA Replication and Genetic Complementation in Cell-Free Reactions. *In* B. L. Semler and E. Wimmer (ed.), Molecular Biology of Picornaviruses. ASM Press, Washington, DC.

21. **Barton, D. J., and J. B. Flanegan.** 1997. Synchronous replication of poliovirus RNA: initiation of negative-strand RNA synthesis requires the guanidine-inhibited activity of protein 2C. J Virol **71:**8482-9.

22. **Barton, D. J., B. J. Morasco, L. Eisner-Smerage, P. S. Collis, S. E. Diamond, M. J. Hewlett, M. A. Merchant, B. J. O'Donnell, and J. B. Flanegan.** 1996. Poliovirus RNA polymerase mutation 3D-M394T results in a temperature-sensitive defect in RNA synthesis. Virology **217:**459-69.

23. **Barton, D. J., B. J. Morasco, and J. B. Flanegan.** 1996. Assays for poliovirus polymerase, 3D(Pol), and authentic RNA replication in HeLa S10 extracts. Methods Enzymol **275:**35-57.

24. **Barton, D. J., B. J. Morasco, and J. B. Flanegan.** 1999. Translating ribosomes inhibit poliovirus negative-strand RNA synthesis. J Virol **73:**10104-12.

25. **Barton, D. J., B. J. O'Donnell, and J. B. Flanegan.** 2001. 5' cloverleaf in poliovirus RNA is a cis-acting replication element required for negative-strand synthesis. Embo J **20:**1439-48.

26. **Beckman, M. T., and K. Kirkegaard.** 1998. Site size of cooperative single-stranded RNA binding by poliovirus RNA-dependent RNA polymerase. J Biol Chem **273:**6724-30.

27. **Bienz, K., D. Egger, and L. Pasamontes.** 1987. Association of polioviral proteins of the P2 genomic region with the viral replication complex and virus-induced membrane synthesis as visualized by electron microscopic immunocytochemistry and autoradiography. Virology **160:**220-6.

28. **Bienz, K., D. Egger, T. Pfister, and M. Troxler.** 1992. Structural and functional characterization of the poliovirus replication complex. J Virol **66:**2740-7.

29. **Brandenburg, B., L. Y. Lee, M. Lakadamyali, M. J. Rust, X. Zhuang, and J. M. Hogle.** 2007. Imaging poliovirus entry in live cells. PLoS Biol **5:**e183.

30. **Cameron, C. E., D. W. Gohara, and J. J. Arnold.** 2002. Poliovirus RNA-dependent RNA Polymerase (3Dpol): Structure, Function, and Mechanism. *In* B. L. Semler and E. Wimmer (ed.), Molecular Biology of Picornaviruses. ASM Press, Washington, D.C.

31. **Cameron, C. E., H. Suk Oh, and I. M. Moustafa.** 2010. Expanding knowledge of P3 proteins in the poliovirus lifecycle. Future Microbiol **5:**867-81.

32. **Campagnola, G., M. Weygandt, K. Scoggin, and O. Peersen.** 2008. Crystal structure of coxsackievirus B3 3Dpol highlights the functional importance of residue 5 in picornavirus polymerases. J Virol **82:**9458-64.

33. **Castro, C., J. J. Arnold, and C. E. Cameron.** 2005. Incorporation fidelity of the viral RNA-dependent RNA polymerase: a kinetic, thermodynamic and structural perspective. Virus Res **107:**141-9.

34. **Chetwynd, J., C. Botting, and D. Hogan.** 1993. Postpolio syndrome in New Zealand: a survey of 700 polio survivors. N Z Med J **106:**406-8.

35. **Cho, M. W., O. C. Richards, T. M. Dmitrieva, V. Agol, and E. Ehrenfeld.** 1993. RNA duplex unwinding activity of poliovirus RNA-dependent RNA polymerase 3Dpol. J Virol **67:**3010-8.

36. **Collis, P. S., B. J. O'Donnell, D. J. Barton, J. A. Rogers, and J. B. Flanegan.** 1992. Replication of poliovirus RNA and subgenomic RNA transcripts in transfected cells. J Virol **66:**6480-8.

37. **Corver, J., E. Lenches, K. Smith, R. A. Robison, T. Sando, E. G. Strauss, and J. H. Strauss.** 2003. Fine mapping of a cis-acting sequence element in yellow fever virus RNA that is required for RNA replication and cyclization. J Virol **77:**2265-70.

38. **Crotty, S., C. E. Cameron, and R. Andino.** 2001. RNA virus error catastrophe: direct molecular test by using ribavirin. Proc Natl Acad Sci U S A **98:**6895-900.

39. **Crotty, S., D. Maag, J. J. Arnold, W. Zhong, J. Y. Lau, Z. Hong, R. Andino, and C. E. Cameron.** 2000. The broad-spectrum antiviral ribonucleoside ribavirin is an RNA virus mutagen. Nat Med **6:**1375-9.

40. **Dalakas, M. C.** 1995. Post-polio syndrome 12 years later. How it all started. Ann N Y Acad Sci **753:**11-8.

41. **Darnell, J. E., Jr.** 1962. Early events in poliovirus infection. Cold Spring Harb Symp Quant Biol **27:**149-58.

42. **Datta, K., N. P. Johnson, V. J. LiCata, and P. H. von Hippel.** 2009. Local conformations and competitive binding affinities of single- and double-stranded primer-template DNA at the polymerization and editing active sites of DNA polymerases. J Biol Chem **284:**17180-93.

43. **Datta, K., N. P. Johnson, and P. H. von Hippel.** 2006. Mapping the conformation of the nucleic acid framework of the T7 RNA polymerase elongation complex in solution using low-energy CD and fluorescence spectroscopy. J Mol Biol **360:**800-13.

44. **De Jesus, N. H.** 2007. Epidemics to eradication: the modern history of poliomyelitis. Virol J **4**.

45. **Diamond, S. E., and K. Kirkegaard.** 1994. Clustered charged-to-alanine mutagenesis of poliovirus RNA-dependent RNA polymerase yields multiple temperature-sensitive mutants defective in RNA synthesis. J Virol **68:**863-76.

46. **Domingo, E.** 1997. Rapid evolution of viral RNA genomes. J Nutr **127:**958S-961S.

47. **Domingo, E., E. Baranowski, C. Escarmis, F. Sobrino, and J. J. Holland.** 2002. Error Frequencies of Picornavirus RNA Polymerase: Evoulutionary Implications for Virus Populations. *In* B. L. Semler and E. Wimmer (ed.), Molecular Biology of Picornaviruses, Washington, D.C.

48. **Duggal, R.** 2002. Cell-Free Genetics of Poliovirus. *In* E. W. B.L. Semler (ed.), Molecular Biology of Picornaviruses. ASM Press.

49. **Dunn, G., N. T. Begg, N. Cammack, and P. D. Minor.** 1990. Virus excretion and mutation by infants following primary vaccination with live oral poliovaccine from two sources. J Med Virol **32:**92-5.

50. **Eggers, H. J.** 2002. History of Poliomyelitis and Poliomyelitis Research. *In* B. L. Semler and E. Wimmer (ed.), Molecular Biology of Picornaviruses. ASM Press, Washington D.C.

51. **Enders, J. F., T. H. Weller, and F. C. Robbins.** 1949. Cultivation of the Lansing Strain of Poliomyelitis Virus in Cultures of Various Human Embryonic Tissues. Science **109:**85-7.

52. **Etchison, D., S. C. Milburn, I. Edery, N. Sonenberg, and J. W. Hershey.** 1982. Inhibition of HeLa cell protein synthesis following poliovirus infection correlates with the proteolysis of a 220,000-dalton polypeptide associated with eucaryotic initiation factor 3 and a cap binding protein complex. J Biol Chem **257:**14806-10.

53. **Ferrer-Orta, C., A. Arias, R. Perez-Luque, C. Escarmis, E. Domingo, and N. Verdaguer.** 2007. Sequential structures provide insights into the fidelity of RNA replication. Proc Natl Acad Sci U S A **104:**9463-8.

54. **Ferrer-Orta, C., A. Arias, R. Perez-Luque, C. Escarmis, E. Domingo, and N. Verdaguer.** 2004. Structure of foot-and-mouth disease virus RNA-dependent RNA polymerase and its complex with a template-primer RNA. J Biol Chem **279:**47212-21.

55. **Flanegan, J. B., R. F. Petterson, V. Ambros, N. J. Hewlett, and D. Baltimore.** 1977. Covalent linkage of a protein to a defined nucleotide sequence at the 5'-terminus of virion and replicative intermediate RNAs of poliovirus. Proc Natl Acad Sci U S A **74:**961-5.

56. **Gamarnik, A. V., and R. Andino.** 1998. Switch from translation to RNA replication in a positive-stranded RNA virus. Genes Dev **12:**2293-304.

57. **Gohara, D. W., J. J. Arnold, and C. E. Cameron.** 2004. Poliovirus RNA-dependent RNA polymerase (3Dpol): kinetic, thermodynamic, and structural analysis of ribonucleotide selection. Biochemistry **43:**5149-58.

58. **Gohara, D. W., C. S. Ha, S. Kumar, B. Ghosh, J. J. Arnold, T. J. Wisniewski, and C. E. Cameron.** 1999. Production of "authentic" poliovirus RNA-dependent RNA polymerase (3D(pol)) by ubiquitin-protease-mediated cleavage in Escherichia coli. Protein Expr Purif **17:**128-38.

59. **Gong, P., G. Campagnola, and O. B. Peersen.** 2009. A quantitative stopped-flow fluorescence assay for measuring polymerase elongation rates. Anal Biochem **391:**45-55.

60. **Gong, P., and O. B. Peersen.** 2010. Structural basis for active site closure by the poliovirus RNA-dependent RNA polymerase. Proc Natl Acad Sci U S A **107:**22505-10.

61. **Goodfellow, I. G., C. Polacek, R. Andino, and D. J. Evans.** 2003. The poliovirus 2C cis-acting replication element-mediated uridylylation of VPg is not required for synthesis of negative-sense genomes. J Gen Virol **84:**2359-63.

62. **Graci, J. D., and C. E. Cameron.** 2006. Mechanisms of action of ribavirin against distinct viruses. Rev Med Virol **16:**37-48.

63. **Gromeier, M., L. Alexander, and E. Wimmer.** 1996. Internal ribosomal entry site substitution eliminates neurovirulence in intergeneric poliovirus recombinants. Proc Natl Acad Sci U S A **93:**2370-5.

64. **Gruez, A., B. Selisko, M. Roberts, G. Bricogne, C. Bussetta, I. Jabafi, B. Coutard, A. M. De Palma, J. Neyts, and B. Canard.** 2008. The crystal structure of coxsackievirus B3 RNA-dependent RNA polymerase in complex with its protein primer VPg confirms the existence of a second VPg binding site on Picornaviridae polymerases. J Virol **82:**9577-90.

65. **Halstead, L. S., and J. K. Silver.** 2000. Nonparalytic polio and postpolio syndrome. Am J Phys Med Rehabil **79:**13-8.

66. **Han, J. Q., H. L. Townsend, B. K. Jha, J. M. Paranjape, R. H. Silverman, and D. J. Barton.** 2007. A phylogenetically conserved RNA structure in the poliovirus open reading frame inhibits the antiviral endoribonuclease RNase L. J Virol **81:**5561-72.

67. **Hansen, J. L., A. M. Long, and S. C. Schultz.** 1997. Structure of the RNA-dependent RNA polymerase of poliovirus. Structure **5:**1109-22.

68. **Hellen, C. U., T. V. Pestova, M. Litterst, and E. Wimmer.** 1994. The cellular polypeptide p57 (pyrimidine tract-binding protein) binds to multiple sites in the poliovirus 5' nontranslated region. J Virol **68:**941-50.

69. **Herold, J., and R. Andino.** 2000. Poliovirus requires a precise 5' end for efficient positive-strand RNA synthesis. J Virol **74:**6394-400.

70. **Herold, J., and R. Andino.** 2001. Poliovirus RNA replication requires genome circularization through a protein-protein bridge. Mol Cell **7:**581-91.

71. **Hobdey, S. E., B. J. Kempf, B. P. Steil, D. J. Barton, and O. B. Peersen.** 2010. Poliovirus polymerase residue 5 plays a critical role in elongation complex stability. J Virol **84:**8072-84.

72. **Hogle, J. M., M. Chow, and D. J. Filman.** 1985. Three-dimensional structure of poliovirus at 2.9 A resolution. Science **229:**1358-65.

73. **Holland, J., K. Spindler, F. Horodyski, E. Grabau, S. Nichol, and S. VandePol.** 1982. Rapid evolution of RNA genomes. Science **215:**1577-85.

74. **Holmgren, A.** 1985. Thioredoxin. Annu Rev Biochem **54:**237-71.

75. **Huber, H. E., S. Tabor, and C. C. Richardson.** 1987. Escherichia coli thioredoxin stabilizes complexes of bacteriophage T7 DNA polymerase and primed templates. J Biol Chem **262:**16224-32.

76. **Kelman, Z., J. Hurwitz, and M. O'Donnell.** 1998. Processivity of DNA polymerases: two mechanisms, one goal. Structure **6:**121-5.

77. **Kitamura, N., B. L. Semler, P. G. Rothberg, G. R. Larsen, C. J. Adler, A. J. Dorner, E. A. Emini, R. Hanecak, J. J. Lee, S. van der Werf, C. W. Anderson, and E. Wimmer.** 1981. Primary structure, gene organization and polypeptide expression of poliovirus RNA. Nature **291:**547-53.

78. **Kitamura, N., and E. Wimmer.** 1980. Sequence of 1060 3'-terminal nucleotides of poliovirus RNA as determined by a modification of the dideoxynucleotide method. Proc Natl Acad Sci U S A **77:**3196-200.

79. **Kohlstaedt, L. A., J. Wang, J. M. Friedman, P. A. Rice, and T. A. Steitz.** 1992. Crystal structure at 3.5 A resolution of HIV-1 reverse transcriptase complexed with an inhibitor. Science **256:**1783-90.

80. **Koike, S., C. Taya, T. Kurata, S. Abe, I. Ise, H. Yonekawa, and A. Nomoto.** 1991. Transgenic mice susceptible to poliovirus. Proc Natl Acad Sci U S A **88:**951-5.

81. **Korneeva, V. S., and C. E. Cameron.** 2007. Structure-function relationships of the viral RNA-dependent RNA polymerase: fidelity, replication speed, and initiation mechanism determined by a residue in the ribose-binding pocket. J Biol Chem **282:**16135-45.

82. **Krenn, B. M., E. Gaudernak, B. Holzer, K. Lanke, F. J. Van Kuppeveld, and J. Seipelt.** 2009. Antiviral activity of the zinc ionophores pyrithione and hinokitiol against picornavirus infections. J Virol **83:**58-64.

83. **Kroon, F. P., H. T. Weiland, A. M. van Loon, and R. van Furth.** 1995. Abortive and subclinical poliomyelitis in a family during the 1992 epidemic in The Netherlands. Clin Infect Dis **20:**454-6.

84. **Lakowicz, J. R.** 2006. Principles of Fluorescence Spectroscopy, 3rd ed. Springer Science+Business Media, LLC.

85. **Lambert, D. A., E. Giannouli, and B. J. Schmidt.** 2005. Postpolio syndrome and anesthesia. Anesthesiology **103:**638-44.

86. **Landsteiner, K., Popper, E.** 1909. Ubertargung der Poliomyelitis acuta auf Affen. Zeitchr. Immunitatsforsch **2:**377-390.

87. **Lanke, K., B. M. Krenn, W. J. Melchers, J. Seipelt, and F. J. van Kuppeveld.** 2007. PDTC inhibits picornavirus polyprotein processing and RNA replication by transporting zinc ions into cells. J Gen Virol **88:**1206-17.

88. **Levy, H. C., M. Bostina, D. J. Filman, and J. M. Hogle.** 2010. Catching a virus in the act of RNA release: a novel poliovirus uncoating intermediate characterized by cryo-electron microscopy. J Virol **84:**4426-41.

89. **Lindberg, A. M., P. O. Stalhandske, and U. Pettersson.** 1987. Genome of coxsackievirus B3. Virology **156:**50-63.

90. **Liu, Y., C. Wang, S. Mueller, A. V. Paul, E. Wimmer, and P. Jiang.** 2010. Direct interaction between two viral proteins, the nonstructural protein 2C and the capsid protein VP3, is required for enterovirus morphogenesis. PLoS Pathog **6**.

91. **Lopez, P. J., J. Guillerez, R. Sousa, and M. Dreyfus.** 1997. The low processivity of T7 RNA polymerase over the initially transcribed sequence can limit productive initiation in vivo. J Mol Biol **269:**41-51.

92. **Love, R. A., K. A. Maegley, X. Yu, R. A. Ferre, L. K. Lingardo, W. Diehl, H. E. Parge, P. S. Dragovich, and S. A. Fuhrman.** 2004. The crystal structure of the RNA-dependent RNA polymerase from human rhinovirus: a dual function target for common cold antiviral therapy. Structure **12:**1533-44.

93. **Lu, H. H., and E. Wimmer.** 1996. Poliovirus chimeras replicating under the translational control of genetic elements of hepatitis C virus reveal unusual properties of the internal ribosomal entry site of hepatitis C virus. Proc Natl Acad Sci U S A **93:**1412-7.

94. **Lyle, J. M., E. Bullitt, K. Bienz, and K. Kirkegaard.** 2002. Visualization and functional analysis of RNA-dependent RNA polymerase lattices. Science **296:**2218-22.

95. **Lyons, T., K. E. Murray, A. W. Roberts, and D. J. Barton.** 2001. Poliovirus 5'-terminal cloverleaf RNA is required in cis for VPg uridylylation and the initiation of negative-strand RNA synthesis. J Virol **75:**10696-708.

96. **Ma, K., D. Temiakov, M. Anikin, and W. T. McAllister.** 2005. Probing conformational changes in T7 RNA polymerase during initiation and termination by using engineered disulfide linkages. Proc Natl Acad Sci U S A **102:**17612-7.

97. **Mark, D. F., and C. C. Richardson.** 1976. Escherichia coli thioredoxin: a subunit of bacteriophage T7 DNA polymerase. Proc Natl Acad Sci U S A **73:**780-4.

98. **Mendelsohn, C. L., E. Wimmer, and V. R. Racaniello.** 1989. Cellular receptor for poliovirus: molecular cloning, nucleotide sequence, and expression of a new member of the immunoglobulin superfamily. Cell **56:**855-65.

99. **Mestas, S. P., A. J. Sholders, and O. B. Peersen.** 2007. A fluorescence polarization-based screening assay for nucleic acid polymerase elongation activity. Anal Biochem **365:**194-200.

100. **Molla, A., A. V. Paul, and E. Wimmer.** 1991. Cell-free, de novo synthesis of poliovirus. Science **254:**1647-51.

101. **Mueller, S., and E. Wimmer.** 2003. Recruitment of Nectin-3 to cell-cell junctions through trans-heterophilic interaction with CD155, a vitronectin and poliovirus receptor that localizes to avb3 integrin containing membrane microdomains. J Biol Chem.

102. **Muller, D. K., C. T. Martin, and J. E. Coleman.** 1988. Processivity of proteolytically modified forms of T7 RNA polymerase. Biochemistry **27:**5763-71.

103. **Murray, K. E., and D. J. Barton.** 2003. Poliovirus CRE-dependent VPg uridylylation is required for positive-strand RNA synthesis but not for negative-strand RNA synthesis. J Virol **77:**4739-50.

104. **Murray, K. E., B. P. Steil, A. W. Roberts, and D. J. Barton.** 2004. Replication of poliovirus RNA with complete internal ribosome entry site deletions. J Virol **78:**1393-402.

105. **Nathanson, N., and P. Fine.** 2002. Virology. Poliomyelitis eradication--a dangerous endgame. Science **296:**269-70.

106. **Nathanson, N., and O. M. Kew.** 2010. From emergence to eradication: the epidemiology of poliomyelitis deconstructed. Am J Epidemiol **172:**1213-29.

107. **Nathanson, N., and J. R. Martin.** 1979. The epidemiology of poliomyelitis: enigmas surrounding its appearance, epidemicity, and disappearance. Am J Epidemiol **110:**672-92.

108. **Neufeld, K. L., J. M. Galarza, O. C. Richards, D. F. Summers, and E. Ehrenfeld.** 1994. Identification of terminal adenylyl transferase activity of the poliovirus polymerase 3Dpol. J Virol **68:**5811-8.

109. **Ng, K. K., J. J. Arnold, and C. E. Cameron.** 2008. Structure-function relationships among RNA-dependent RNA polymerases. Curr Top Microbiol Immunol **320:**137-56.

110. **Ng, K. K., N. Pendas-Franco, J. Rojo, J. A. Boga, A. Machin, J. M. Alonso, and F. Parra.** 2004. Crystal structure of norwalk virus polymerase reveals the carboxyl terminus in the active site cleft. J Biol Chem **279:**16638-45.

111. **Nomoto, A., N. Kitamura, F. Golini, and E. Wimmer.** 1977. The 5'-terminal structures of poliovirion RNA and poliovirus mRNA differ only in the genome-linked protein VPg. Proc Natl Acad Sci U S A **74:**5345-9.

112. **Novak, J. E., and K. Kirkegaard.** 1991. Improved method for detecting poliovirus negative strands used to demonstrate specificity of positive-strand encapsidation and the ratio of positive to negative strands in infected cells. J Virol **65:**3384-7.

113. **Nugent, C. I., K. L. Johnson, P. Sarnow, and K. Kirkegaard.** 1999. Functional coupling between replication and packaging of poliovirus replicon RNA. J Virol **73:**427-35.

114. **Oh, H. S., H. B. Pathak, I. G. Goodfellow, J. J. Arnold, and C. E. Cameron.** 2009. Insight into poliovirus genome replication and encapsidation obtained from studies of 3B-3C cleavage site mutants. J Virol **83:**9370-87.

115. **Pata, J. D., S. C. Schultz, and K. Kirkegaard.** 1995. Functional oligomerization of poliovirus RNA-dependent RNA polymerase. Rna **1:**466-77.

116. **Paul, A. V.** 2002. Possible Unifying Mechanism of Picornavirus Genome Replication. *In* B. L. Semler and E. Wimmer (ed.), Molecular Biology of Picornaviruses. ASM Press, Washington, DC.

117. **Paul, A. V., E. Rieder, D. W. Kim, J. H. van Boom, and E. Wimmer.** 2000. Identification of an RNA hairpin in poliovirus RNA that serves as the primary template in the in vitro uridylylation of VPg. J Virol **74:**10359-70.

118. **Paul, A. V., J. H. van Boom, D. Filippov, and E. Wimmer.** 1998. Protein-primed RNA synthesis by purified poliovirus RNA polymerase. Nature **393:**280-4.

119. **Paul, A. V., J. Yin, J. Mugavero, E. Rieder, Y. Liu, and E. Wimmer.** 2003. A "slide-back" mechanism for the initiation of protein-primed RNA synthesis by the RNA polymerase of poliovirus. J Biol Chem **278:**43951-60.

120. **Pelletier, J., G. Kaplan, V. R. Racaniello, and N. Sonenberg.** 1988. Cap-independent translation of poliovirus mRNA is conferred by sequence elements within the 5' noncoding region. Mol Cell Biol **8:**1103-12.

121. **Pelletier, J., and N. Sonenberg.** 1988. Internal initiation of translation of eukaryotic mRNA directed by a sequence derived from poliovirus RNA. Nature **334:**320-5.

122. **Pfeiffer, J. K., and K. Kirkegaard.** 2005. Increased fidelity reduces poliovirus fitness and virulence under selective pressure in mice. PLoS Pathog **1:**e11.

123. **Pfeiffer, J. K., and K. Kirkegaard.** 2003. A single mutation in poliovirus RNA-dependent RNA polymerase confers resistance to mutagenic nucleotide analogs via increased fidelity. Proc Natl Acad Sci U S A **100:**7289-94.

124. **Pfister, T., and E. Wimmer.** 1999. Characterization of the nucleoside triphosphatase activity of poliovirus protein 2C reveals a mechanism by which guanidine inhibits poliovirus replication. J Biol Chem **274:**6992-7001.

125. **Pincus, S. E., D. C. Diamond, E. A. Emini, and E. Wimmer.** 1986. Guanidine-selected mutants of poliovirus: mapping of point mutations to polypeptide 2C. J Virol **57:**638-46.

126. **Polatnick, J., and H. L. Bachrach.** 1978. Effect of zinc and other chemical agents on foot-and-mouth-disease virus replication. Antimicrob Agents Chemother **13:**731-4.

127. **Poranen, M. M., M. R. Koivunen, and D. H. Bamford.** 2008. Nontemplated terminal nucleotidyltransferase activity of double-stranded RNA bacteriophage phi6 RNA-dependent RNA polymerase. J Virol **82:**9254-64.

128. **Prevention, C. f. D. C. a.** March 10, 2011 2011, posting date. Emerging Infectious Diseases. [Online.]

129. **Racaniello, V. R.** 2006. One hundred years of poliovirus pathogenesis. Virology **344:**9-16.

130. **Racaniello, V. R., and D. Baltimore.** 1981. Cloned poliovirus complementary DNA is infectious in mammalian cells. Science **214:**916-9.

131. **Reich, E., R. M. Franklin, A. J. Shatkin, and E. L. Tatum.** 1961. Effect of actinomycin D on cellular nucleic acid synthesis and virus production. Science **134:**556-7.

132. **Richards, O. C., S. C. Martin, H. G. Jense, and E. Ehrenfeld.** 1984. Structure of poliovirus replicative intermediate RNA. Electron microscope analysis of RNA cross-linked in vivo with psoralen derivative. J Mol Biol **173:**325-40.

133. **Rieder, E., A. V. Paul, D. W. Kim, J. H. van Boom, and E. Wimmer.** 2000. Genetic and biochemical studies of poliovirus cis-acting replication element cre in relation to VPg uridylylation. J Virol **74:**10371-80.

134. **Rodriguez-Wells, V., S. J. Plotch, and J. J. DeStefano.** 2001. Primer-dependent synthesis by poliovirus RNA-dependent RNA polymerase (3D(pol)). Nucleic Acids Res **29:**2715-24.

135. **Rodriguez, P. L., and L. Carrasco.** 1995. Poliovirus protein 2C contains two regions involved in RNA binding activity. J Biol Chem **270:**10105-12.

136. **Rodriguez, P. L., and L. Carrasco.** 1993. Poliovirus protein 2C has ATPase and GTPase activities. J Biol Chem **268:**8105-10.

137. **Sabin, A. B.** 1956. Pathogenesis of poliomyelitis; reappraisal in the light of new data. Science **123:**1151-7.

138. **Sabin, A. B.** 1959. Present position of immunization against poliomyelitis with live virus vaccines. Br Med J **1:**663-80.

139. **Sonenberg, N.** 1987. Regulation of translation by poliovirus. Adv Virus Res **33:**175-204.

140. **Sousa, R., Y. J. Chung, J. P. Rose, and B. C. Wang.** 1993. Crystal structure of bacteriophage T7 RNA polymerase at 3.3 A resolution. Nature **364:**593-9.

141. **Sowers, L. C., G. V. Fazakerley, R. Eritja, B. E. Kaplan, and M. F. Goodman.** 1986. Base pairing and mutagenesis: observation of a protonated base pair between 2-aminopurine and cytosine in an oligonucleotide by proton NMR. Proc Natl Acad Sci U S A **83:**5434-8.

142. **Stanway, G., Hovi, T., Knowles, N.J., Hyypia, T.,.** 2001. Molecular and Biological Basis of Picornavirus Taxonomy. *In* B. L. Semler, Wimmer, E. (ed.), Molecular Biology of Picornaviruses. ASM Press, Washington, DC.

143. **Steil, B. P., B. J. Kempf, and D. J. Barton.** 2010. Poly(A) at the 3' end of positive-strand RNA and VPg-linked poly(U) at the 5' end of negative-strand RNA are reciprocal templates during replication of poliovirus RNA. J Virol **84:**2843-58.

144. **Steitz, T. A.** 1993. DNA- and RNA-dependent DNA polymerases. Current Opinion in Structural Biology **3:**31-38.

145. **Stukenberg, P. T., P. S. Studwell-Vaughan, and M. O'Donnell.** 1991. Mechanism of the sliding beta-clamp of DNA polymerase III holoenzyme. J Biol Chem **266:**11328-34.

146. **Tabor, S., H. E. Huber, and C. C. Richardson.** 1987. Escherichia coli thioredoxin confers processivity on the DNA polymerase activity of the gene 5 protein of bacteriophage T7. J Biol Chem **262:**16212-23.

147. **Tabor, S., and C. C. Richardson.** 1987. DNA sequence analysis with a modified bacteriophage T7 DNA polymerase. Proc Natl Acad Sci U S A **84:**4767-71.

148. **Tainer, J. A., V. A. Roberts, and E. D. Getzoff.** 1992. Protein metal-binding sites. Curr Opin Biotechnol **3:**378-87.

149. **Tang, G. Q., V. S. Anand, and S. S. Patel.** 2011. Fluorescence-based assay to measure the real-time kinetics of nucleotide incorporation during transcription elongation. J Mol Biol **405:**666-78.

150. **te Velthuis, A. J., J. J. Arnold, C. E. Cameron, S. H. van den Worm, and E. J. Snijder.** 2010. The RNA polymerase activity of SARS-coronavirus nsp12 is primer dependent. Nucleic Acids Res **38:**203-14.

151. **Thompson, A. A., R. A. Albertini, and O. B. Peersen.** 2007. Stabilization of Poliovirus Polymerase by NTP Binding and Fingers-Thumb Interactions. J Mol Biol **366:**1459-74.

152. **Thompson, A. A., and O. B. Peersen.** 2004. Structural basis for proteolysis-dependent activation of the poliovirus RNA-dependent RNA polymerase. Embo J **23:**3462-71.

153. **Vignuzzi, M., J. K. Stone, J. J. Arnold, C. E. Cameron, and R. Andino.** 2006. Quasispecies diversity determines pathogenesis through cooperative interactions in a viral population. Nature **439:**344-8.

154. **Vignuzzi, M., E. Wendt, and R. Andino.** 2008. Engineering attenuated virus vaccines by controlling replication fidelity. Nat Med **14:**154-61.

155. **Viruses, I. C. o. T. o.** 2009. Virus Taxonomy: 2009 Release.

156. **Vogt, D. A., and R. Andino.** 2010. An RNA element at the 5'-end of the poliovirus genome functions as a general promoter for RNA synthesis. PLoS Pathog **6:**e1000936.

157. **Ward, C. D., M. A. Stokes, and J. B. Flanegan.** 1988. Direct measurement of the poliovirus RNA polymerase error frequency in vitro. J Virol **62:**558-62.

158. **Weller, T. H., F. C. Robbins, and J. F. Enders.** 1949. Cultivation of poliomyelitis virus in cultures of human foreskin and embryonic tissues. Proc Soc Exp Biol Med **72:**153-5.

159. **Wells, V. R., S. J. Plotch, and J. J. DeStefano.** 2001. Determination of the mutation rate of poliovirus RNA-dependent RNA polymerase. Virus Res **74:**119-32.

160. **Wimmer, E., and A. Nomoto.** 1993. Molecular biology and cell-free synthesis of poliovirus. Biologicals **21:**349-56.

161. **Xiang, W., A. Cuconati, D. Hope, K. Kirkegaard, and E. Wimmer.** 1998. Complete protein linkage map of poliovirus P3 proteins: interaction of polymerase 3Dpol with VPg and with genetic variants of 3AB. J Virol **72:**6732-41.

162. **Yang, X., J. L. Welch, J. J. Arnold, and D. D. Boehr.** 2010. Long-range interaction networks in the function and fidelity of poliovirus RNA-dependent RNA polymerase studied by nuclear magnetic resonance. Biochemistry **49:**9361-71.

163. **Zamyatkin, D. F., F. Parra, J. M. Martin Alonso, D. A. Harki, B. R. Peterson, P. Grochulski, and K. K. Ng.** 2008. Structural insights into mechanisms of catalysis and inhibition in norwalk virus polymerase. J Biol Chem.